UNIVERSITY OF CALIFORNIA SAN DIEGO

Targeting Cytosolic Cathepsin B: Leveraging pH-Dependent Cleavage Preferences with Selective Inhibitors to Rescue Cell Death and Mitigate TBI-Induced Motor Deficits

A Dissertation submitted in partial satisfaction of the requirements
for the degree Doctor of Philosophy

in

Biomedical Sciences

by

Von V. Phan

Committee in charge:

Professor Vivian Hook, Chair
Professor Conor Caffrey, Co-Chair
Professor Richard Daneman
Professor William Gerwick
Professor Anthony O'Donoghue

2024

The Dissertation of Von V. Phan is approved, and it is acceptable in quality and form for publication on microfilm and electronically.

University of California San Diego

2024

DEDICATION

This dissertation is dedicated to my parents, brother, sisters, and Mr. Ali.

TABLE OF CONTENTS

LIST OF FIGURES

LIST OF TABLES

ACKNOWLEDGEMENTS

I am grateful for the unwavering support and mentorship provided by Dr. Vivian Hook, who served as the chair of my committee and as my PhD advisor, and Dr. Conor Caffrey, my co-chair. Their guidance across diverse domains including neuroscience, enzymology, and drug discovery has been instrumental in shaping my journey to success in the field.

Additionally, I extend my appreciation to Drs. Anthony O'Donoghue, William Gerwick, and Richard Daneman for their invaluable contributions as committee members. Their expertise and mentorship have been a source of inspiration and motivation.

I am also indebted to my esteemed colleagues, both past and present, namely Michael C. Yoon, Sonia Podvin, and Charles Mosier, whose mentorship, contributions, and shared knowledge in the laboratory have greatly enriched this thesis.

Furthermore, I extend my gratitude to our esteemed collaborators, including William Gerwick, Evgenia Glukhov, Jehad Almaliti, and Mitchel Christy, for their expertise in marine natural products chemistry, as well as Robert Rissman, Jazmin Florio, Brian Spencer, and Mike Mante for their contributions in traumatic brain injury and mouse handling.

I would like to express my sincere gratitude for the financial support provided by the NIH grants R01NS109075 (granted to Dr. Vivian Hook), T32GM007752 (granted to Drs. Joan Heller Brown and Tracy Handel), and T32AG066596 (granted to Dr. Edward Koo), and Skaggs School of Pharmacy and Pharmaceutical Sciences (Dr. Conor Caffrey). This support has been pivotal in facilitating my research endeavors and academic pursuits.

Furthermore, I extend my appreciation to the UC San Diego Biomedical Sciences Graduate Program and the UC San Diego Skaggs School of Pharmacy and Pharmaceutical Sciences Program

for their unwavering support and resources, which have played a crucial role in my academic and professional development.

Lastly, I am profoundly thankful to my family and friends whose unwavering support has been the cornerstone of my journey through the PharmD and PhD programs at UC San Diego, making this chapter of my life truly enjoyable.

Chapter 2, in full, is a reprint of the material as it appears in Biochemistry in American Chemical Society. Michael C. Yoon, Mitchell P. Christy, Von V. Phan, William H. Gerwick, Gregory Hook, Anthony J. O'Donoghue, and Vivian Hook, American Chemical Society, 2022. The dissertation author was co-author of this paper.

Chapter 3, in full, is a reprint of the material as it appears in ACS Omega in American Chemical Society. Von V. Phan, Charles Mosier, Michael C. Yoon, Evgenia Glukhov, Conor R Caffrey, Anthony J O'Donoghue, William H. Gerwick, and Vivian Hook, American Chemical Society, 2022. The dissertation author was the primary researcher and author of this material.

Chapter 4, in full, is a reprint of the material as it appears in Biochemistry in American Chemical Society. Michael C. Yoon, Von V. Phan, Sonia Podvin, Charles Mosier, Anthony J. O'Donoghue, and Vivian Hook, American Chemical Society, 2023. The dissertation author was a co-author of this material.

Chapter 5, in part, is currently being prepared for submission for publication of the material. Von V. Phan, Sonia Podvin, Charles Mosier, Michael C. Yoon, Dennis Wolan, Anthony J. O'Donoghue, and Vivian Hook. The dissertation author was the primary researcher and author of this material.

Chapter 6, in part, is currently being prepared for submission for publication of the material. Sonia Podvin, Jazmin Florio, Charles Mosier, Brian Spencer, Mike Mante, Michael C.

Yoon, Von V. Phan, Jehad Almaliti, William Gerwick, Anthony J. O'Donoghue, Robert Rissman, and Vivian Hook. The dissertation author was a co-author of this material.

VITA

2011 – 2015 Bachelor of Science in Marine Biology, University of California Los Angeles

2019 – 2024 Doctor of Philosophy in Biomedical Sciences, University of California San Diego

2017 – 2019 Doctor of Pharmacy, University of California San Diego, expected completion date: May 2026

PUBLICATIONS

Phan VV, Mosier C, Yoon MC, Glukhov E, Caffrey CR, O'Donoghue AJ, Gerwick WH, Hook V. Discovery of pH-Selective Marine and Plant Natural Product Inhibitors of Cathepsin B Revealed by Screening at Acidic and Neutral pH Conditions. *ACS Omega.* 2022 Jul 12;7(29):25346-25352. doi: 10.1021/acsomega.2c02287. PMID: 35910167.

Yoon MC, Christy MP, **Phan VV**, Gerwick WH, Hook G, O'Donoghue AJ, Hook V. Molecular Features of CA-074 pH-Dependent Inhibition of Cathepsin B. *Biochemistry.* 2022 Feb 15;61(4):228-238. doi: 10.1021/acs.biochem.1c00684. Epub 2022 Feb 4. PMID: 35119840.

Yoon MC, **Phan VV**, Podvin S, Mosier C, O'Donoghue AJ, Hook V. Distinct Cleavage Properties of Cathepsin B Compared to Cysteine Cathepsins Enable the Design and Validation of a Specific Substrate for Cathepsin B over a Broad pH Range. Biochemistry. 2023 Aug 1;62(15):2289-2300. doi: 10.1021/acs.biochem.3c00139. Epub 2023 Jul 17. PMID: 37459182.

Phan VV, Podvin S, Mosier C, Yoon MC, Wolan D, O'Donoghue AJ, Hook V. Involvement of Cytosolic Cathepsin B in Cell Death Induced by Low Nutrient Stress in Microglia Cells. For submission in 2024, in preparation.

Podvin S., Florio J, Mosier C, Spencer B, Mante M, Yoon MC, **Phan VV**, Almaliti J, Gerwick WH, O'Donoghue AJ, Rissman R, Hook V. Traumatic Brain Injury Induces Cytosolic Cathepsin B and Motor Deficits. For submission in 2024, in preparation.

ABSTRACT OF THE DISSERTATION

Targeting Cytosolic Cathepsin B: Leveraging pH-Dependent Cleavage Preferences with Selective Inhibitors to Rescue Cell Death and Mitigate TBI-Induced Motor Deficits

by

Von V. Phan

Doctor of Philosophy in Biomedical Sciences

University of California San Diego, 2024

Professor Vivian Hook, Chair
Professor Conor Caffrey, Co-Chair

The dissertation addresses the imperative need to understand the molecular mechanisms underlying Alzheimer's disease (AD), traumatic brain injury (TBI), and other neurological disorders. AD, a prevalent neurodegenerative disease, and TBI, a significant risk factor for AD, impose severe cognitive deficits and memory loss, emphasizing the urgency for advancing our comprehension of their pathogenic mechanisms. Cytosolic cathepsin B has been implicated in cell death and neuroinflammation in AD and TBI, making it a potential therapeutic target. Pathogenic, cytosolic cathepsin B in disease conditions results from lysosomal leakage of cathepsin B to the cytosol. Research has shown elevated levels of cathepsin B in various neurological disorders,

including AD and TBI, highlighting its involvement in disease pathology. Notably, cathepsin B displays distinct cleavage properties at lysosomal acidic pH 4.6 and cytosolic neutral pH 7.2, suggesting its dynamic role in different cellular compartments. To investigate this further, pH-selective inhibitors, such as Z-Arg-Lys-AOMK and CA-074, were developed to target cathepsin B in specific pH environments. Additionally, a novel fluorescent substrate, Z-Nle-Lys-Arg-AMC, was designed to monitor cathepsin B activity across a wide pH range with high specificity. Utilizing these tools, the study aims to assess the role of cytosolic cathepsin B in cell death in mouse microglia BV2 cells and TBI mouse models. Experimental studies in a mouse model of traumatic brain injury (TBI) show that injury increases cytosolic cathepsin B associated with motor behavioral deficits, modulated by the neutral pH selective inhibitor of cathepsin B, Z-Arg-Lys-AOMK. Treatment of TBI mice with Z-Arg-Lys-AOMK improved neuromotor function, and inhibited TBI-induced cytosolic cathepsin B. Further *in vivo* investigation of the role of cytosolic cathepsin B in behavioral deficits and neuropathology in animal models of neurological diseases are needed to evaluate the therapeutic potential of targeting cathepsin B in particular brain disorders. In conclusion, this dissertation sheds light on the complex role of cathepsin B in neurological disorders and offers novel insights into its therapeutic targeting. By elucidating the molecular mechanisms underlying AD, and TBI, this research paves the way for the development of innovative treatments for future therapeutic interventions in neurological disorders.

Chapter 1 INTRODUCTION: Assessment of Neutral pH, cytosolic Cathepsin B in Neurological Disorders

1.1 Need for Characterizing the involvement of Cathepsin B in Pathogenic Mechanisms of Alzheimer's Disease, Traumatic Brain Injury, and other Neurological Disorders

Alzheimer's disease (AD) is an age-related neurodegenerative disease that results in severe cognitive deficit and memory loss. (1) It accounts for up to 80% of dementia cases, with one in three people over the age of 85 diagnosed with AD. AD is preceded by the early stage of mild cognitive impairment that transitions into the severe dementia of AD, which is often fatal. (2-4) Traumatic brain injury (TBI) is a significant risk factor for AD (5,6); described as an external force that causes damage to the brain leading to brain dysfunction and cognitive deficits. TBI impacts approximately 2.8 million individuals annually in the United States and is the leading cause of death in young adults. (7) TBI is associated with short-term and long-term effects, patients that experience TBI have a greater likelihood of developing AD in their lifetime. Given the substantial prevalence of AD and TBI, there is an imperative to advance our comprehension of the molecular mechanisms of brain dysfunction that may provide future drug targets for drug discovery. More specifically, cathepsin B has been shown to participate in the underlying mechanisms of cell death and neuroinflammation that contribute to dysfunctions and neuropathology of AD and TBI (Figure 1.0). This dissertation addresses the scientific question of whether the inhibition of cytosolic cathepsin B can mitigate neurodegeneration and neuroinflammation, thereby preventing the motor deficits associated with TBI—a recognized risk factor for AD. The applicability of this dissertation extends to scenarios where cathepsin B play a role in pathology of various neurological diseases.

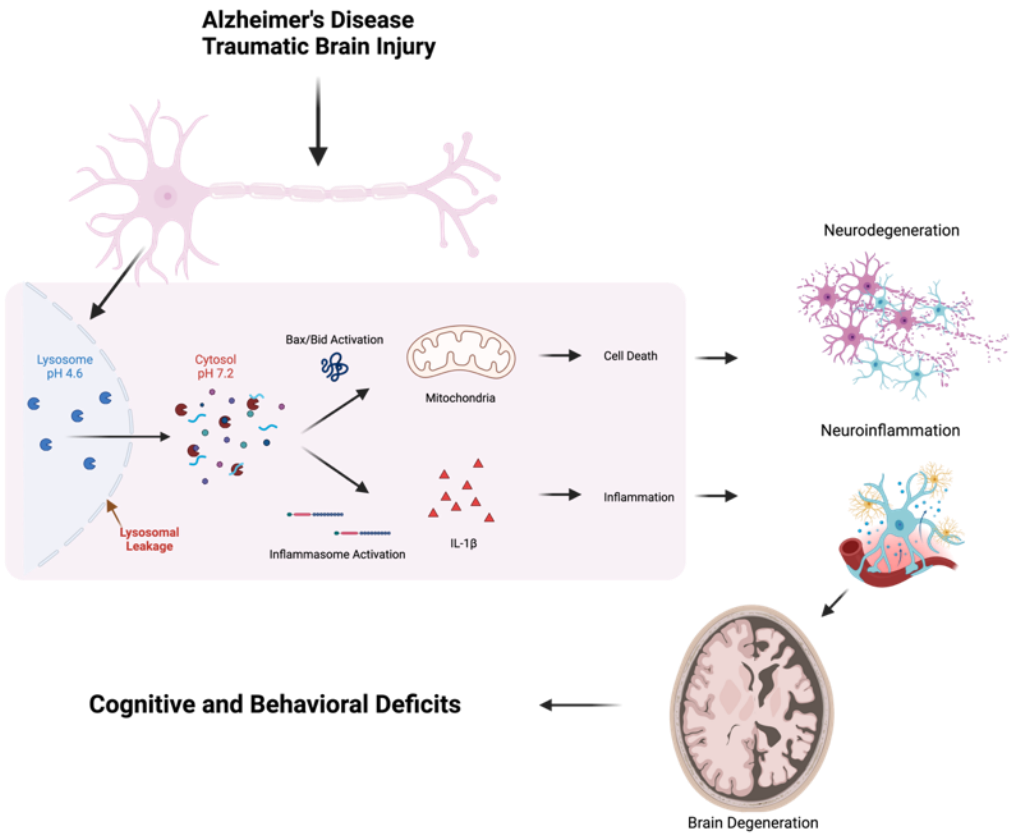

Figure 1.1 Lysosomal leakage in AD and TBI leads to neurodegeneration and neuroinflammation, contributing to observed cognitive and behavioral deficits.

1.2 Evidence for Cathepsin B Participation in AD, TBI, and other Neurologic Disorders

Cathepsin B is a lysosomal protease that is primarily involved in maintaining homeostasis. (8,9) It is a member of the Papain-like family of lysosomal cysteine proteases, containing 11 members that include cathepsins B, C, F, H, K, L, O, S, V, W, and X. Cathepsin B contains a unique feature known as the occluding loop, and uniquely expresses both endopeptidase and dicarboxypeptidase activity. (10) Although cathepsin B is normally found in the lysosome at pH 4.6 (11), it can also be found in the cytosol at pH 7.2 (12), and extracellular locations at pH 5.5 (13). Lysosomal leakage leads to Cathepsin B translocating to the cytosol, activating various responses such as apoptosis, necrosis, ferroptosis, pyroptosis, and lysosome-dependent cell death. (14-16) Additionally, cathepsin B is present in secretory vesicles at pH 5.5, proteolytically

processing and producing peptide neurotransmitters. (13) Significantly, cathepsin B has been implicated in many neurologic diseases. Elevated levels of Cathepsin B are observed in the cortex, serum, cerebrospinal fluid (CSF), and plasma of AD patients, as well as in the brain plasma and monocytes of HIV patients, the spinal cord of ALS patients, and the CSF of both TBI patients and aging individuals. (17,18) Elevated expression or activity of Cathepsin B is also observed in animal models of AD, TBI, trauma, Huntington's disease, hemorrhage, hypoxia/ischemia, brain aneurysm, sepsis, inflammation, amyotrophic lateral sclerosis (ALS), and epilepsy. (18) In animal models, studies have demonstrated that cathepsin B gene knockouts improve pathology by enhancing memory loss and reducing neurotoxic Aβ in AD models, as well as ameliorating neuromotor deficits and brain tissue lesions in TBI models. (19) It is evident that cathepsin B functions across diverse environments and pH conditions and is involved in numerous of biological pathways and disorders. To elucidate the role of extra-lysosomal cathepsin B in TBI and AD, this study seeks to leverage the dynamic properties of cathepsin B across varying pH environments.

1.3 Cathepsin B Displays Specific Cleavage Properties at Cytosolic Neutral pH 7.2 Compared to Lysosomal Acidic pH 4.6

Cathepsin B stands out within the family of human cysteine proteases due to its distinctive features, encompassing both endopeptidase and dicarboxypeptidase activity, along with a unique occluding loop structure. (8-10) It retains its proteolytic activity across varying pH environments that allows it to continue maintaining homeostasis and process peptides. Yet, recent studies reveal that cathepsin B exhibits distinct cleavage properties in various pH environments, specifically distinguishing between lysosomal acidic pH 4.6 and cytosolic neutral pH 7.2 in different subcellular compartments. (14) The study employed Multiplex Substrate Profiling by Mass Spectrometry (MSP-MS) to ascertain the pH-dependent cleavage preferences of cathepsin B at pH 4.6 and 7.2 (20), unveiling distinctive peptide cleavage preferences that are solely pH-dependent.

Utilizing these distinctive preferences, substrates and subsequent inhibitors were developed with pH-dependent characteristics. Notably, Z-Arg-Lys-AOMK emerged as an irreversible, neutral pH-selective inhibitor of cathepsin B. This specificity is attributed to interactions between the P2 Arg of the inhibitor and the Glu245 residue on cathepsin B. Given that Glu245 has a pKa of 5.1, it carries a negative charge at neutral pH 7.2, facilitating favorable interactions with the positively charged P2 Arg on the inhibitor. (14) The inhibitor underwent assays against other cathepsins within the cysteine protease family and was incubated with SHSY-5Y human neuroblastoma cells; it exhibited specific inhibitory properties against cathepsin B and demonstrated cell-permeable characteristics.

The development of Z-Arg-Lys-AOMK established a neutral pH-selective and cathepsin B specific inhibitor that will be utilized in this study to elucidate the role of cathepsin B in varying pH environments on biological pathways related to cell death and inflammation, and ultimately for drug discovery efforts in models of TBI, a risk factor for AD. While the neutral pH-selective inhibitor showed success, the acid pH-selective inhibitor did not fare as well and an acid pH-selective inhibitor is necessary to distinguish cathepsin B activity in varying pH environments. Consequently, we propose the characterization of an acid pH-selective inhibitor, drawing inspiration from known inhibitor, CA-074, and incorporating current knowledge of pH-selective cleavage events into novel inhibitor screening, as elaborated in the following section.

1.4 Strategy for Characterizing neutral pH-selective inhibitors of Cathepsin B

Given the evidence suggesting distinct substrates and inhibitors for cathepsin B at different pH levels, exemplified by the success of the neutral pH-selective Z-Arg-Lys-AOMK, our studies involve the search for acid pH-selective inhibitors. These would enable selective inhibition in either neutral or acidic pH environments, corresponding to cytosolic or lysosomal conditions. Our exploration began with an investigation into the canonical cathepsin B-specific inhibitor, CA-074.

CA-074 (N-(L-3-trans-propylcarbamoyloxirane-2-carbonyl)-L-isoleucyl-L-proline) is an epoxysuccinyl peptide inhibitor (21,22), originally derived from E-64 (L-trans-epoxysuccinyl-leucylamido(4-guanidino)butane), a natural product isolated from *Aspergillus japonicus* (23 Specifically designed for potent and selective inhibition of cathepsin B over other cysteine cathepsins, CA-074 is widely employed in the field for this purpose. Its methyl ester form, CA-074Me, is also commonly utilized in cell and animal studies as a cell-permeable inhibitor, undergoing conversion to CA-074 by intracellular esterases. (24)

Despite its extensive use, the inhibition profile of CA-074 has not been characterized for the pH-dependent inhibition of cathepsin B. Therefore, this study aimed to assess the inhibition profile of cathepsin B by CA-074 and CA-074Me across a range of acidic and neutral pH values (Chapter 2). The investigation encompasses inhibitor potency, kinetic evaluation, molecular properties, and protease specificity of CA-074 inhibition at pH 4.6, 5.5, and 7.2. The findings indicate that CA-074 is 120-fold more potent at pH 4.6 compared to pH 7.2 for inhibiting cathepsin B, establishing it as an acid-pH selective inhibitor.

In addition, this study also employed a pH-dependent screening effort to identify pH-selective modulators of cathepsin B activity from a library of pure marine natural products (Chapter 3). The difference in the acidic pH (4.6) of lysosomes compared to the neutral pH (7.2) of the cytosol suggests that screening at different pH conditions may identify pH-selective modulators of cathepsin B. A diverse collection of pure marine and plant natural product (NP) compounds, along with synthetic compounds, underwent screening at pH 4.6 and pH 7.2 in cathepsin B assays. This led to the discovery of GER-12 (Crossbyanol B) and GER-24 ((7Z,9Z,12Z)-octadeca-7,9,12-trien-5-ynoic acid) marine NP inhibitors exhibiting activity at acidic pH but not at neutral pH. While these inhibitors are less potent compared to previously

characterized Z-Arg-Lys-AOMK and CA-074 at pH 7.2 and 4.6 respectively, the results underscore that screening natural products at distinct biological pH conditions can identify pH-selective cathepsin B modulators.

Following the characterization of an acid pH-selective inhibitor, CA-074, and the existence of a neutral pH-selective inhibitor, Z-Arg-Lys-AOMK, our objective was to formulate and create a fluorescent substrate capable of measuring cathepsin B activity across a wide pH range. This substrate aims to surpass the capabilities of current substrates employed for cathepsin B, as detailed in the subsequent section.

1.5 Strategy for Development of a Novel Fluorescent Substrate that Monitors Cathepsin B Specific Activity over a Broad pH Range

This study aimed to address the lack of substrates that specifically monitor cathepsin B activity across a broad pH range without interference from other cysteine cathepsins (Chapter 4). Current substrates, such as Z-Phe-Arg-AMC, used for cathepsin B assays, also detect cathepsin L and other proteases. (25) Although Z-Arg-Arg-AMC is specific for cathepsin B, it predominantly monitors neutral pH activity, neglecting acidic activity. (25) The strategy involved designing selective peptide-AMC substrates based on cathepsin B's pH-dependent cleavage properties at both acidic (pH 4.6) and neutral (pH 7.2) conditions. Using MSP-MS (20), the unique cleavage properties of cathepsin B were compared with other cysteine cathepsins. The novel substrate Z-Nle-Lys-Arg-AMC was identified, demonstrating high specific activity for cathepsin B across a broad pH range, while remaining specific to cathepsin B over other cathepsins. Kinetic studies revealed its greater efficiency compared to the currently used substrate, Z-Arg-Arg-AMC. Importantly, Z-Nle-Lys-Arg-AMC specifically measured cathepsin B activity in neuronal and glial cells, showcasing its potential for assessing cathepsin B activity under in cell studies at physiological pH conditions. Overall, this novel substrate offers significant advantages in

monitoring specific cathepsin B activity across a wide pH range, making it valuable for physiological assessments. To analyze the impact of extra-lysosomal cathepsin B on cell death and inflammation, this study utilizes the neutral pH-selective inhibitor Z-Arg-Lys-AOMK, the acid pH-selective inhibitor CA-074 (Chapter 2), and the broad pH-active fluorescent substrate Z-Nle-Lys-Arg-AMC (Chapter 4). These tools are applied to dissect the role of cytosolic cathepsin B in mouse microglia BV2 (Chapter 5) and in mouse models of TBI, a recognized risk factor for AD (Chapter 6), discussed in the following section.

1.6 Evaluation of Cytosolic Cathepsin B with neutral pH-selective inhibitor in Mouse Microglia Cells and Cell Stress

Cathepsin B contributes significantly to cellular homeostasis through protein degradation. Its involvement in various normal biological processes and diseases, including AD and TBI, is well-established. Under neurologic conditions, Cathepsin B translocate from the lysosome to the cytosol, where it retains its proteolytic activity, leading to cell death and inflammation. (10, 15-16) Targeting Cathepsin B has emerged as a therapeutic strategy, with studies showing improved outcomes in AD and TBI mouse models upon its inhibition. (18-19) However, existing inhibitors lack specificity for cytosolic Cathepsin B. To address this, a pH-selective inhibitor, Z-R-K-AOMK, was developed to target cytosolic Cathepsin B while sparing lysosomal Cathepsin B. (14)

Nutrient stress, resulting from limited access to nutrients and glucose, is a common stress factor in various disorders, particularly evident in neurodegenerative conditions where nutrient sources may be constrained due to brain degeneration or other factors. Nutrient stress in TBI arises from the physical inaccessibility of nutrients to neuronal cells, coupled with metabolic disorders such as reduced glucose metabolism. (26) Furthermore, the restricted availability of energy resources in the brain is hypothesized to play a crucial role in the pathogenesis of AD, with AD patients exhibiting evident deficiencies in energy metabolism. (27-30) Additionally, nutrient stress

induces lysosomal membrane permeabilization, causing Cathepsin B leakage into the cytosol, exacerbating pathological processes. (31) These studies employ nutrient deprivation as a relevant stressor for AD and TBI to investigate the role of cathepsin B in cell death and neurodegeneration. Mouse microglia are cultured with pH-selective inhibitor Z-R-K-AOMK, inhibiting cathepsin B activity in cytosolic compartments within the cell (Chapter 5). The research reveals lysosomal leakage during stress, and the associated cell death is mediated by the inhibition of cathepsin B activity with Z-R-K-AOMK.

1.7 Treatment of Traumatic Brain Injury in Mice with Z-Arg-Lys-AOMK Inhibitor of Cathepsin B at Neutral pH

As previously discusses, cathepsin B gene knockouts have shown improvement in pathology, alleviating neuromotor deficits and brain tissue lesions in TBI models. (17,18) In this section, the impact of cytosolic cathepsin B on neuromotor deficits in a mouse controlled cortical impact (CCI) model of TBI (32) was investigated using the novel neutral pH-selective inhibitor Z-Arg-Lys-AOMK (14) (Chapter 6). The inhibitor's efficacy was tested at different doses, and the most effective dose was used in subsequent TBI animal studies. Following CCI injury, the inhibitor was administered daily for five days, and motor function was assessed using the rotarod assay. Cathepsin B activity in cortex and hippocampus brain regions was measured at various time points. Synaptosomes from CCI-TBI and control sham mice was used to assess neuropeptidome signatures, comparing results to control brains. (13) Cathepsin B activity was assessed in sub-cellular compartments. The data suggests that CCI-TBI induces lysosomal leakage and translocation of cathepsin B activity, which is inhibited by treatment with the cathepsin B inhibitor, Z-Arg-Lys-AOMK. Treatment with Z-Arg-Lys-AOMK also mediates neuromotor dysfunction, where mice treated with the inhibitor show significant improvement in neuromotor dysfunction, quantified by latency to falls in rotarod assay.

1.8 Exploring Cathepsin B: A Molecular Investigation into its Role in Neurodegeneration, Neuroinflammation, and the Impact on Alzheimer's Disease and Traumatic Brain Injury

In summary, AD is a prevalent neurodegenerative disorder, and TBI is a significant risk factor for AD. This dissertation explores the molecular mechanisms involving cathepsin B in neurodegeneration and neuroinflammation, focusing on its role in TBI, a recognized risk for AD. The study introduces the development of pH-selective inhibitors, Z-Arg-Lys-AOMK and CA-074 (Chapters 1 and 2), and a novel substrate, Z-Nle-Lys-Arg-AMC (Chapter 4), to monitor cathepsin B activity across varying pH environments. The investigation encompasses the effects of extra-lysosomal cathepsin B on cell death and inflammation using these tools in mouse microglia BV2 (Chapter 5) and TBI mouse models (Chapter 6). Moreover, the dissertation examines the impact of cytosolic cathepsin B on neuromotor deficits in a CCI model of TBI, revealing that Z-Arg-Lys-AOMK treatment mitigates neuromotor dysfunction. The research underscores the critical role of cathepsin B in the pathogenesis of AD and TBI, providing insights into potential drug targets for future therapeutic interventions in neurological disorders.

1.9 References

1. 2021 Alzheimer's disease facts and figures. Alzheimer's and Dementia. 2021 Mar 1;17(3):327–406.

2. Aisen PS, Cummings J, Jack CR Jr, Morris JC, Sperling R, Frölich L, Jones RW, Dowsett SA, Matthews BR, Raskin J, Scheltens P, Dubois B. On the path to 2025: understanding the Alzheimer's disease continuum. Alzheimers Res Ther. 2017 Aug 9;9(1):60. PMCID: PMC5549378.

3. Kirova AM, Bays RB, Lagalwar S. Working memory and executive function decline across normal aging, mild cognitive impairment, and Alzheimer's disease. Biomed Res Int. 2015;2015:748212. PMCID: PMC4624908.

4. Wang C, Xu T, Yu W, Li T, Han H, Zhang M, Tao M. Early diagnosis of Alzheimer's disease and mild cognitive impairment based on electroencephalography: From the perspective of event related potentials and deep learning. Int J Psychophysiol. 2022 Oct 26:S0167-8760(22)00247-1. PMID: 36309183.

5. Sivanandam TM, Thakur MK. Traumatic brain injury: a risk factor for Alzheimer's disease. Neurosci Biobehav Rev. 2012 May;36(5):1376-81. PMID: 22390915.

6. Djordjevic J, Sabbir MG, Albensi BC. Traumatic Brain Injury as a Risk Factor for Alzheimer's Disease: Is Inflammatory Signaling a Key Player? Curr Alzheimer Res. 2016;13(7):730-8. PMID: 26899581.

7. Centers for Disease Control and Prevention. (2014). Report to Congress on Traumatic Brain Injury in the United States: Epidemiology and Rehabilitation. National Center for Injury Prevention and Control; Division of Unintentional Injury Prevention. Atlanta, GA.

8. Turk V, Stoka V, Vasiljeva O, Renko M, Sun T, Turk B, et al. Cysteine cathepsins: From structure, function and regulation to new frontiers. Biochimica et Biophysica Acta - Proteins and Proteomics. 2012;1824(1):68–88.

9. Turk B, Turk D, Turk V. Lysosomal cysteine proteases: more than scavengers. Biochim Biophys Acta. 2000 Mar 7;1477(1-2):98-111.

10. Yoon MC, Hook V, O'Donoghue AJ. Cathepsin B Dipeptidyl Carboxypeptidase and Endopeptidase Activities Demonstrated across a Broad pH Range. Biochemistry. 2022 Sep 6;61(17):1904-1914. doi: 10.1021/acs.biochem.2c00358. Epub 2022 Aug 18. PMID: 35981509; PMCID: PMC9454093.

11. Mindell JA. Lysosomal acidification mechanisms. Annu Rev Physiol. 2012;74:69-86. doi: 10.1146/annurev-physiol-012110-142317. PMID: 22335796.

12. Madshus IH. Regulation of intracellular pH in eukaryotic cells. Biochem J. 1988 Feb 15;250(1):1-8. doi: 10.1042/bj2500001. PMID: 2965576; PMCID: PMC1148806.

13. Jiang Z, Lietz CB, Podvin S, Yoon MC, Toneff T, Hook V, O'Donoghue AJ. Differential Neuropeptidomes of Dense Core Secretory Vesicles (DCSV) Produced at Intravesicular and Extracellular pH Conditions by Proteolytic Processing. ACS Chem Neurosci. 2021 Jul 7;12(13):2385-2398. doi: 10.1021/acschemneuro.1c00133. Epub 2021 Jun 21. PMID: 34153188; PMCID: PMC8267839.

14. Yoon MC, Solania A, Jiang Z, Christy MP, Podvin S, Mosier C, Lietz CB, Ito G, Gerwick WH, Wolan DW, Hook G, O'Donoghue AJ, Hook V. Selective Neutral pH Inhibitor of Cathepsin B Designed Based on Cleavage Preferences at Cytosolic and Lysosomal pH Conditions. ACS Chem Biol. 2021 Sep 17;16(9):1628-1643. doi: 10.1021/acschembio.1c00138. Epub 2021 Aug 20. PMID: 34416110; PMCID: PMC9104225.

15. de Castro MA, Bunt G, Wouters FS. Cathepsin B launches an apoptotic exit effort upon cell death-associated disruption of lysosomes. Cell Death Discov. 2016 Feb 29;2:16012. doi: 10.1038/cddiscovery.2016.12. PMID: 27551506; PMCID: PMC4979493.

16. Wang F, Gómez-Sintes R, Boya P. Lysosomal membrane permeabilization and cell death. Traffic. 2018 Dec;19(12):918-931. doi: 10.1111/tra.12613. Epub 2018 Sep 12. PMID: 30125440.

17. Hook V, Yoon M, Mosier C, Ito G, Podvin S, Head BP, Rissman R, O'Donoghue AJ, Hook G. Cathepsin B in neurodegeneration of Alzheimer's disease, traumatic brain injury, and related brain disorders. Biochim Biophys Acta Proteins Proteom. 2020 Aug;1868(8):140428. doi: 10.1016/j.bbapap.2020.140428. Epub 2020 Apr 17. PMID: 32305689; PMCID: PMC7261628.

18. Hook G, Reinheckel T, Ni J, Wu Z, Kindy M, Peters C, Hook V. Cathepsin B Gene Knockout Improves Behavioral Deficits and Reduces Pathology in Models of Neurologic Disorders. Pharmacol Rev. 2022 Jul;74(3):600-629. doi: 10.1124/pharmrev.121.000527. PMID: 35710131; PMCID: PMC9553114.

19. Kindy MS, Yu J, Zhu H, El-Amouri SS, Hook V, Hook GR. Deletion of the cathepsin B gene improves memory deficits in a transgenic Alzheimer's disease mouse model expressing APP containing the wild-type -secretase site sequence. J Alzheimers Dis. 2012;29(4):827-40. PMCID: PMC4309289

20. O'Donoghue AJ, Eroy-Reveles AA, Knudsen GM, Ingram J, Zhou M, Statnekov JB, Greninger AL, Hostetter DR, Qu G, Maltby DA, Anderson MO, Derisi JL, McKerrow JH, Burlingame AL, Craik CS. Global identification of peptidase specificity by multiplex substrate profiling. Nat Methods. 2012 Nov;9(11):1095-100. doi: 10.1038/nmeth.2182. Epub 2012 Sep 30. PMID: 23023596; PMCID: PMC3707110.

21. Towatari T, Nikawa T, Murata M, Yokoo C, Tamai M, Hanada K, Katunuma N. Novel epoxysuccinyl peptides. A selective inhibitor of cathepsin B, in vivo. FEBS Lett. 1991 Mar 25;280(2):311-5. doi: 10.1016/0014-5793(91)80319-x. PMID: 2013329.

22. Montaser M, Lalmanach G, Mach L. CA-074, but not its methyl ester CA-074Me, is a selective inhibitor of cathepsin B within living cells. Biol Chem. 2002 Jul-Aug;383(7-8):1305-8. doi: 10.1515/BC.2002.147. PMID: 12437121.

23. Barrett AJ, Kembhavi AA, Brown MA, Kirschke H, Knight CG, Tamai M, Hanada K. L-trans-Epoxysuccinyl-leucylamido(4-guanidino)butane (E-64) and its analogues as inhibitors of cysteine proteinases including cathepsins B, H and L. Biochem J. 1982 Jan 1;201(1):189-98. doi: 10.1042/bj2010189. PMID: 7044372; PMCID: PMC1163625.

24. Buttle DJ, Murata M, Knight CG, Barrett AJ. CA074 methyl ester: a proinhibitor for intracellular cathepsin B. Arch Biochem Biophys. 1992 Dec;299(2):377-80. doi: 10.1016/0003-9861(92)90290-d. PMID: 1444478.

25. Poreba M, Groborz K, Vizovisek M, Maruggi M, Turk D, Turk B, Powis G, Drag M, Salvesen GS. Fluorescent probes towards selective cathepsin B detection and visualization in cancer cells and patient samples. Chem Sci. 2019 Jul 31;10(36):8461-8477. doi: 10.1039/c9sc00997c. PMID: 31803426; PMCID: PMC6839509.

26. Lai JQ, Shi YC, Lin S, Chen XR. Metabolic disorders on cognitive dysfunction after traumatic brain injury. Trends Endocrinol Metab. 2022 Jul;33(7):451-462. doi: 10.1016/j.tem.2022.04.003. Epub 2022 May 7. PMID: 35534336.

27. Blonz ER. Alzheimer's Disease as the Product of a Progressive Energy Deficiency Syndrome in the Central Nervous System: The Neuroenergetic Hypothesis. J Alzheimers Dis. 2017;60(4):1223-1229. doi: 10.3233/JAD-170549. PMID: 28946565; PMCID: PMC5676979.

28. Yao J, Irwin RW, Zhao L, Nilsen J, Hamilton RT, Brinton RD. Mitochondrial bioenergetic deficit precedes Alzheimer's pathology in female mouse model of Alzheimer's disease. Proc Natl Acad Sci U S A. 2009 Aug 25;106(34):14670-5. doi: 10.1073/pnas.0903563106. Epub 2009 Aug 10. PMID: 19667196; PMCID: PMC2732886.

29. Gupta S, Kass GE, Szegezdi E, Joseph B. The mitochondrial death pathway: a promising therapeutic target in diseases. J Cell Mol Med. 2009 Jun;13(6):1004-33. doi: 10.1111/j.1582-4934.2009.00697.x. Epub 2009 Feb 9. PMID: 19220575; PMCID: PMC4496101.

30. Kalkavan H, Green DR. MOMP, cell suicide as a BCL-2 family business. Cell Death Differ. 2018 Jan;25(1):46-55. doi: 10.1038/cdd.2017.179. Epub 2017 Oct 20. PMID: 29053143; PMCID: PMC5729535.

31. Gerónimo-Olvera C, Montiel T, Rincon-Heredia R, Castro-Obregón S, Massieu L. Autophagy fails to prevent glucose deprivation/glucose reintroduction-induced neuronal death due to calpain-mediated lysosomal dysfunction in cortical neurons. Cell Death Dis. 2017 Jun 29;8(6):e2911. doi: 10.1038/cddis.2017.299. PMID: 28661473; PMCID: PMC5520945.

32. Onyszchuk G, Al-Hafez B, He YY, Bilgen M, Berman NE, Brooks WM. A mouse model of sensorimotor controlled cortical impact: characterization using longitudinal magnetic resonance imaging, behavioral assessments and histology. J Neurosci Methods. 2007 Mar 15;160(2):187-96. doi: 10.1016/j.jneumeth.2006.09.007. Epub 2006 Oct 16. PMID: 17049995; PMCID: PMC1941707.

Chapter 2 Molecular Features of CA-074 pH-Dependent Inhibition of Cathepsin B

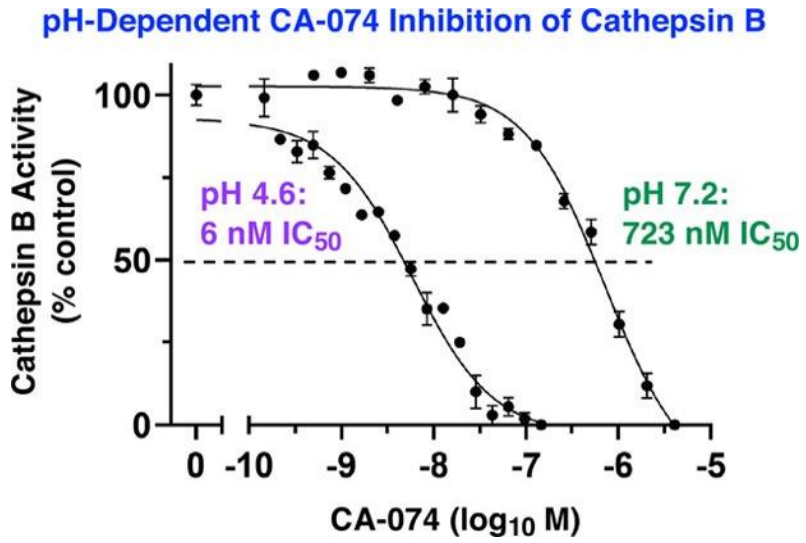

Figure 2.1 Chapter 2 Graphical Abstract. CA-074 is a selective inhibitor of cathepsin B, a lysosomal cysteine protease. CA-074 has been utilized in numerous studies to demonstrate the role of this protease in cellular and physiological functions. Cathepsin B in numerous human disease mechanisms involves its translocation from acidic lysosomes of pH 4.6 to neutral pH 7.2 of cellular locations, including the cytosol and extracellular environment. To gain in-depth knowledge of CA-074 inhibition under these different pH conditions, this study evaluated the molecular features, potency, and selectivity of CA-074 for cathepsin B inhibition under acidic and neutral pH conditions. This study demonstrated that CA-074 is most effective at inhibiting cathepsin B at an acidic pH of 4.6 with nM potency, which was more than 100-fold more potent than its inhibition at a neutral pH of 7.2. The pH-dependent inhibition of CA-074 was abolished by methylation of its C-terminal proline, indicating the requirement for the free C-terminal carboxyl group for pH-dependent inhibition. Under these acidic and neutral pH conditions, CA-074 maintained its specificity for cathepsin B over other cysteine cathepsins, displayed irreversible inhibition, and inhibited diverse cleavages of peptide substrates of cathepsin B assessed by profiling mass spectrometry. Molecular docking suggested that pH-dependent ionic interactions of the C-terminal carboxylate of CA-074 occur with His110 and His111 residues in the S2′ subsite of the enzyme at pH 4.6, but these interactions differ at pH 7.2. While high levels of CA-074 or CA-074Me (converted by cellular esterases to CA-074) are used in biological studies to inhibit cathepsin B at both acidic and neutral pH locations, it is possible that adjusted levels of CA-074 or CA-074Me may be explored to differentially affect cathepsin B activity at these different pH values. Overall, the results of this study demonstrate the molecular, kinetic, and protease specificity features of CA-074 pH-dependent inhibition of cathepsin B.

2.1 Introduction

Cathepsin B is a lysosomal cysteine protease that participates in protein degradation for cellular protein homeostasis. (1−3) Significantly, cathepsin B generates biologically active protein fragments that regulate functions in numerous human diseases, including neurological disorders such as Alzheimer's disease (AD) and traumatic brain injury (TBI), (3−8) ischemia, (9) cancer, (10−12) autoinflammatory disease conditions, such as rheumatoid arthritis, (13−15) atherosclerosis, (16,17) and others. (18,19) The use of the selective cathepsin B inhibitor, CA-074, has facilitated studies of cathepsin B inhibition that ameliorates dysfunctional phenotypes in cell and animal models of human disease conditions. (3) For example, CA-074 improves memory deficits and neuropathology in an AD mouse model, (6) and CA-074 reduces the severity of ischemia and provides neuroprotection. (9) These animal studies administered the proinhibitor CA-074Me that is converted by esterases in vivo to the potent CA-074 inhibitor. (6,9)

CA-074 is an epoxysuccinyl peptide known as N-(l-3-trans-propylcarbamoyloxirane-2-carbonyl)-l-isoleucyl-l-proline that was designed as a derivative of E-64 (l-trans-epoxysuccinyl-leucylamido(4-guanidino)butane, (20,21) a natural product molecule originally isolated from Aspergillus japonicus. (22) CA-074 has been reported to potently inhibit cathepsin B with nanomolar potency (20,21) and selectivity for inhibition of cathepsin B compared to the related cysteine cathepsins L, H, and S. (20−22) These inhibitory properties of CA-074 used purified rat cathepsin B activity monitored at pH 5.5 with the fluorogenic substrate Z-Arg-Arg-AMC. (21)

While cathepsin B normally functions at a lysosomal pH of 4.6, (23,24) evidence shows that in numerous human disease conditions, lysosomal leakage results in movement of cathepsin B to the cytosol of neutral pH 7.2. (25,26) Cathepsin B in the cytosol is proteolytically active and initiates inflammation and cell death in numerous neurological disorders. (3) Cell death lysis results in extracellular cathepsin B that causes damage through proteolysis at neutral pH. (27,28)

Cathepsin B also translocates to the nucleus of neutral pH (29) where it results in telomere-related chromosome segregation defects (30) and degradation of sirtuins that promote aging. (31) Furthermore, cathepsin B functions in secretory vesicles at a moderately acidic pH of 5.5 for production of peptide neurotransmitters. (32) These results indicate that cathepsin B functions under neutral pH conditions which differs from its function in acidic lysosomes.

To gain more in-depth knowledge of CA-074 inhibition of cathepsin B under neutral pH conditions compared to acidic pH conditions, this study examined the potency, molecular properties, and protease specificity of CA-074 inhibition at pH 4.6, 5.5, and 7.2. At pH 4.6, CA-074 was 7-fold and 120-fold more potent than that at pH 5.5 and pH 7.2, respectively, for inhibiting cathepsin B. CA-074 retained specificity for inhibition of cathepsin B compared to other cysteine cathepsin family members under the acidic and neutral pH conditions. Notably, the methylated form of CA-074, CA-074Me, (33) did not display pH-dependent inhibition and was much less potent than CA-074. These findings reveal the pH-dependent inhibitory properties of CA-074 for specific inhibition of cathepsin B.

2.2 Results

2.2.1 CA-074 Displays Preference for Inhibition of Cathepsin B at the Acidic pH of Lysosomes Compared to Neutral pH of the Cytosol

We assessed cathepsin B activity under acidic to neutral pH conditions using the fluorogenic substrate, Z-Phe-Arg-7-amino-4-methylcoumarin (Z-Phe-Arg-AMC). Z-Phe-Arg-AMC monitors cathepsin B activity from acidic to neutral pH conditions (Figure 2.2). Data show that robust cathepsin B activity occurs between pH 4.6 and pH 7.2 (Figure 2.2). These results showed that cathepsin B is active at pH 4.6 of acidic lysosomes, (23,24) pH 5.5 of mildly acidic secretory vesicles, (29) and neutral pH 7.2 of cytosol, (25,26) nuclei, (29) and extracellular locations. (29) Thus, cathepsin B is active over a wide pH range that correlated with the environment of multiple subcellular and extracellular locations.

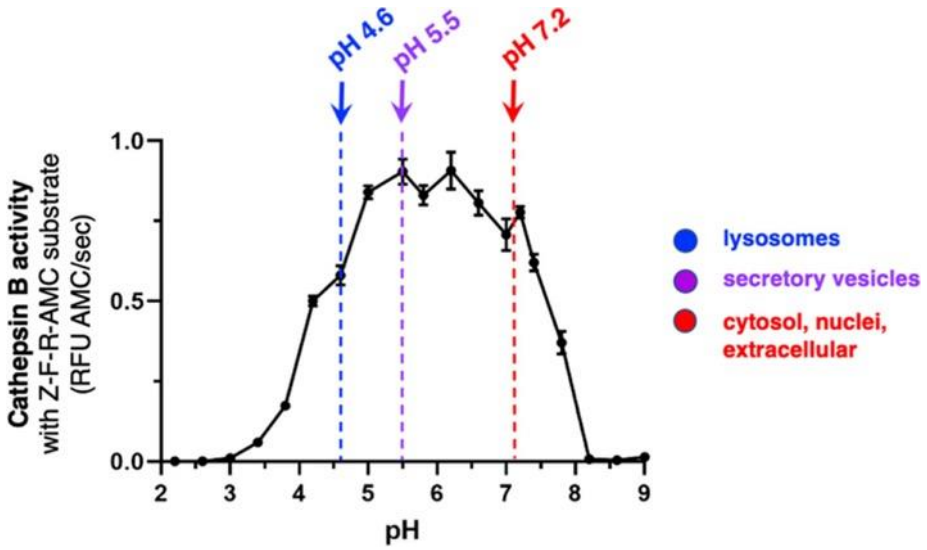

Figure 2.2 Cathepsin B activity under acidic to neutral pH conditions representing the varying pH environments of cellular organelles from lysosomes to cytosol and extracellular locations. Cathepsin B activity was monitored at pH 2.2 to pH 9.0 in increments of 0.4 pH units with addition of pH 7.2. The substrate Z-Phe-Arg-AMC (Z-F-R-AMC) was utilized in the cathepsin B assays. The biological pH conditions of lysosomes at pH 4.6, (23,24) secretory vesicles at pH 5.5, (29,32) and neutral cellular compartments of the cytosol, nuclei, and extracellular locations (28−30) are indicated.

2.2.2 CA-074 Potently Inhibits Cathepsin B at Acidic pH, Corresponding to its Normal Location in Lysosomes

The potency of CA-074 inhibition of cathepsin B was assessed at pH 4.6, 5.5, and 7.2 (Figure 2.3a). At a lysosomal pH of 4.6, CA-074 was an effective inhibitor with an IC_{50} value of 6 nM (IC_{50}, concentration of inhibitor for 50% inhibition), but at neutral pH 7.2 it was 120-fold less potent with an IC_{50} value of 723 nM (Figure 2.3a.ii). Inhibition at pH 5.5 was also assessed because cathepsin B is present in secretory vesicles. (32) The pH of 5.5 was used in the original studies of CA-074 (21) and is also the pH condition that is routinely used in the field. (34,35) At pH 5.5, CA-074 inhibited cathepsin B with an IC_{50} value of 44 nM (Figure 2.3a.ii). These data show that CA-074 at pH 4.6 is 7-fold and 120-fold more potent than that at pH 5.5 and pH 7.2, respectively, demonstrating the pH-dependent properties of CA-074 for cathepsin B inhibition.

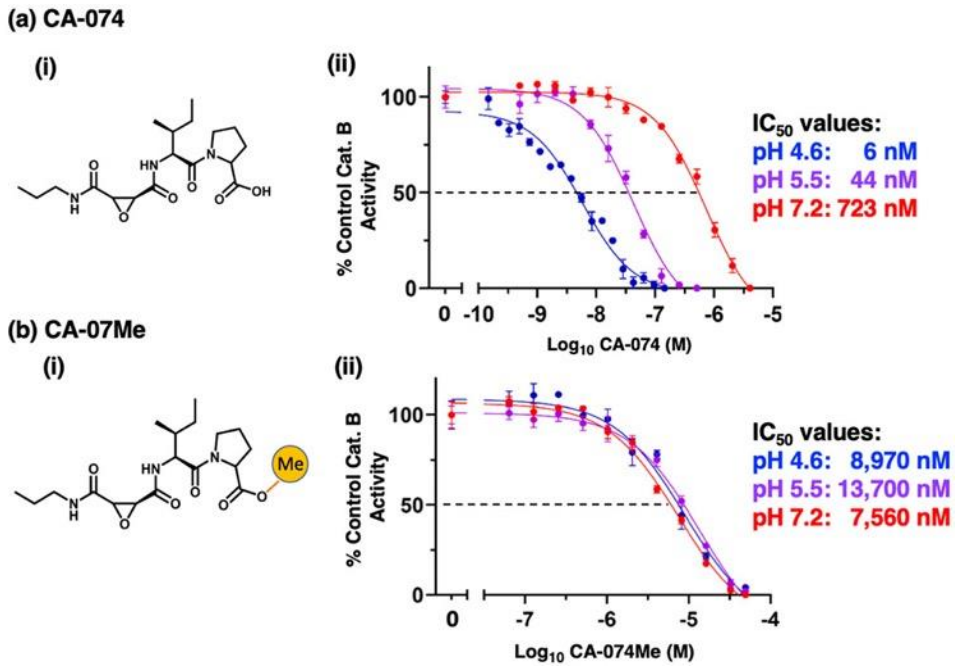

Figure 2.3 CA-074 pH-dependent inhibition of cathepsin B under acidic to neutral pH conditions requires unmodified C-terminal proline. (a) Effective pH-dependent CA-074 inhibition of cathepsin B at pH 4.6, 5.5, and 7.2. (i) CA-074 structure. The chemical structure of CA-074 [N-3-trans-propylcarbamoyl-exirane-2-carbonyl)-l-isoleucyl-l-proline] is illustrated. CA-074 is an epoxysuccinyl inhibitor of cathepsin B. (20,21) (ii) Potent, pH-dependent CA-074 inhibition of cathepsin B under acidic to neutral pH conditions. Potencies of CA-074 inhibition of cathepsin B were assessed at pH 4.6, pH 5.5, and pH 7.2 over a range of concentrations of CA-074. Inhibitory potencies were assessed by IC_{50} values, representing inhibitor concentrations that reduced cathepsin B activity by 50%. (b) Poor CA-074Me inhibition of cathepsin B at pH 4.6, 5.5, and 7.2. (i) CA-074Me structure. The chemical structure of CA-074Me is illustrated, showing methylation of the carboxylate group of the C-terminal proline of CA-074. (33) (ii) Poor CA-074Me inhibition of cathepsin B under acidic to neutral pH conditions. Potencies of CA-074 inhibition of cathepsin B were assessed at pH 4.6, pH 5.5, and pH 7.2 over a range of concentrations of CA-074Me. Inhibitory potencies were evaluated by IC_{50} values, representing inhibitor concentrations that reduced cathepsin B by 50%.

2.2.3 Methylation of CA-074 Abolishes Its pH-dependent Inhibition and Reduces Potency

Importantly, methylation of the C-terminal proline of CA-074, generating CA-074Me, resulted in no pH-dependent inhibition of cathepsin B (Figure 2.3b). These data indicate that the nonmethylated C-terminal carboxylate of the proline residue of CA-074 is necessary for its potency and pH-dependent inhibition. Compared to CA-074, CA-074Me was a weak inhibitor of cathepsin B under acidic and neutral pH conditions, shown by its high IC_{50} values of 8.9, 13.7, and

7.6 μM at pH 4.6, 5.5, and 7.2, respectively (Figure 2.3b.ii). Thus, CA-074Me was less potent than CA-074 by 1495-fold, 311-fold, and 10-fold at pH 4.6, pH 5.5, and pH 7.2, respectively.

2.2.4 Irreversible Mechanism of CA-074 Inhibition under Acidic and Neutral pH Conditions

CA-074 has been proposed as an irreversible inhibitor based on structural binding analyses of the inhibitor to the cathepsin B protein structure. (36,37) However, direct evaluation of the irreversible nature of CA-074 inhibition has not yet been assessed. Therefore, the irreversible or reversible nature of protease inhibitors was assessed for CA-074. CA-074 was incubated with cathepsin B for 30 min at pH 4.6, pH 5.5, and pH 7.2 at 10 times the IC_{50} concentrations and then diluted 100-fold followed by addition of the Z-F-R-AMC substrate (Figure 2.4). The lack of cathepsin B activity after dilution demonstrates the irreversible inhibitory mechanism of CA-074 under all three pH conditions. As a control, cathepsin B was preincubated without an inhibitor and displayed a linear formation of products in the assay (Figure 2.4). These data show that inhibition of cathepsin B with CA-074 is irreversible under acidic and neutral pH conditions.

In addition, CA-074Me also displays irreversible inhibition of cathepsin B at pH 4.6, 5.5, and 7.2 (Figure 2.S1). These results illustrate the irreversible mechanism of the weak inhibitor CA-074Me.

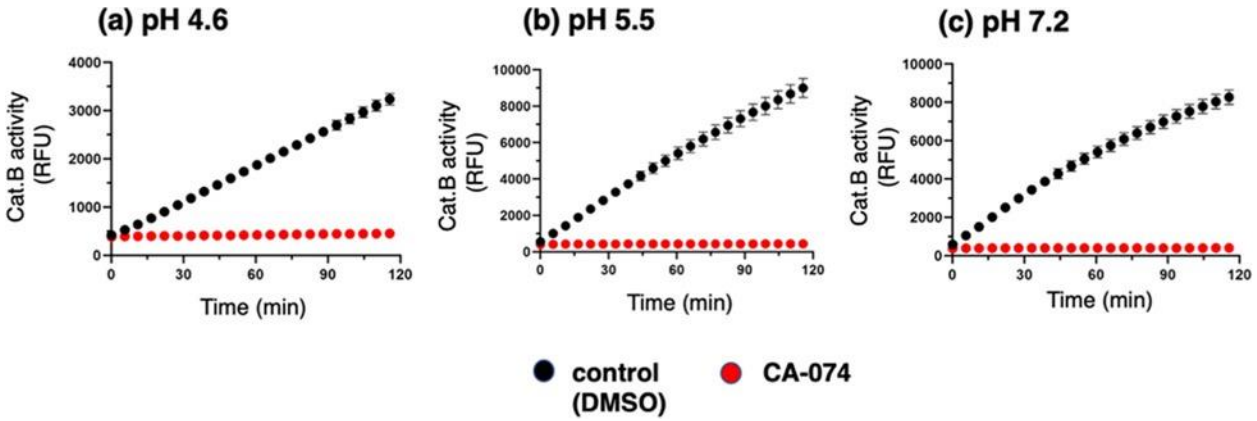

Figure 2.4 Irreversible CA-074 inhibition of cathepsin B at pH 4.6, pH 5.5, and pH 7.2. CA-074 at pH 4.6 (panel a), pH 5.5 (panel b), and pH 7.2 (panel c) was evaluated for irreversible or reversible inhibition of cathepsin B by dilution experiments. Cathepsin B was preincubated with inhibitor at 10 times the IC_{50} concentration (corresponding to 58 nM at pH 4.6, 440 nM at pH 5.5, and 7230 nM at pH 7.2) followed by dilution to 1/10 the IC_{50} concentration, addition of substrate (Z-F-R-AMC), and measurement of activity in time-course assays. Inhibition of cathepsin B following dilution indicates the irreversible inhibitory mechanism of CA-074 under acidic and neutral pH conditions.

2.2.5 Kinetic Evaluation of CA-074 K_I and k_{inact} Values for Inhibition of Cathepsin B at Acidic and Neutral pH Values

Kinetic characterization of CA-074 irreversible inhibition was conducted to assess K_I and k_{inact} values based on plots of inhibitor concentration and k_{obs} values. The k_{obs} values were assessed from plots of cathepsin B activity at different inhibitor concentrations (Figure 2.S2). Data showed that CA-074 was most potent at pH 4.6 with a K_I of 22 nM (Figure 2.5) and was a less effective inhibitor at pH 7.2 with a K_I of 1.98 μM (Figure 2.5). Inhibition at pH 5.5 was observed with a moderate K_I value of 211 nM. These K_I values showed that the potency of inhibition at pH 4.6 was about 10-fold and 90-fold greater compared to that at pH 5.5 and pH 7.2, respectively (Table 2.1). Thus, K_I and IC_{50} values both indicated the greater potency of CA-074 under acidic compared to neutral pH conditions (Table 2.1). Evaluation of k_{inact}/K_I values showed more effective inhibition kinetics at pH 4.6 than that at pH 5.5 or pH 7.2. At pH 4.6, the k_{inact}/K_I value of 4.5×10^5 M^{-1} s^{-1} was 4-fold and 52-fold greater than such values at pH 5.5 or pH 7.2 with values of 1.1×10^5 and

8.6×10^3 M^{-1} s^{-1}, respectively (Table 2.1). These data illustrate the kinetic properties of pH-dependent inhibition by CA-074.

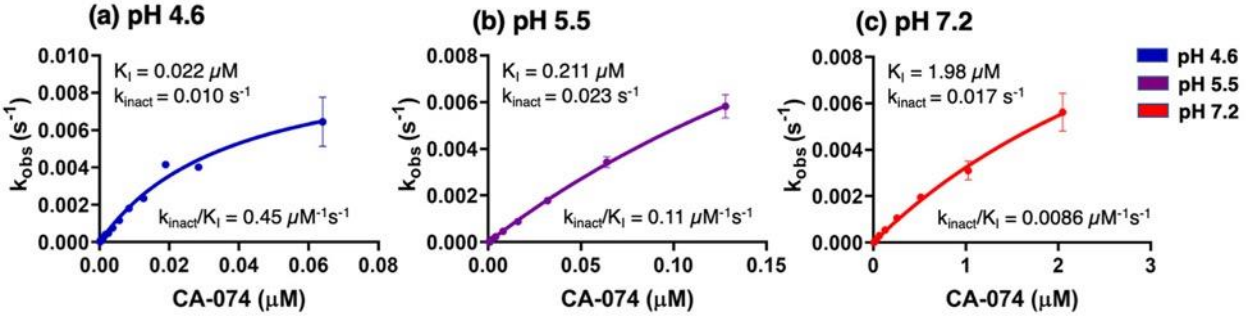

Figure 2.5 Kinetics of CA-074 inhibition of cathepsin B under acidic and neutral pH conditions. Kinetic analyses of CA-074 inhibition of cathepsin B was conducted at pH 4.6 (panel a), pH 5.5 (panel b), and pH 7.2 (panel c) to determine the kinetic values of K_I, k_{inact}, and k_{inact}/K_I, conducted as described in the methods.

Table 2.1 Kinetic Values for CA-074 and CA-074Me Inhibition of Cathepsin B at pH 4.6, pH 5.5, and pH 7.2[a]

kinetic constant	cathepsin B CA-074			cathepsin B CA-074Me		
	pH 4.6	pH 5.5	pH 7.2	pH 4.6	pH 5.5	pH 7.2
IC_{50} (nM)	6	44	723	8970	13,700	7560
K_I (nM)	22	211	1980	52,000	56,000	29,000
k_{inact} (s^{-1})	0.010	0.023	0.017	0.016	0.014	0.014
k_{inact}/K_I (M^{-1} s^{-1})	4.5×10^5	1.1×10^5	8.6×10^3	3.1×10^2	2.5×10^2	4.8×10^2

[a]IC_{50} values were calculated for cathepsin B based on assays with Z-Phe-Arg-AMC substrate in the presence of a range of inhibitor concentrations (from Figure 2.2). The K_I, k_{inact}, and k_{inact}/K_I values were calculated as described in the methods to measure k_{obs} values at different inhibitor concentrations (Figure 2.S2 and Figure 2.S3) for determination of K_I, k_{inact}, and k_{inact}/K_I values shown in this Table. K_I calculation utilized K_m values for Z-Phe-Arg-AMC substrate at pH 4.6, 5.5, and 7.2 (Figure 2.S6).

The kinetic properties of CA-074Me were assessed, indicating its poor inhibition of cathepsin B (Table 2.1 and Figure 2.S3). CA-074Me inhibition of cathepsin B at pH 4.6, pH 5.5,

and pH 7.2 occurred with K_I values of 52, 56, and 29 μM, respectively, which represented lower potencies by 1/2363, 1/265, and 1/15 at these respective pH values compared to CA-074. The k_{inact}/K_I values of CA-074Me also indicated substantially weaker inhibition compared to CA-074 (Table 2.1).

2.2.6 Specificity of CA-074 inhibition of cathepsin B compared to other cysteine cathepsins at acidic and neutral pHs.

Cathepsin B is one among 11 lysosomal cysteine cathepsin proteases consisting of cathepsins B, C, F, H, K, L, O, S, V, W, and X (also known as cathepsin Z). (1,38) While previous studies of CA-074 assessed its selectivity for cathepsin B compared to cathepsins L and H at pH 5.5, (20,21) selectivity for the full spectrum of cysteine cathepsins was not assessed under both acidic and neutral pH conditions. Therefore, we evaluated the selectivity of CA-074 among the cysteine cathepsins at pH 4.6, pH 5.5, and pH 7.2 (Table 2). At pH 4.6, 16 μM CA-074 had no effect on cathepsins C, H, and L; CA-074 at 16 μM displayed minor effects on cathepsins K, S, V, and X of 5–20% inhibition. At pH 5.5, 16 μM CA-074 μM had no effect on these cysteine cathepsins C, H, L, K, V, and X; but cathepsin S was inhibited with an IC_{50} value of 4.8 μM, showing 109-fold less potency than inhibition of cathepsin B. At pH 7.2, CA-074 at 16 μM had no effect on cathepsin C, H, K, and V, and partial inhibition of cathepsin S by 29%; cathepsins L and X were inactive at pH 7.2. These findings illustrate the high specificity of CA-074 for cathepsin B over other cysteine cathepsin enzymes under acidic and neutral pH conditions.

Table 2.2 Specificity of CA-074 and CA-074Me for inhibition of cathepsin B compared to other cysteine cathepsins.[a]

protease	CA-074 IC_{50} (nM) (% inhibition)			CA-074Me IC_{50} (nM) (% inhibition)		
	pH 4.6	pH 5.5	pH 7.2	pH 4.6	pH 5.5	pH 7.2
cathepsin B	6	44	723	8970	13,700	7560
cathepsin C	>16,000	>16,000	>16,000	>16,000	>16,000	>16,000
	0%	0%	0%	5%	0%	4%
cathepsin H	>16,000	>16,000	>16,000	>16,000	>16,000	>16,000
	0%	0%	0%	0%	0%	19%
cathepsin L	>16,000	>16,000	NA	>16,000	>16,000	NA
	0%	0%		0%	0%	
cathepsin K	>16,000	>16,000	>16,000	>16,000	>16,000	>16,000
	8%	0%	0%	0%	0%	16%
cathepsin S	>16,000	4800	>16,000	>16,000	5500	3800
	20%		29%	22%		
cathepsin V	>16,000	>16,000	>16,000	12,000	>16,000	>16,000
	10%	0%	0%	33%	22%	0%
cathepsin X	>16,000	>16,000	NA	>16,000	>16,000	NA
	5%	0%		0%	0%	

[a]Inhibitors were evaluated for protease selectivity among members of the cysteine cathepsin family. The activity of each cathepsin was assessed in the presence of CA-074 or CA-074Me at 0.5 nM to 16 μM (with the exception of 50 μM CA-074Me for cathepsin B). IC_{50} values were determined for CA-074 and CA-074Me for each protease. IC_{50} values are indicated as >16,000 nM when partial inhibition or no inhibition was observed. NA indicates that the enzyme had no activity at the indicated pH.

With respect to CA-074Me, it displayed nearly no inhibition of the cysteine cathepsins assessed at up to 16 μM CA-074Me (Table 2.2). Cathepsin S, however, was inhibited by high concentrations illustrated by the micromolar IC_{50} values of 5.5 μM and 3.8 μM CA-074Me at pH 5.5 and pH 7.2, respectively.

2.2.7 CA-074 inhibition of peptide cleavages of cathepsin B assessed by multiplex substrate profiling by mass spectrometry (MSP-MS).

The inhibitory properties of CA-074 have largely been evaluated with dipeptide-AMC fluorogenic substrates such as Z-Phe-Arg-AMC and Z-Arg-Arg-AMC, (20,21) but the information about CA-074 inhibition of diverse cathepsin B cleavages is needed to characterize the inhibitor effects. To gain knowledge of cathepsin B peptide cleavages that can be inhibited by CA-074 at pH 4.6 and pH 7.2 for broader substrates, we evaluated the ability of CA-074 to inhibit cathepsin B cleavages by a global, unbiased cleavage profiling approach known as MSP-MS. (39,40) The MSP-MS approach uses a substrate library consisting of 228 peptides (14 residues in length) containing 2964 distinct cleavage sites. In the absence and presence of CA-074, cathepsin B cleavage products of the library were identified and quantified by nano-liquid chromatography tandem mass spectrometry (nano-LC–MS/MS). In the presence of 10 nM CA-074, cleavages of peptide substrates of the library were blocked by CA-074 (Figure 2.6). At pH 7.2, 10 nM CA-074 had no effect on cathepsin B cleavage of the Z-Phe-Arg-AMC substrate (Figure 2.3) and, similarly, had no effect on cleaving peptide substrates in the MSP-MS assay (Figure 2.6). These findings confirm that CA-074 has selectivity for inhibiting cathepsin B peptide cleavages at pH 4.6 over pH 7.2 for broader substrates.

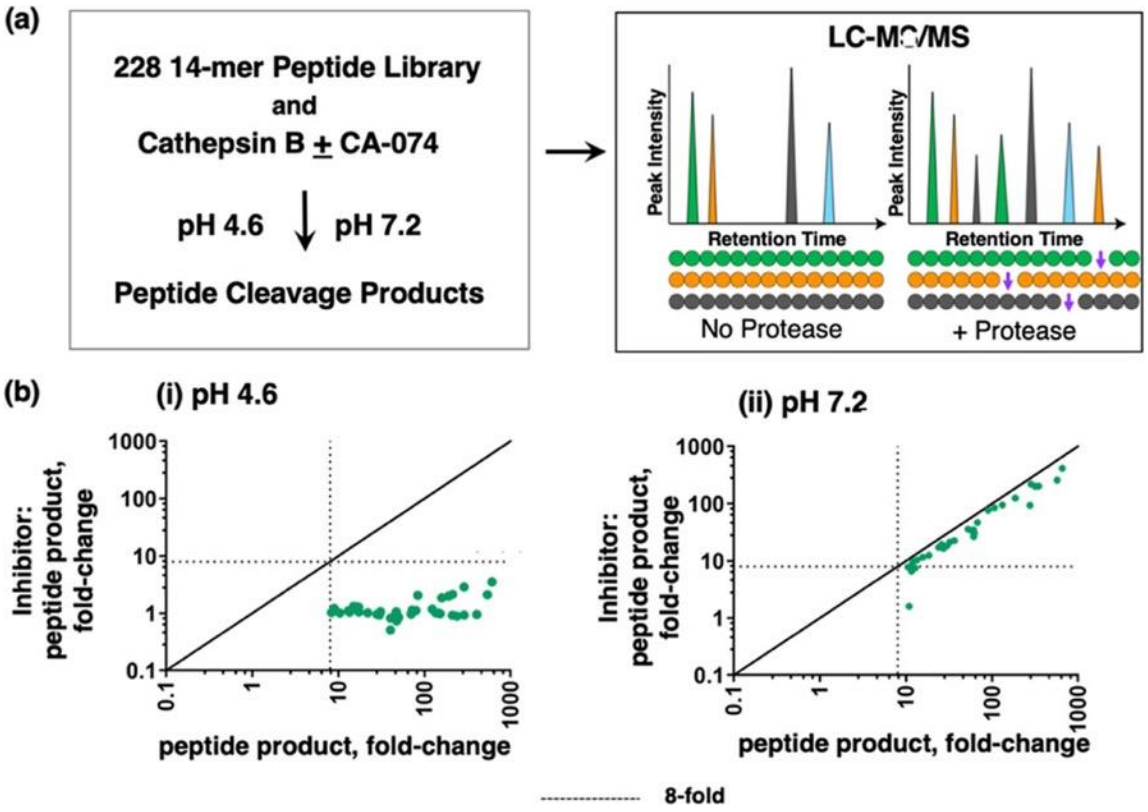

Figure 2.6 CA-074 inhibition of peptide cleavages by cathepsin B analyzed by MSP-MS. (a) MSP-MS approach for cleavage profiling of cathepsin B in the presence or absence of CA-074. Cathepsin B was preincubated with CA-074 (10 nM) at pH 4.6 and pH 7.2 for 30 min at room temperature (RT) and without an inhibitor as the control. These cathepsin B conditions were then subjected to MSP-MS assays by addition of the peptide library and incubation (at RT) for 60 min followed by LC–MS/MS identification and quantification of peptide cleavage products. (b) Cleaved peptide products of cathepsin B in MSP-MS at pH 4.6 (panel i) and pH 7.2 (panel ii). The quantities of each cleaved peptide product generated in the absence of an inhibitor or in the presence of an inhibitor were plotted as the fold-change of each cleaved peptide product relative to no enzyme activity control. Cleaved peptides were defined as those with intensity scores of 8-fold or more (----) above the quenched inactive cathepsin B, evaluated using the ratio of $\log_2$(Cat.B/inactivated enzyme) for each peptide product, with $p < 0.05$ by the two-tailed homoscedastic t-test.

2.2.8 Molecular Docking of CA-074 Interactions with Cathepsin B at Acidic pH 4.6 and Neutral pH 7.2

Modeling of CA-074 binding interactions to cathepsin B at acidic pH 4.6 and neutral pH 7.2 was evaluated using the molecular operating environment (MOE) docking software. (41,42) The MOE modeled CA-074 binding to bovine cathepsin B (PDB: 1QDQ) (36) at pH 4.6 and pH

7.2, showing similar orientation at the active site (Figure 2.7a). Mature human and bovine cathepsin B share 88.3% protein sequence identity and 100% sequence identity for the amino acids (His 110 and His111) that directly interact with CA-074. (37) The docking assessment shows that CA-074 interacts with the S2, S1, S1′, and S2′ subsites of the enzyme according to the Schechter–Berger nomenclature, (43) where the subsites interact with the corresponding amino acids adjacent to the cleavage site indicated as P2-P1-↓P1′-P2′. At pH 4.6, the P2′ residue of CA-074 at the C-terminus (proline residue) shows a strong ionic interaction His110 and His111 in the S2′ subsite of the enzyme (Figure 2.7b), reflected by a total binding energy of −58.3 kcal/mol (Table 2.3 and Figure 2.S4). However, at pH 7.2, the P2′ residue of CA-074 at the C-terminus partially loses ionic interaction with His111 in the S2′ subsite of the enzyme (Figure 2.7c), reflected by the altered binding energy of −43 kcal/mol (Table 2.3 and Figure 2.S5), when compared to the binding energy at pH 4.6. These MOE docking analyses show that CA-074 binds more favorably to cathepsin B at pH 4.6 than at pH 7.2, which supports our experimental data illustrating the greater inhibition by CA-074 under acidic compared to neutral pH conditions.

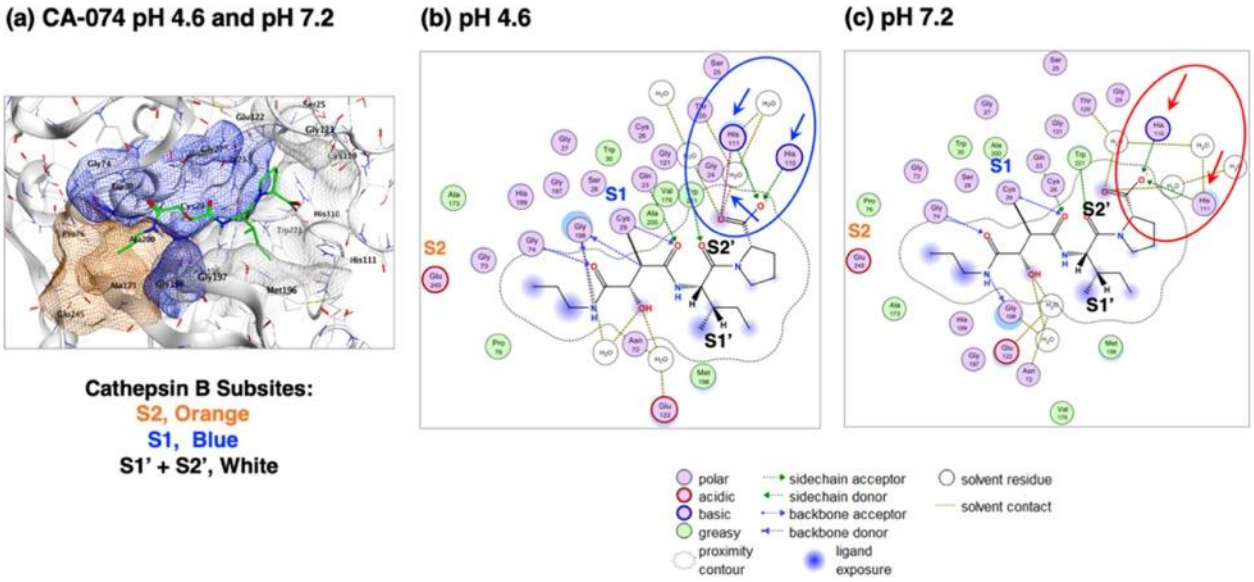

Figure 2.7 Molecular docking of CA-074 to cathepsin B at pH 4.6 and pH 7.2. (a) Model of CA-074 docking to cathepsin B at pH 4.6 and pH 7.2. Analysis of CA-074 inhibitor binding to enzyme was conducted by MOE at pH 4.6 and pH 7.2 to illustrate the predicted docking orientation of the inhibitor to the cathepsin B structure of PDB 1QDQ as the template for analyses. (36,37) CA-074 interacts with S2 to S2′ subsites of the enzyme substrate binding region (Schechter–Berger nomenclature (43)), containing the active site Cys29 residue. Cathepsin B enzyme subsites are shown as the S2 subsite in orange, the S1 subsite in blue, and the S1′ and S2′ subsites in gray-white. (b) Two-dimensional illustration of CA-074 and cathepsin B binding interactions at pH 4.6. At pH 4.6, the P2′ proline residue of CA-074 at its C-terminus shows strong ionic interactions with His110 and His111 in the S2′ subsite of the occluding loop region of the enzyme (panel b, indicated by blue arrows), indicated by the total binding energy of −58.3 kcal/mol (Table 2.3 and Figure 2.S4). (c) Two-dimensional illustration of CA-074 and cathepsin B binding interactions at pH 7.2. At pH 7.2, the P2′ proline residue of CA-074 at the C-terminus partially loses ionic interaction with His111 in the S2′ subsite of the enzyme (panel c, indicated by red arrows), reflected by the altered binding energy of −43 kcal/mol (Table 2.3 and Figure 2.S5), when compared to the binding energy at pH 4.6. These MOE docking analyses predict the differential binding features of CA-074 to the occluding loop domain of cathepsin B at pH 4.6 compared to pH 7.2.

Table 2.3 Binding Energies of CA-074 to Cathepsin B at pH 4.6 and pH 7.2[a]

pH condition	binding energy
pH 4.6	−58.3 kcal/mol
pH 7.2	−43.0 kcal/mol

[a]The more negative binding energy calculated for pH 4.6 compared to pH 7.2 predicts the more favorable interaction of CA-074 to cathepsin B at pH 4.6.

2.3 Discussion

This study demonstrates the potency, molecular features, and protease specificity of CA-074 inhibition of cathepsin B, showing that CA-074 displays preference for inhibition at the acidic lysosomal pH of 4.6 compared to the mildly acidic pH 5.5 of secretory vesicles and the neutral pH of 7.2 of cytosol and extracellular locations. KI values indicate that CA-074 is 90-fold more potent for inhibition of cathepsin B at acidic pH 4.6 compared to neutral pH 7.2. CA-074 at pH 5.5 was about 10-fold less effective than that at pH 4.6 (based on KI) and was 9-fold more potent than that at pH 7.2. These results demonstrate that the potency of CA-074 increases as the pH decreases from pH 7.2 to 4.6. Under these acidic and neutral pH conditions, CA-074 maintains its specificity for cathepsin B over other cysteine cathepsins, displays irreversible inhibition, and inhibits diverse peptide cleavages of cathepsin B assessed by MSP-MS profiling. Molecular docking suggested pH-dependent ionic interactions of the carboxylate group of the C-terminal proline of CA-074 with His110 and His111 residues at the S2 subsite of the enzyme. Notably, CA-074Me showed no pH-dependent inhibition, indicating that methylation of the C-terminal proline of CA-074 abolishes its pH-dependent inhibition of cathepsin B. These results demonstrate the pH-dependent structural and kinetic properties of CA-074 for specific inhibition of cathepsin B.

The distinct features of cathepsin B that result in its preferential inhibition by CA-074 at acidic pH suggest that this enzyme possesses different properties at acidic compared to neutral pH environments. Indeed, cathepsin B has been shown to possess different cleavage specificities at pH 4.6 compared to pH 7.2, (44) observed during unbiased cleavage profiling analyses by MSP-MS. (44) Based on the peptide substrate preferences of cathepsin B under the two different pH conditions, a neutral pH-selective substrate was modified with the AOMK warhead to generate Z-Arg-Lys-AOMK that displayed neutral pH-selective inhibition of cathepsin B with high potency. (44) These new findings distinguish cathepsin B properties in its normal acidic environment of

lysosomes, versus its abnormal location in the cytosol and extracellularly in numerous human diseases. Together, these data support the hypothesis that neutral pH cathepsin B may represent a pathogenic form of the enzyme involved in disease mechanisms.

Our molecular docking studies by MOE demonstrated the more favorable interaction of the C-terminal region of CA-074 with the occluding loop of cathepsin B at pH 4.6 rather than at pH 7.2. Our molecular docking assessment by the MOE at pH 4.6 and pH 7.2 using X-ray crystallography data for cathepsin B (36) shows the importance of the enzyme occluding loop interaction with the C-terminal carboxylate of CA-074. Binding energies of docking at pH 4.6 compared to pH 7.2 support the hypothesis that CA-074 at pH 4.6 displays preferable interaction with the occluding loop through its C-terminal proline carboxylate interaction with His110 and His111 of the enzyme. His110 and His111 have been shown to be key residues for cathepsin B exopeptidase activity. Mutagenesis of His110 to Gln, or His111 to Ala, results in reduction of cathepsin B activity to less than 1% of the wild-type cathepsin B activity when using substrates containing P2′ residues with a C-terminal carboxylic acid group. (45) Notably, methylation at the carboxylate residue of CA-074, forming CA-074Me, abolished the pH-dependent property of CA-074 with substantially decreased potency at acidic and neutral pH values. These findings indicate that the C-terminus of CA-074 participates in its pH-dependent inhibition and potency. These findings advance previous knowledge (20,21,36,46,47) concerning the importance of His110 and His111 of the occluding loop for interacting with the C-terminus of CA-074 in a pH-dependent manner.

In cellular and animal studies, the prodrug CA-074Me is widely used for CA-074 inhibition of cathepsin B. (3) Treatment of cells with CA-074Me has been shown to more effectively inhibit intracellular cathepsin B compared to incubating cells with CA-074. (33) It has been hypothesized

that CA-074Me is more cell permeable and is converted by intracellular esterases to CA-074. (33) In numerous cellular studies, the concentration of CA-074Me used to inhibit intracellular cathepsin B generally ranges from 10 to 50 μM. (4,48−50) With the assumption that most of the proinhibitors are converted to CA-074, the high concentration of CA-074 would be sufficient to inhibit cathepsin B located in different subcellular pH conditions of acidic lysosomes and neutral pH locations including cytosol. In animal studies, CA-074Me concentrations in the approximate range of 4–10 mg/kg and higher have been administered, (6,51−54) which may correspond to micromolar and greater levels of the inhibitor that would inhibit cathepsin B at acidic to neutral pH cellular locations. Measurements of CA-074 and CA-074Me in vivo levels and clearance in animal studies will be important in future studies to assess in vivo inhibitor concentrations.

The new findings of this study suggest that adjustment of CA-074 concentrations may allow assessment of cathepsin B functions in acidic lysosomes compared to neutral pH locations such as the cytosol, nuclei, and extracellular environment. (3,11,27,30,55−57) We previously discovered that Z-Arg-Lys-AOMK is >100-fold selective at inhibiting cathepsin B at pH 7.2 over pH 4.6, (44) while in this study CA-074 has the opposite property for preferring inhibition at acidic pH 4.6. Use of these two inhibitors in cellular studies, at concentrations where they maintain pH selectivity, may allow evaluation of the functional roles of lysosomal compared to nonlysosomal cathepsin B.

In summary, this study has demonstrated the pH-dependent inhibitory properties of CA-074 inhibition of cathepsin B with respect to its potency, molecular features, and specificity. At appropriate concentrations, CA-074 may potentially serve as a selective acidic pH inhibitor of cathepsin B, with specificity for cathepsin B over other cysteine cathepsins. The proof-of concept of these findings shows that it may be possible to develop other pH-selective inhibitors. Novel pH-

selective inhibitors may allow studies in the future to specifically probe the role of cathepsin B in distinct pH cellular compartments such as the cytosol that have implicated to be involved in brain disorders and other human diseases.

2.4 Methods and Materials

2.4.1 Inhibitors, Enzymes, Peptides, and Reagents

CA-074 inhibitor was purchased from Calbiochem (Millipore Sigma #205530, St. Louis, MO). CA-074Me was purchased from Sigma (#205531). Recombinant human cathepsin B (accession NP_001899.1) and cysteine cathepsin proteases were from R & D Systems (Minneapolis, MN) or Abcam (Cambridge, MA) consisting of cathepsin B (R & D #953-CY-010), cathepsin L (R & D #952-CY-010), cathepsin V (R & D #1080-CY-010), cathepsin S (R & D #1183-CY-010), cathepsin K (Abcam #ab157067), cathepsin C (R & D #1071-CY-010), cathepsin H (R & D #75116-CY-010), and cathepsin X (R & D #934-CY)-010). Fluorogenic substrates consisted of Z-Phe-Arg-AMC ((#AS-24096, Anaspec, Fremont, CA), Gly-Arg-AMC and Arg-AMC from Bachem ((#4002196 and (#I-1050, respectively, Torrance, CA), and MCA-Arg-Pro-Pro-Gly-Phe-Ser-Ala-Phe-Lys(Dnp)OH ((#AMYD-111A, CPC Scientific, San Jose, CA). MSP-MS assays utilized a library of 228 peptides of 14 amino acids in length, designed, and synthesized to contain all neighbor and near-neighbor diversity in residues, as described previously. (39,40) These assays utilized buffer components of citric acid monohydrate (Merck #1.00244.0500, Burlington, MA), sodium phosphate dibasic anhydrous (EMD #SX-072305, Burlington, MA), sodium acetate (Fisher Scientific #BP-333-500, Fair Lawn, NJ), EDTA (Calbiochem #324503, Burlington, MA), sodium chloride (Fisher Chemical #S271-1, Pittsburgh, PA), dithiothreitol (DTT) (Promega #V351, Madison, WI), and urea (Teknova #U2222, Hollister, CA). Peptide extraction reagents consisted of C18 LTS tips (Rainin #PT-LC18-960, Oakland, CA) and C18 for SPE stage-tips (3 M company #2215-C18, Maplewood, MN), and (3) nano-LC–MS/MS reagents

consisting of the BEH C18 packing material (Waters Corporation #186004661, Milford, MA), acetonitrile (Fisher Chemical #A955-4, Pittsburgh, PA), formic acid (FA) (Fisher Chemical #A117-50, Pittsburgh, PA), trifluoroacetic acid (TFA) (Fisher Chemical #A116-50, Pittsburgh, PA), and HPLC-grade water (Fisher Chemical #W6-4).

2.4.2 Cathepsin B Activity Assay

Procathepsin B (recombinant) was activated to mature cathepsin B by incubation at 37 °C for 30 min in 20 mM Na-acetate pH 5.5, 1 mM EDTA, 5 mM DTT, and 100 mM NaCl. Assay of cathepsin B activity utilized final buffer conditions of 0.04 ng/μL cathepsin B, 40 μM Z-Phe-Arg-AMC, 40 mM citrate phosphate (pH 4.6, pH 5.5, or pH 7.2), 1 mM EDTA, 100 mM NaCl, 5 mM DTT, and 0.01% Tween-20. Assays were conducted at RT (25 °C) in quadruplicate, and relative fluorescence readings (RFUs) (excitation 360 nm, emission 460 nm) were recorded every 46 s over a period of 30 min (for inhibitor assays) in a Biotek HTX microplate plate reader. For other assays, RFUs were recorded every 101, 30, and 70 s for studies of pH dependence (Figure 2.1), irreversibility (Figure 2.3), and K_m values (Figure 2.S6), respectively. Enzyme velocity (RFU/sec) calculations used the highest slope recorded for 10 consecutive fluorescent readings. RFU/s were converted to specific activity of pmol/min/μg using AMC standards. Specific activity was defined as pmol/min/μg enzyme. Data analysis was conducted using Prism GraphPad software.

For the pH curve experiment (Figure 2.1), cathepsin B activity was also monitored over the entire pH range of 2.2 to 9.0 in 40 mM citrate phosphate (pH 2.2 to pH 7.4) or 40 mM Tris–HCl (pH 7.8 to 9.0), 1 mM EDTA, 5 mM DTT, 100 mM NaCl, and 0.01% Tween-20, with preincubation in each pH buffer for 10 min prior to initiating the assay by adding a substrate. We noted that preincubation at pH values of 3.0 or 8.0 resulted in reduced activity when compared with our previous studies (44) that had no preincubation step.

2.4.3 Inhibition of Cathepsin B by CA-074 and CA-074Me in Kinetic Studies

Kinetic analyses of CA-074 and CA-074Me inhibition of cathepsin B were conducted at pH 4.6, pH 5.5, and pH 7.2 to determine IC_{50}, K_I, k_{obs}, and k_{inact}/K_I. The CA-074 inhibitor concentrations ranged from 4096 to 0.5 nM (2-fold serial dilution) or 144 to 0.5 nM (1.5-fold serial dilution). CA-074Me inhibitor concentrations ranged from 65,536 to 64 nM (2-fold serial dilution) or 50,000 to 64 nM (1.5-fold dilution). Inhibitors were added to the enzyme at the start of the incubation period (at RT); thus, there was no preincubation. A vehicle control assay without inhibitor contained enzyme, substrate, and 2% (v/v) DMSO. Cathepsin B proteolytic assays with CA-074 were conducted as described above. IC_{50} values were calculated as the inhibitor concentration that reduced cathepsin B activity by 50%.

For determination of K_I and k_{inact}/K_I kinetic inhibition constants, k_{obs} constants were determined for each inhibitor concentration by plots of cathepsin B activity in time courses with various inhibitor concentrations by curve fitting slope data of RFU versus time into $Y = Y_0 \times e^{(-k_{obs} \times X)}$, where Y_0 is the activity for the control with no inhibitor, Y is the activity in the presence of the inhibitor, and X is time. K_I and k_{inact} values were determined by plots of k_{obs} and inhibitor concentration, combined with curve fitting the k_{obs} values with the equation $k_{obs} = k_{inact} \times [I]/(K_I + [I])$, where $[I]$ is inhibitor concentration, k_{inact} is the maximum rate of inactivation at saturating inhibitor concentrations, and $K_{I,app}$ is the x-axis inhibitor concentration where $y = k_{inact}/2$. (58,59)K_I, values were determined from $K_{I,app}$ and K_m values by the equation $K_{I,app} = K_I \times (1 + [S]_0/K_m)$. Determination of K_m values is described in the next paragraph. These analyses are for irreversible inhibitor kinetic characterization.

K_m values were determined for Cathepsin B (Z-Phe-Arg-AMC substrate), Cathepsin C (Gly-Arg-AMC), Cathepsin H (Arg-AMC), Cathepsin L (Z-Phe-Arg-AMC), Cathepsin K (Z-Phe-Arg-AMC), Cathepsin S (Z-Phe-Arg-AMC), Cathepsin V (Z-Phe-Arg-AMC), and Cathepsin X

(MCA-Arg-Pro-Pro-Gly-Phe-Ser-Ala-Phe-Lys(Dnp)-OH) at pH 4.6, pH 5.5, and pH 7.2 (Figure 2.S6). Enzymes were assayed at different substrate concentrations ranging from 225 to 4 μM (1.5-fold serial dilution), and the slope of RFU per unit time was determined for each substrate concentration; plots of substrate concentration and velocity were assessed by Prism 9 by curve fitting using the equation $v_0 = V_{max} \times [S]/(K_m + [S])$ to determine K_m values. These kinetic methods are for irreversible inhibitor kinetic characterization.

2.4.4 Irreversible Inhibition Mechanism

The irreversible mechanisms of CA-074 and CA-074Me inhibition of cathepsin B were conducted at pH 4.6, pH 5.5, and pH 7.2. Cathepsin B was preincubated with each inhibitor at 10 times the IC_{50} concentration followed by dilution to 1/10 the IC_{50} concentration, addition of substrate (Z-F-R-AMC), and monitoring activity in time-course assays. Inhibition of cathepsin B following dilution indicates the irreversible inhibitory mechanism of CA-074 and CA-074Me under acidic and neutral pH conditions.

2.4.5 Selectivity of CA-074 for Cathepsin B and Cysteine Cathepsin Proteases

The selectivity of CA-074 and CA-074Me was assessed by comparing its inhibitory potencies for cathepsin B compared to other cysteine cathepsin proteases consisting of cathepsin V, L, K, S, X, H, and C. IC_{50} values were determined for pH 4.6, pH 5.5, and pH 7.2 conditions (with no preincubation of inhibitor and enzyme), consisting of 40 mM citrate phosphate, 1 mM EDTA, 5 mM DTT, and 100 mM NaCl. The inhibitor concentrations ranged from 16.38 μM to 256 nM in 2-fold serial dilutions. When activity (RFU/s) in the presence of 16.38 μM inhibitor was reduced by <50%, the IC_{50} value was indicated as >16 μM. Cathepsin L (0.03 ng/μL), cathepsin K (0.10 ng/μL), cathepsin S (0.20 ng/uL), and cathepsin V (0.04 ng/μL) were assayed with 40 μM Z-Phe-Arg-AMC. Cathepsin C (0.51 ng/uL), cathepsin H (0.1 ng/μL), and cathepsin X (0.20 ng/uL) were assayed with 40 μM of MCA-Arg-Pro-Pro-Gly-Phe-Ser-Ala-Phe-

Lys(*Dnp*)OH, Gly-Arg-AMC, and Arg-AMC, respectively. Activation of procathepsin H to cathepsin H was achieved by incubation of cathepsin H (4.4 ng/μL) with cathepsin L (1.1 ng/μL) at RT for 2 h in 20 mM citrate phosphate pH 6.0, 5 mM DTT, and 100 mM NaCl. Cathepsin C (13.78 ng/μL) was activated by incubation with cathepsin L (3.4 ng/μL) at RT for 1 h in 20 mM citrate phosphate, pH 6.0, 100 mM NaCl, and 5 mM DTT. Cathepsin L did not cleave the cathepsin C and cathepsin H substrates Gly-Arg-AMC and Arg-AMC, respectively. These fluorogenic assays used a fluorescent microplate reader as described for cathepsin B. For assay of cathepsin X, the reader was set to excitation 320 nm and emission 400 nm. To convert RFU/s to picomol/min, 10 μM to 0.005 μM (in 2-fold dilutions) of MCA-Arg-Pro-Pro-Gly-Phe-Ser-Ala-Phe-Lys(*Dnp*)OH was fully hydrolyzed with excess Cathepsin X, and a standard curve was generated using the fluorescence values measured at each concentration.

2.4.6 CA-074 Inhibition of Cathepsin B Peptide Cleavages Assessed by MSP-MS

CA-074 inhibition of peptide cleavages was evaluated by MSP-MS assays of cathepsin B. Cathepsin B was preincubated at 25 °C for 30 min with 10 nM of CA-074 in pH 4.6 buffer or pH 7.2 buffer. As a control, cathepsin B was preincubated with 2.5% DMSO in each assay buffer. In a total volume of 10 μL, cathepsin B (0.1 ng/μL) preincubated with CA-074 was incubated with a mixture of 228 14-mer peptides (0.5 μM for each peptide) in assay buffer composed of 40 mM citrate phosphate at pH 4.6 or pH 7.2, 1 mM EDTA, 100 mM NaCl, and 5 mM DTT for 60 min at 25 °C. After 60 min incubation, the 10 μL aliquot was combined with 60 μL of 8 M urea. A control assay used activated cathepsin B in each assay buffer mixed with 8 M urea for 60 min at 25 °C for inactivation, prior to addition of the peptide library. Assays were conducted in quadruplicate. Samples were acidified by addition of 40 μL of 2% TFA, enriched, and desalted using C18 LTS Tips (Rainin), evaporated to dryness in a vacuum centrifuge, and placed at −70 °C. Samples were resuspended in 40 μL of 0.1% FA (solvent A), and 4 μL was used for LC–MS/MS.

LC–MS/MS was performed on a Q-Exactive Mass Spectrometer (Thermo) equipped with an Ultimate 3000 HPLC (Thermo Fisher). Peptides were separated by reverse-phase chromatography on a C18 column (1.7 μm bead size, 75 μm × 20 cm, 65 °C) heated to 65 °C at a flow rate of 400 nL/min using solvent A and 0.1% FA in acetonitrile (solvent B). LC separation used a 50-minute linear gradient of 5–30% solvent B with a subsequent 15-minute linear gradient of 30–75% solvent B. Survey scans were recorded over a 200–2000 *m*/*z* range (70,000 resolutions at 200 *m*/*z*, AGC target 1×10^6, 75 ms maximum). MS/MS was performed in data-dependent acquisition mode with HCD fragmentation (30 normalized collision energy) on the 10 most intense precursor ions (17,500 resolutions at 200 *m*/*z*, AGC target 5×10^4, 120 ms maximum, dynamic exclusion 15 s).

MS/MS data analysis was performed using PEAKS (v 8.5) software (Bioinformatics Solutions Inc.). MS^2 data were searched against the 228-member tetradecapeptide library sequences, and a decoy search was conducted with sequences in reverse order. A precursor tolerance of 20 ppm and 0.01 Da for MS^2 fragments was defined. No protease digestion was specified. Data were filtered to 1% peptide and protein level false discovery rates with the target-decoy strategy. Peptides were quantified with label-free quantification, and data were normalized by the Loess-G algorithm and filtered by 0.5 peptide quality. Using R scripts, outliers from replicates were removed by Dixon's Q testing. Missing and zero values are imputed with random normally distributed numbers in the range of the average of smallest 5% of the data ± SD. Analysis of variance testing was performed for peptide data of control and 60 min incubation conditions; those with $p < 0.05$ were considered for further analysis. Criteria for cleaved peptide products were those with intensity scores of 8-fold or more above the quenched inactive cathepsin B, evaluated

by $\log_2$(active/inactivated enzyme) ratios for each peptide product; with $p < 0.05$ by the two-tailed homoscedastic t-test.

2.4.7 MOE Modeling of CA-074 Interactions with Cathepsin B under Acidic and Neutral pH Conditions

The MOE molecular modeling tool was used to model CA-074 binding to cathepsin B using the crystal structure of bovine cathepsin B (PDB 1QDQ) and a co-crystal template with the inhibitor CA-074 as the default binding ligand. The builder function of the MOE was used to examine binding poses that considered polar contacts and hydrogen bonds between the ligand and the active site pocket of 1QDQ at pH 4.6 and pH 7.2. Docking simulations used energy-minimized structures to assess ligand flexibility and poses.

2.4.8 Data availability

LC-MS/MS files for the MSP-MS experiments can be accessed at www.massive.ucsd.edu under the dataset identifier numbers MSV000086449 and MSV000086447.

2.5 Supporting Information

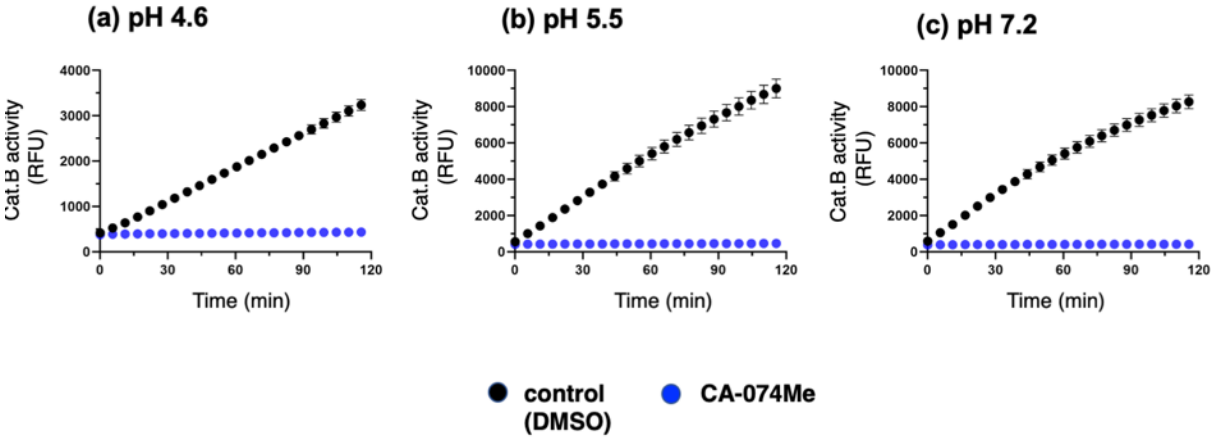

Figure 2.S1 Irreversible mechanism of CA-074Me inhibition of cathepsin B at pH 4.6, pH 5.5, and pH 7.2. CA-074Me at pH 4.6 (panel a), pH 5.5 (panel b), and pH 7.2 (panel c) was evaluated for irreversible or reversible inhibition of cathepsin B. Cathepsin B was pre-incubated with inhibitor at 10 times the IC50 concentration (consisting of CA-074Me at 90 µM at pH 4.6, 137 µM at pH 5.5, and 75 nM at pH 7.2), followed by dilution to 1/10 the IC50 concentration, addition of substrate (Z-F-R-AMC), and measurement of activity in time-course assays. Inhibition of cathepsin B following dilution indicates the irreversible inhibitory mechanism of CA-074Me.

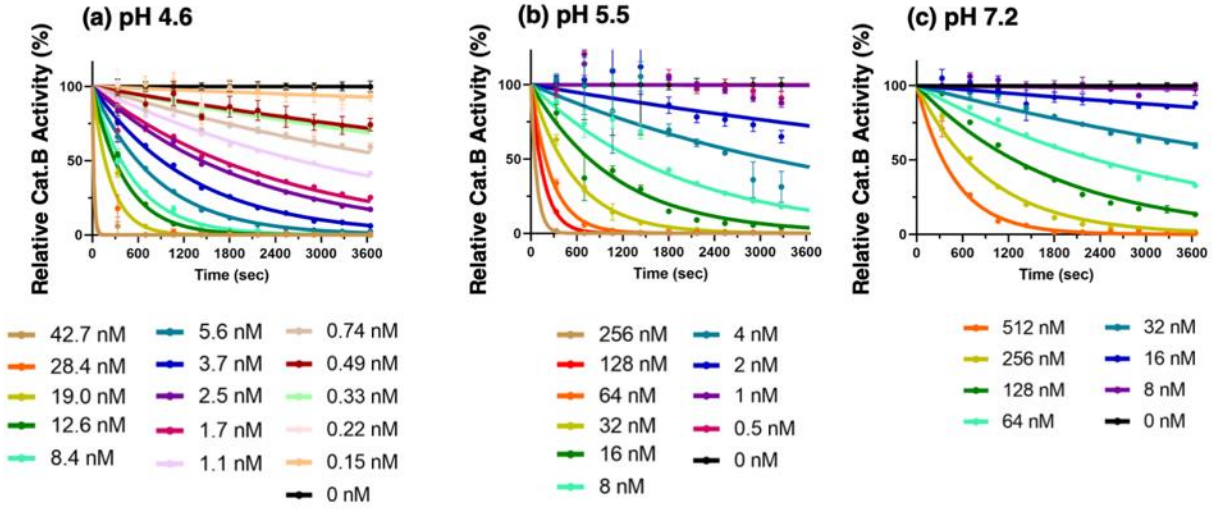

Figure 2.S2 Kinetic analysis of CA-074 inhibition of cathepsin B at acidic to neutral pH conditions. Cathepsin B activity was monitored in time-course assays at different concentrations of CA-074, conducted at pH 4.6 (panel a), pH 5.5 (panel b), and pH 7.2 (panel c). Values for k_{obs} were calculated by Prism using the equation $Y=Y0*e^{(-kobs*X)}$ where X is time and Y/Y0 is activity (measured as slope of RFU vs time) with inhibitor relative to activity with no inhibitor. The k_{obs} values were used to calculate k_{inact} and K_I values by plotting k_{obs} vs inhibitor concentration (shown in Figure 3).

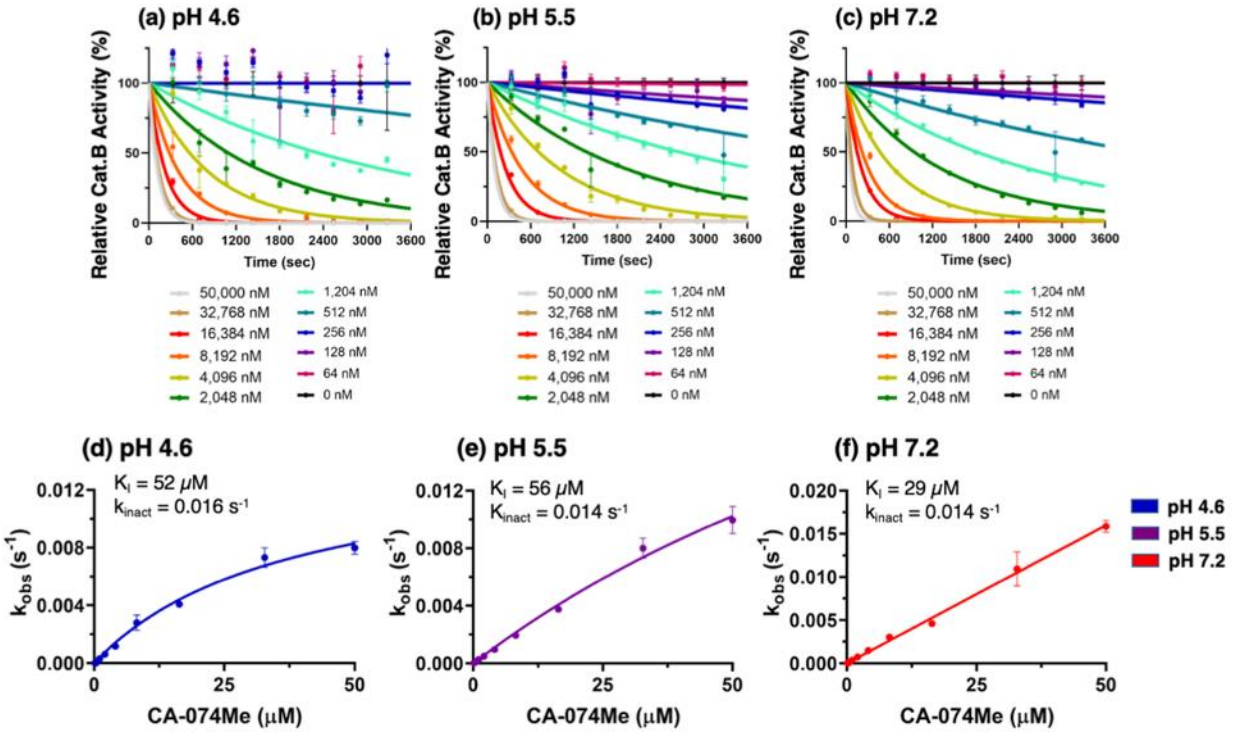

Figure 2.S3 Kinetic analysis of CA-074Me inhibition of cathepsin B at acidic to neutral pH conditions. (a) to (c). CA-074Me and cathepsin B in kinetic studies for k_{obs} values. Cathepsin B activity was monitored in time-course assays at different concentrations of CA-074, conducted at pH 4.6 (panel a), pH 5.5 (panel b), and pH 7.2 (panel c). Values for k_{obs} were calculated by the equation $Y=Y0*e^{(-kobs*X)}$ where X is time and Y/Y0 is activity with inhibitor relative to activity with no inhibitor. The k_{obs} values were used to calculate k_{inact} and K_I values by plotting k_{obs} vs inhibitor concentration (shown in d-f). (d) to (f). CA-074Me inhibition of cathepsin B kinetics for K_I, k_{inact}, and k_{inact} /K_I values. Kinetic analyses of CA-074Me inhibition of cathepsin B was conducted at pH 4.6 (panel d), pH 5.5 (panel e), and pH 7.2 (panel f) to determine K_I, k_{inact}, and k_{inact} /K_I values, conducted as described in the methods.

Ligand Interactions Report

Mon Oct 12 12:58:04 2020 (MOE 2019.01)

1QDQ: HYDROLASE / 1QDQ: HYDROLASE

Inhibitor		Enzyme				Interaction	Distance	E (kcal/mol)
N1	11	O	GLY	198	(A)	H-donor	2.84	-2.0
O2	17	O	HOH	399	(A)	H-donor	2.61	-1.6
C6	19	O	GLY	198	(A)	H-donor	3.37	-0.5
O1	14	N	GLY	74	(A)	H-acceptor	3.04	-2.3
O2	17	O	HOH	282	(A)	H-acceptor	2.86	-1.2
O3	22	NE2	GLN	23	(A)	H-acceptor	2.90	-1.4
O3	22	N	CYS	29	(A)	H-acceptor	3.26	-1.9
O4	28	NE1	TRP	221	(A)	H-acceptor	2.89	-4.2
O	46	O	HOH	388	(A)	H-acceptor	2.62	-1.1
O	46	O	HOH	395	(A)	H-acceptor	2.65	-3.3
OT	56	ND1	HIS	110	(A)	H-acceptor	2.70	-11.2
OT	56	NE2	HIS	111	(A)	H-acceptor	2.73	-10.9
O	46	NE2	HIS	111	(A)	Ionic	3.19	-3.3
OT	56	ND1	HIS	110	(A)	Ionic	2.70	-6.8
OT	56	NE2	HIS	111	(A)	Ionic	2.73	-6.6

CA074:
Bound @ pH4.6

Total Interactions:
-58.3 kcal/mol

Nuc-E Distance: N/Å

Figure 2.S4 Binding energy of CA-074 bound to cathepsin B at pH 4.6. Components comprising the binding energy of CA-074 binding to cathepsin B at pH 4.6 were assessed by the MOE docking software. Energies of the binding interactions of the inhibitor with the enzyme (specific residues are indicated) are shown, combined with the total binding energy indicated as -58.3 kcal/mol.

Ligand Interactions Report

Mon Oct 12 13:33:09 2020 (MOE 2019.01)

1QDQ: HYDROLASE / 1QDQ: HYDROLASE

Inhibitor		Enzyme				Interaction	Distance	E (kcal/mol)
N1	11	O	GLY	198	(A)	H-donor	2.84	-2.0
O2	17	O	HOH	399	(A)	H-donor	2.61	-1.6
O1	14	N	GLY	74	(A)	H-acceptor	3.04	-2.3
O2	17	O	HOH	282	(A)	H-acceptor	2.87	-1.2
O3	22	NE2	GLN	23	(A)	H-acceptor	2.90	-1.3
O3	22	N	CYS	29	(A)	H-acceptor	3.26	-1.9
O4	28	NE1	TRP	221	(A)	H-acceptor	2.90	-4.4
O	46	O	HOH	388	(A)	H-acceptor	2.61	-1.1
O	46	O	HOH	395	(A)	H-acceptor	2.62	-3.1
OT	56	ND1	HIS	110	(A)	H-acceptor	2.69	-11.1
OT	56	NE2	HIS	111	(A)	H-acceptor	2.83	-6.1
OT	56	ND1	HIS	110	(A)	Ionic	2.69	-6.9

CA074:
Bound @ pH7.2

Total Interactions:
-43.0 kcal/mol

Nuc-E Distance: N/Å

Figure 2.S5 Binding energy of CA-074 bound to cathepsin B at pH 7.2. Components comprising the binding energy of CA-074 binding to cathepsin B at pH 7.2 were assessed by the MOE docking software. Energies of the binding interactions of the inhibitor with the enzyme (residues are indicated) are shown, combined with the total binding energy indicated as -43.0 kcal/mol.

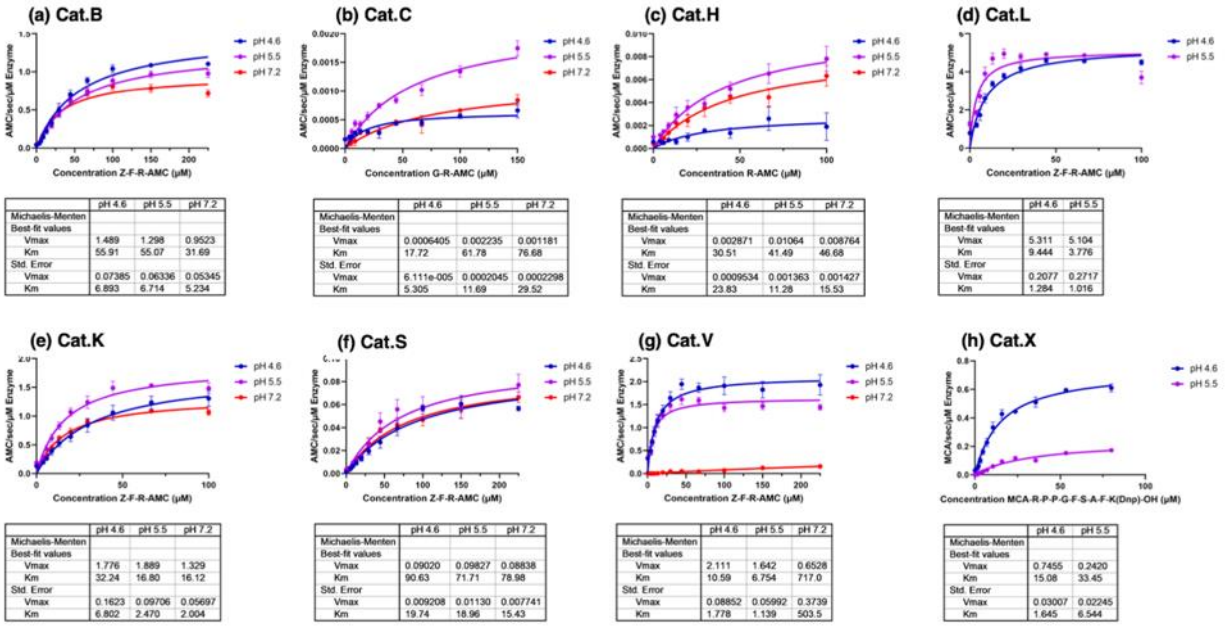

Cat.B	pH 4.6	pH 5.5	pH 7.2
Michaelis-Menten Best-fit values			
Vmax	1.489	1.298	0.9523
Km	55.91	55.07	31.69
Std. Error			
Vmax	0.07385	0.06336	0.05345
Km	6.893	6.714	5.234

Cat.C	pH 4.6	pH 5.5	pH 7.2
Michaelis-Menten Best-fit values			
Vmax	0.0006405	0.002235	0.001181
Km	17.72	61.78	76.68
Std. Error			
Vmax	6.111e-005	0.0002045	0.0002298
Km	5.305	11.69	29.52

Cat.H	pH 4.6	pH 5.5	pH 7.2
Michaelis-Menten Best-fit values			
Vmax	0.002871	0.01064	0.008764
Km	30.51	41.49	46.68
Std. Error			
Vmax	0.0009534	0.001363	0.001427
Km	23.83	11.28	15.53

Cat.L	pH 4.6	pH 5.5
Michaelis-Menten Best-fit values		
Vmax	5.311	5.104
Km	9.444	3.776
Std. Error		
Vmax	0.2077	0.2717
Km	1.284	1.016

Cat.K	pH 4.6	pH 5.5	pH 7.2
Michaelis-Menten Best-fit values			
Vmax	1.776	1.889	1.329
Km	32.24	16.80	16.12
Std. Error			
Vmax	0.1623	0.09706	0.05697
Km	6.802	2.470	2.004

Cat.S	pH 4.6	pH 5.5	pH 7.2
Michaelis-Menten Best-fit values			
Vmax	0.09020	0.09827	0.08838
Km	90.63	71.71	78.98
Std. Error			
Vmax	0.009208	0.01130	0.007741
Km	19.74	18.96	15.43

Cat.V	pH 4.6	pH 5.5	pH 7.2
Michaelis-Menten Best-fit values			
Vmax	2.111	1.642	0.6528
Km	10.59	6.754	717.0
Std. Error			
Vmax	0.08852	0.05992	0.3739
Km	1.778	1.139	503.5

Cat.X	pH 4.6	pH 5.5
Michaelis-Menten Best-fit values		
Vmax	0.7455	0.2420
Km	15.08	33.45
Std. Error		
Vmax	0.03007	0.02245
Km	1.645	6.544

Figure 2.S6 K_m plots for cathepsin B and cysteine cathepsins at pH 4.6, 5.5, and 7.2. K_m values were determined for cathepsin B (panel a) and the cysteine cathepsins (cathepsins C, H, L K, S, V, and X with each of their indicated substrates, shown in panels b, c, d, e, f, g, and h, respectively. Michaelis-Menten kinetics was used for K_m data analysis (conducted as described in the methods) using the equation $v_0=V_{max}*[S]/(K_m+[S]$ with curve-fitting using Prism 9. Cathepsin L and cathepsin X had no activity at pH 7.2 and, therefore, K_m was determined for pH 4.6 and 5.5.

2.6 References

1. Turk, V.; Stoka, V.; Vasiljeva, O.; Renko, M.; Sun, T.; Turk, B.; Turk, D. Cysteine cathepsins: from structure, function and regulation to new frontiers. Biochim. Biophys. Acta 2012, 1824, 68−88.

2. Reiser, J.; Adair, B.; Reinheckel, T. Specialized roles for cysteine cathepsins in health and disease. J. Clin. Invest. 2010, 120, 3421− 3431.

3. Hook, V.; Yoon, M.; Mosier, C.; Ito, G.; Podvin, S.; Head, B. P.; Rissman, R.; O'Donoghue, A. J.; Hook, G. Cathepsin B in neurodegeneration of Alzheimer's disease, traumatic brain injury, and related brain disorders. Biochim. Biophys. Acta, Proteins Proteomics 1868, 1868, No. 140428.

4. Wu, Z.; Ni, J.; Liu, Y.; Teeling, J. L.; Takayama, F.; Collcutt, A.; Ibbett, P.; Nakanishi, H. Cathepsin B plays a critical role in inducing Alzheimer's disease-like phenotypes following chronic systemic exposure to lipopolysaccharide from Porphyromonas gingivalis in mice. Brain, Behav., Immun. 2017, 65, 350−361.

5. Kindy, M. S.; Yu, J.; Zhu, H.; El-Amouri, S. S.; Hook, V.; Hook, G. R. Deletion of the cathepsin B gene improves memory deficits in a transgenic Alzheimer's disease mouse

model expressing AβPP containing the wild-type β-secretase site sequence. J. Alzheimers Dis. 2012, 29, 827−840.

6. Hook, V. Y.; Kindy, M.; Hook, G. Inhibitors of cathepsin B improve memory and reduce beta-amyloid in transgenic Alzheimer disease mice expressing the wild-type, but not the Swedish mutant, beta-secretase site of the amyloid precursor protein. J. Biol. Chem. 2008, 283, 7745−7753.

7. Hook, G. R.; Yu, J.; Sipes, N.; Pierschbacher, M. D.; Hook, V.; Kindy, M. S. The cysteine protease cathepsin B is a key drug target and cysteine protease inhibitors are potential therapeutics for traumatic brain injury. J. Neurotrauma. 2014, 31, 515−529.

8. Boutté, A. M.; Hook, V.; Thangavelu, B.; Sarkis, G. A.; Abbatiello, B. N.; Hook, G.; Jacobsen, J. S.; Robertson, C. S.; Gilsdorf, J.; Yang, Z.; Wang, K. K. W.; Shear, D. A. Penetrating Traumatic Brain Injury Triggers Dysregulation of Cathepsin B Protein Levels Independent of Cysteine Protease Activity in Brain and Cerebral Spinal Fluid. J. Neurotrauma. 2020, 37, 1574−1586.

9. Zuo, X.; Hou, Q.; Jin, J.; Chen, X.; Zhan, L.; Tang, Y.; Shi, Z.; Sun, W.; Xu, E. Inhibition of Cathepsins B Induces Neuroprotection Against Secondary Degeneration in Ipsilateral Substantia Nigra After Focal Cortical Infarction in Adult Male Rats. Front Aging Neurosci. 2018, 10, 125.

10. Aggarwal, N.; Sloane, B. F. Cathepsin B: multiple roles in cancer. Proteomics Clin. Appl. 2014, 8, 427−437.

11. Victor, B. C.; Anbalagan, A.; Mohamed, M. M.; Sloane, B. F.; Cavallo-Medved, D. Inhibition of cathepsin B activity attenuates extracellular matrix degradation and inflammatory breast cancer invasion. Breast Cancer Res. 2011, 13, R115.

12. Bian, B.; Mongrain, S.; Cagnol, S.; Langlois, M. J.; Boulanger, J.; Bernatchez, G.; Carrier, J. C.; Boudreau, F.; Rivard, N. Cathepsin B promotes colorectal tumorigenesis, cell invasion, and metastasis. Mol. Carcinog. 2016, 55, 671−687.

13. Mort, J. S.; Recklies, A. D.; Poole, A. R. Extracellular presence of the lysosomal proteinase cathepsin B in rheumatoid synovium and its activity at neutral pH. Arthritis Rheum. 1984, 27, 509−515.

14. Fujisawa, A.; Kambe, N.; Saito, M.; Nishikomori, R.; Tanizaki, H.; Kanazawa, N.; Adachi, S.; Heike, T.; Sagara, J.; Suda, T.; Nakahata, T.; Miyachi, Y. Disease-associated mutations in CIAS1 induce cathepsin B-dependent rapid cell death of human THP-1 monocytic cells. Blood 2007, 109, 2903−2911.

15. Toomey, C. B.; Cauvi, D. M.; Hamel, J. C.; Ramirez, A. E.; Pollard, K. M. Cathepsin B regulates the appearance and severity of mercury-induced inflammation and autoimmunity. Toxicol. Sci. 2014, 142, 339−349.

16. Rajamäki, K.; Lappalainen, J.; Oörni, K.; Välimäki, E.; Matikainen, S.; Kovanen, P. T.; Eklund, K. K. Cholesterol crystals activate the NLRP3 inflammasome in human macrophages: a novel link between cholesterol metabolism and inflammation. PLoS One 2010, 5, e11765.

17. Gonzalez, E. A.; Martins, G. R.; Tavares, A. M. V.; Viegas, M.; Poletto, E.; Giugliani, R.; Matte, U.; Baldo, G. Cathepsin B inhibition attenuates cardiovascular pathology in mucopolysaccharidosis I mice. Life Sci. 2018, 196, 102−109.

18. Van Acker, G. J.; Saluja, A. K.; Bhagat, L.; Singh, V. P.; Song, A. M.; Steer, M. L. Cathepsin B inhibition prevents trypsinogen activation and reduces pancreatitis severity. Am. J. Physiol.: Gastro- intest. Liver Physiol. 2002, 283, G794−G800.

19. Cantres-Rosario, Y. M.; Ortiz-Rodríguez, S. C.; Santos- Figueroa, A. G.; Plaud, M.; Negron, K.; Cotto, B.; Langford, D.; Melendez, L. M. HIV Infection Induces Extracellular Cathepsin B Uptake and Damage to Neurons. Sci. Rep. 2019, 9, 8006.

20. Towatari, T.; Nikawa, T.; Murata, M.; Yokoo, C.; Tamai, M.; Hanada, K.; Katunuma, N. Novel epoxysuccinyl peptides A selective inhibitor of cathepsin B, in vivo. FEBS Lett. 1991, 280, 311−315.

21. Murata, M.; Miyashita, S.; Yokoo, C.; Tamai, M.; Hanada, K.; Hatayama, K.; Towatari, T.; Nikawa, T.; Katunuma, N. Novel epoxysuccinyl peptides Selective inhibitors of cathepsin B, in vitro. FEBS Lett. 1991, 280, 307−310.

22. Barrett, A. J.; Kembhavi, A. A.; Brown, M. A.; Kirschke, H.; Knight, C. G.; Tamai, M.; Hanada, K. L-trans-Epoxysuccinyl- leucylamido(4-guanidino)butane (E-64) and its analogues as inhibitors of cysteine proteinases including cathepsins B, H and L. Biochem. J. 1982, 201, 189−198.

23. Mindell, J. A. Lysosomal acidification mechanisms. Annu. Rev. Physiol. 2012, 74, 69−86.

24. Ishida, Y.; Nayak, S.; Mindell, J. A.; Grabe, M. A model of lysosomal pH regulation. J. Gen. Physiol. 2013, 141, 705−720.

25. Bright, G. R.; Fisher, G. W.; Rogowska, J.; Taylor, D. L. Fluorescence ratio imaging microscopy: temporal and spatial measurements of cytoplasmic pH. J. Cell Biol. 1987, 104, 1019−1033.

26. Madshus, I. H. Regulation of intracellular pH in eukaryotic cells. Biochem. J. 1988, 250, 1−8.

27. Wang, F.; Gómez-Sintes, R.; Boya, P. Lysosomal membrane permeabilization and cell death. Traffic 2018, 19, 918−931.

28. Porter, K.; Lin, Y.; Liton, P. B. Cathepsin B is up-regulated and mediates extracellular matrix degradation in trabecular meshwork cells following phagocytic challenge. PLoS One 2013, 8, e68668.

29. Casey, J. R.; Grinstein, S.; Orlowski, J. Sensors and regulators of intracellular pH. Nat. Rev. Mol. Cell Biol. 2010, 11, 50−61.

30. Hämälistö, S.; Stahl, J. L.; Favaro, E.; Yang, Q.; Liu, B.; Christoffersen, L.; Loos, B.; Guasch Boldú, C.; Joyce, J. A.; Reinheckel, T.; Barisic, M.; Jättelä, M. Spatially and temporally defined lysosomal leakage facilitates mitotic chromosome segregation. Nat. Commun. 2020, 11, 229.

31. Meng, J.; Liu, Y. C.; Xie, Z.; Qing, H.; Lei, P.; Ni, J. Nucleus distribution of cathepsin B in senescent microglia promotes brain aging through degradation of sirtuins. Neurobiol. Aging 2020, 96, 255−266.

32. Jiang, Z.; Lietz, C. B.; Podvin, S.; Yoon, M. C.; Toneff, T.; Hook, V.; O'Donoghue, A. J. Differential Neuropeptidomes of Dense Core Secretory Vesicles (DCSV) Produced at Intravesicular and Extracellular pH Conditions by Proteolytic Processing. ACS Chem. Neurosci. 2021, 12, 2385−2398.

33. Buttle, D. J.; Murata, M.; Knight, C. G.; Barrett, A. J. CA074 methyl ester: a proinhibitor for intracellular cathepsin B. Arch. Biochem. Biophys. 1992, 299, 377−380.

34. Choe, Y.; Leonetti, F.; Greenbaum, D. C.; Lecaille, F.; Bogyo, M.; Brömme, D.; Ellman, J. A.; Craik, C. S. Substrate profiling of cysteine proteases using a combinatorial peptide library identifies functionally unique specificities. J. Biol. Chem. 2006, 281, 12824−12832.

35. Poreba, M.; Groborz, K.; Vizovisek, M.; Maruggi, M.; Turk, D.; Turk, B.; Powis, G.; Drag, M.; Salvesen, G. S. Fluorescent probes towards selective cathepsin B detection and visualization in cancer cells and patient samples. Chem. Sci. 2019, 10, 8461−8477.

36. Yamamoto, A.; Tomoo, K.; Hara, T.; Murata, M.; Kitamura, K.; Ishida, T. Substrate specificity of bovine cathepsin B and its inhibition by CA074, based on crystal structure refinement of the complex. J. Biochem. 2000, 127, 635−643.

37. Yamamoto, A.; Hara, T.; Tomoo, K.; Ishida, T.; Fuji, T.; Hata, Y.; Murata, M.; Kitamura, K. Binding mode of CA074, a specific irreversible inhibitor, to bovine cathepsin B as determined by X-ray crystal analysis of the complex. J. Biochem. 1997, 121, 974−977.

38. Hsu, A.; Podvin, S.; Hook, V. Lysosomal Cathepsin Protease Gene Expression Profiles in the Human Brain During Normal Development. J. Mol. Neurosci. 2018, 65, 420−431.

39. O'Donoghue, A. J.; Eroy-Reveles, A. A.; Knudsen, G. M.;Ingram, J.; Zhou, M.; Statnekov, J. B.; Greninger, A. L.; Hostetter, D. R.; Qu, G.; Maltby, D. A.; Anderson, M. O.; Derisi, J. L.; McKerrow, J. H.; Burlingame, A. L.; Craik, C. S. Global identification of peptidase specificity by multiplex substrate profiling. Nat. Methods 2012, 9, 1095−1100.

40. Lapek, J. D., Jr.; Jiang, Z.; Wozniak, J. M.; Arutyunova, E.; Wang, S. C.; Lemieux, M. J.; Gonzalez, D. J.; O'Donoghue, A. J. Quantitative Multiplex Substrate Profiling of Peptidases by Mass Spectrometry. Mol. Cell. Proteomics 2019, 18, 968−981.

41. Vilar, S.; Cozza, G.; Moro, S. Medicinal chemistry and the molecular operating environment (MOE): application of QSAR and molecular docking to drug discovery. Curr. Top. Med. Chem. 2008, 8, 1555−1572.

42. Roy, U.; Luck, L. A. Molecular modeling of estrogen receptor using molecular operating environment. Biochem. Mol. Biol. Educ. 2007, 35, 238−243.

43. Schechter, I. Mapping of the active site of proteases in the 1960s and rational design of inhibitors/drugs in the 1990s. Curr. Protein Pept. Sci. 2005, 6, 501−512.

44. Yoon, M. C.; Solania, A.; Jiang, Z.; Christy, M. P.; Podvin, S.; Mosier, C.; Lietz, C. B.; Ito, G.; Gerwick, W. H.; Wolan, D. W.; Hook, G.; O'Donoghue, A. J.; Hook, V. Selective Neutral pH Inhibitor of Cathepsin B Designed Based on Cleavage Preferences at Cytosolic and Lysosomal pH Conditions. ACS Chem. Biol. 2021, 16, 1626− 1643.

45. Krupa, J. C.; Hasnain, S.; Nägler, D. K.; Ménard, R.; Mort, J. S. S2' substrate specificity and the role of His110 and His111 in the exopeptidase activity of human cathepsin B. Biochem. J. 2002, 361, 613−619.

46. Turk, D.; Podobnik, M.; Popovic, T.; Katunuma, N.; Bode, W.; Huber, R.; Turk, V. Crystal structure of cathepsin B inhibited with CA030 at 20-A resolution: A basis for the design of specific epoxysuccinyl inhibitors. Biochemistry 1995, 34, 4791−4797.

47. Katunuma, N. Structure-based development of specific inhibitors for individual cathepsins and their medical applications. Proc. Jpn. Acad., Ser. B 2011, 87, 29−39.

48. Jiang, M.; Meng, J.; Zeng, F.; Qing, H.; Hook, G.; Hook, V.; Wu, Z.; Ni, J. Cathepsin B inhibition blocks neurite outgrowth in cultured neurons by regulating lysosomal trafficking and remodeling. J. Neurochem. 2020, 155, 300−312.

49. Matarrese, P.; Ascione, B.; Ciarlo, L.; Vona, R.; Leonetti, C.; Scarsella, M.; Mileo, A. M.; Catricalà, C.; Paggi, M. G.; Malorni, W. Cathepsin B inhibition interferes with metastatic potential of human melanoma: an in vitro and in vivo study. Mol. Cancer 2010, 9, 207.

50. Asai, M.; Yagishita, S.; Iwata, N.; Saido, T. C.; Ishiura, S.; Maruyama, K. An alternative metabolic pathway of amyloid precursor protein C-terminal fragments via cathepsin B in a human neuroglioma model. FASEB J. 2011, 25, 3720−3730.

51. Yamashima, T.; Kohda, Y.; Tsuchiya, K.; Ueno, T.; Yamashita, J.; Yoshioka, T.; Kominami, E. Inhibition of ischaemic hippocampal neuronal death in primates with cathepsin B inhibitor CA-074: a novel strategy for neuroprotection based on 'calpain-cathepsin hypothesis'. Eur. J. Neurosci. 1998, 10, 1723−1733.

52. Yoshida, M.; Yamashima, T.; Zhao, L.; Tsuchiya, K.; Kohda, Y.; Tonchev, A. B.; Matsuda, M.; Kominami, E. Primate neurons show different vulnerability to transient ischemia and response to cathepsin inhibition. Acta. Neuropathol. 2002, 104, 267−272.

53. Zhang, L.; Fu, X. H.; Yu, Y.; Shui, R. H.; Li, C.; Zeng, H. Y.; Qiao, Y. L.; Ni, L. Y.; Wang, Q. Treatment with CA-074Me, a Cathepsin B inhibitor, reduces lung interstitial inflammation and fibrosis in a rat model of polymyositis. Lab. Invest. 2015, 95, 65−77.

54. Van Acker, G. J.; Weiss, E.; Steer, M. L.; Perides, G. Cause- effect relationships between zymogen activation and other early events in secretagogue-induced acute pancreatitis. Am. J. Physiol.: Gastrointest. Liver Physiol. 2007, 292, G1738−G1746.

55. Stoka, V.; Turk, V.; Turk, B. Lysosomal cathepsins and their regulation in aging and neurodegeneration. Ageing Res. Rev. 2016, 32, 22−37.

56. Tedelind, S.; Poliakova, K.; Valeta, A.; Hunegnaw, R.; Yemanaberhan, E. L.; Heldin, N. E.; Kurebayashi, J.; Weber, E.; Kopitar-Jerala, N.; Turk, B.; Bogyo, M.; Brix, K. Nuclear cysteine cathepsin variants in thyroid carcinoma cells. Biol. Chem. 2010, 391, 923−935.

57. Sloane, B. F.; Yan, S.; Podgorski, I.; Linebaugh, B. E.; Cher, M. L.; Mai, J.; Cavallo-Medved, D.; Sameni, M.; Dosescu, J.; Moin, K. Cathepsin B and tumor proteolysis: contribution of the tumor microenvironment. Semin. Cancer Biol. 2005, 15, 149−157.

58. Strelow, J. M. A Perspective on the Kinetics of Covalent and Irreversible Inhibition. SLAS Discov. 2017, 22, 3−20.

59. Tonge, P. J. Quantifying the Interactions between Biomole- cules: Guidelines for Assay Design and Data Analysis. ACS Infect. Dis. 2019, 5, 796−808.

Acknowledgements

Chapter 2, in full, is a reprint of the material as it appears in Biochemistry in American Chemical Society. Michael C. Yoon, Mitchell P. Christy, Von V. Phan, William H. Gerwick, Gregory Hook, Anthony J. O'Donoghue, and Vivian Hook, American Chemical Society, 2022. The dissertation author was co-author of this paper.

Chapter 3 Discovery of pH-Selective Marine and Plant Natural Product Inhibitors of Cathepsin B Revealed by Screening at Acidic and Neutral pH Conditions

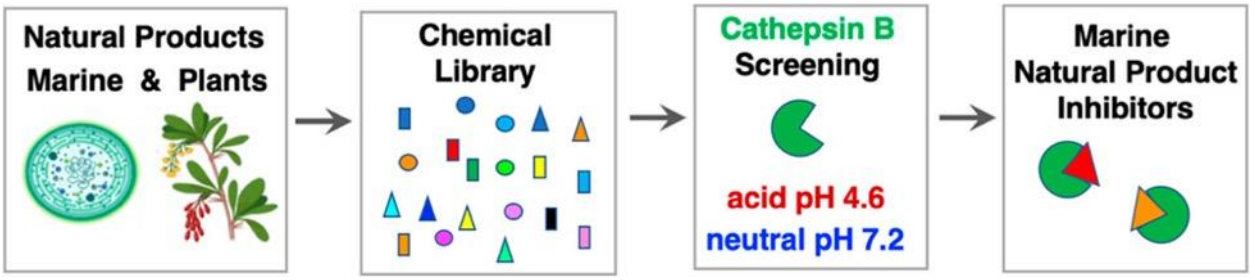

Figure 3.1 Chapter 3 Graphical Abstract. Dysregulation of cathepsin B, which involves the translocation of the enzyme from acidic pH lysosomes to the neutral pH cytosol, followed by the initiation of cell death and inflammation, occurs in numerous brain disorders. The wide difference in the acidic pH (4.6) of lysosomes compared to the neutral pH (7.2) of the cytosol suggests that screening at different pH conditions may identify pH-selective modulators of cathepsin B. Therefore, a collection of pure marine and plant natural product (NP) compounds, with synthetic compounds, was screened at pH 4.6 and pH 7.2 in cathepsin B assays, which led to the identification of GER-12 (Crossbyanol B) and GER-24 ((7*Z*,9*Z*,12*Z*)-octadeca-7,9,12-trien-5-ynoic acid) marine NP inhibitors at acidic pH but not at neutral pH. GER-12 was effective for the reversible inhibition of cathepsin B, with an IC_{50} of 3 μM. GER-24 had an IC_{50} of 16 μM and was found to be an irreversible inhibitor. These results show that NP screening at distinct biological pH conditions can lead to the identification of pH-selective cathepsin B modulators. These findings suggest that screening efforts for molecular probes and drug discovery may consider the biological pH environment of the target in the disease process.

3.1 Introduction

Cathepsin B is a lysosomal cysteine protease that is normally involved in molecular pathways that maintain cellular homeostasis through proteolysis and protein catabolism. (1,2) Dysregulation of cathepsin B has been implicated in brain disorders, including Alzheimer's disease (AD), traumatic brain injury (TBI), and others, (2) as well as cancer (3) and inflammatory diseases. (4,5) The inhibition of cathepsin B activity has been an area of interest to assess the mechanistic role of cathepsin B in disease pathogenicity and drug discovery efforts.

Evidence for the participation of cathepsin B in brain disorder pathogenicity has spurred much investigation into agents that inhibit cathepsin B to ameliorate dysfunctions associated with neurodegenerative diseases. Cathepsin B is involved in the inflammatory pathways and cell death pathways of AD and TBI, which are hypothesized to involve the leakage of lysosomal cathepsin B into the cytosol. (2) In vivo inhibition or gene silencing of cathepsin B in AD mouse models results in improved memory deficits and alleviates neuropathology. (6−8) In vivo studies of TBI mouse models show that gene knockout of cathepsin B improves motor dysfunction and reduces brain tissue loss. (9) Furthermore, clinical patient studies indicate elevated levels of cathepsin B in AD and TBI. (10,11) Thus, there is interest in the field to discover new cathepsin B inhibitors.

Marine and plant natural products (NP) provide rich sources of chemically diverse compounds that are biologically active and useful as active therapeutic agents. (12,13) Studies have shown that potent and effective protease inhibitors can be identified from NP sources. (14,15) For example, gallinamide A is a potent and selective inhibitor of the lysosomal cysteine protease cathepsin L discovered from marine cyanobacteria, (16) which has the potential to reduce SARS-CoV-2 infection. (17) Natural products, both marine and terrestrial, account for ∼50% of small-molecule drugs approved for the treatment of cancer and related conditions; this includes their

novel structures as well as their derivatives. (18) Thus, NP small-molecule libraries provide rich and novel resources to search for selective inhibitors of cathepsin B activity.

Screening of small molecules in drug discovery efforts has traditionally utilized optimal enzyme assay conditions for the assessment of effective modulators. However, drug targets in biological systems may be located at different pH conditions within subcellular and extracellular locations in diseases compared to normal healthy conditions. For example, cathepsin B in numerous brain disorders (2) and cancer (3) mediates disease deficits at abnormal neutral pH locations, including the cytosol and extracellular locations; however, cathepsin B is normally located in lysosomes containing an acidic internal pH. (1,2) The large pH differences between pathogenic and normal enzyme locations in biological systems suggest that drug discovery should target the pathogenic pH form of the enzyme in screening programs.

Significantly, our previous studies showed that cathepsin B is selectively inhibited by Z-Arg-Lys-AOMK at neutral pH 7.2 with a nanomolar (nM) potency, with no inhibition at acidic pH 4.6 at nM inhibitor concentrations. (19) The Z-Arg-Lys-AOMK inhibitor was designed using the pH 7.2 preferences of residues adjacent to the cleavage sites of cathepsin B proteolysis. Cleavage profiling analysis of cathepsin B using a defined library of diverse peptide substrates led to the design of the neutral-pH-selective substrate Z-Arg-Lys-AMC and an acid-pH-selective substrate Z-Glu-Lys-AMC. We propose that the use of these pH-selective substrates in compound screening efforts may uncover pH-selective modulators of cathepsin B.

For these reasons, the goal of this study was to evaluate the hypothesis for differential screening outcomes of natural product (NP) modulators, from marine and plant organisms, of cathepsin B by comparing screening assays conducted at the acidic lysosomal pH of 4.6 to those conducted at the neutral cytosolic pH of pH 7.2. Indeed, results of such a screening approach

identified NP inhibitors effective at acidic pH, but not at neutral pH, for inhibition of cathepsin B. These findings indicate that NP compound screening at distinct biological pH conditions can lead to the differential identification of cathepsin B enzyme modulators. Furthermore, the finding of pH-dependent NP modulators may reflect natural pH-dependent activities of NP molecules in their native ecological environments.

3.2 Results

3.2.1 Strategy to Assess Marine and Plant Natural Product (NP) Modulators of Cathepsin B at Acidic and Neutral pH Conditions Using pH-Selective Peptidic Substrates

A collection of purified natural product compounds consisting of 151 chemical molecules from marine organisms of cyanobacteria, Rhodophyta, sponge, mollusk, and Phaeophyceae combined with NP molecules from plants were utilized to discover pH-dependent inhibitory modulators of human cathepsin B proteolytic activity (Figure 3.2). Our unique cathepsin B screening strategy was conducted at the lysosomal pH of 4.6 and the cytosolic pH of 7.2. These cathepsin B assays used pH-selective substrates Z-Glu-Lys-AMC and Z-Arg-Lys-AMC that monitor cathepsin B activity at acidic pH 4.6 and neutral pH 7.2, respectively. (19) NP molecules displaying at least 50% inhibition of cathepsin B activity were further assessed for potency by calculating IC50 values, the reversible or irreversible mechanism of inhibition, and the specificity of the NP inhibition of cathepsin B compared to other cysteine cathepsins.

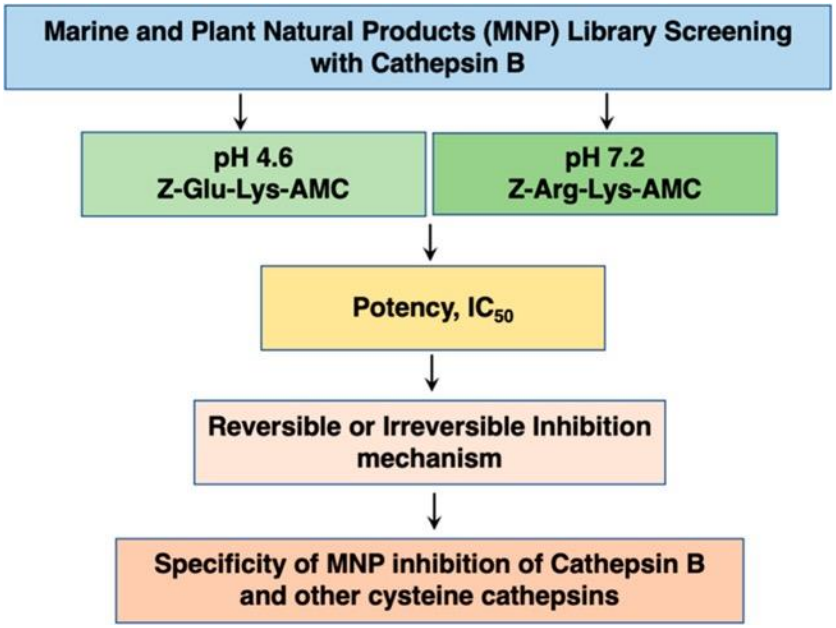

Figure 3.2 Workflow for screening marine and plant natural products (NP), and synthetic compounds, in cathepsin B assays at acidic and neutral pH conditions. A collection of pure NP compounds was assessed for modulators of human cathepsin B using acidic pH 4.6 and neutral pH 7.2 screening assay conditions. NP molecules that inhibited cathepsin B by >50% were characterized for potency, a reversible or irreversible inhibition mechanism, and specificity for cathepsin B compared to other cysteine cathepsins.

3.2.2 Inhibitors of Acidic Cathepsin B Activity Revealed through Screening a Collection of Pure NP Compounds at Neutral and Acidic pH Assay Conditions

The library of pure NPs from marine and plant organisms was assessed for the modulation of human cathepsin B activity. Assays were conducted by preincubating (30 min) each NP with cathepsin B at pH 7.2 and pH 4.6, followed by adding the substrate and monitoring the proteolytic activity. Screening of the NP compounds utilized pH-selective substrates Z-Arg-Lys-AMC at pH 7.2 and Z-Glu-Lys-AMC at pH 4.6, which led to the identification of several active compounds that showed varying degrees of cathepsin B modulation (Figure 3.3). Seven compounds were observed to significantly ($p < 0.05$) inhibit cathepsin B activity at pH 4.6 by at least 50% at NP concentrations of 1–10 μM, with no inhibition of cathepsin B at neutral pH 7.2 (Table 3.1). Furthermore, at pH 4.6, one NP molecule activated cathepsin B at least 200% or greater compared to controls (100%), with no effects at pH 7.2. Additionally, two other NPs activated cathepsin B

at pH 7.2 without effects at pH 4.6 (Table 3.1). These results illustrate the differential discovery of NP inhibitors or activators of cathepsin B activity at acidic pH 4.6 compared to neutral pH 7.2. Inhibition of cathepsin B has been predicted in the field to ameliorate several conditions of brain disorders, cancer, infectious disease, and others. (2−9) Therefore, we continued with the characterization of NP inhibitors of cathepsin B.

Table 3.1 Identification of pH-Selective Marine Natural Product Modulators of Cathepsin B[a]

Natural Product Compound	Concentration	Cathepsin B Activity		Compound Structure
		pH 4.6 Z-E-K-AMC	pH 7.2 Z-R-K-AMC	
None	0	100%	100%	
GER-12	1.6 μM (2 μg/ml)	43 ± 5 *	78 ± 15	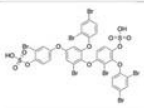
GER-24	8.0 μM (2 μg/ml)	23 ± 1 *	117 ± 5	
GER-151	5.2 μM (2 μg/ml)	205 ± 21 *	109 ± 11	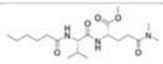
GER-163	2.2 μM (2 μg/ml)	48 ± 7 *	118 ± 11	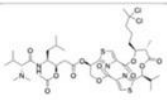
GER-165	8.6 μM (2 μg/ml)	47 ± 4 *	120 ± 13	
GER-169	4.4 μM (2 μg/ml)	38 ± 7 *	128 ± 7	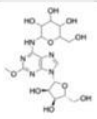
GER-170	6.0 μM (2 μg/ml)	50 ± 4 *	118 ± 3	
ST024730	2.0 μM	50 ± 7 *	173 ± 33	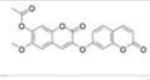
ST024752	2.0 μM	111 ± 33	241 + 21 *	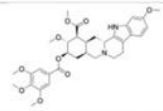
ST024772	2.0 μM	73 ± 22	205 ± 21 *	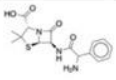

[a]A collection of pure marine natural products (purified) were assessed for the modulation of human cathepsin B activity (with preincubation) by screening them at pH 4.6 and pH 7.2 using pH-selective substrates of Z-E-K-AMC and Z-R-K-AMC, respectively. the asterisk indicates compounds that resulted in a significant inhibition of <50% (blue) or activation of >200% (green) with $*p < 0.05$.

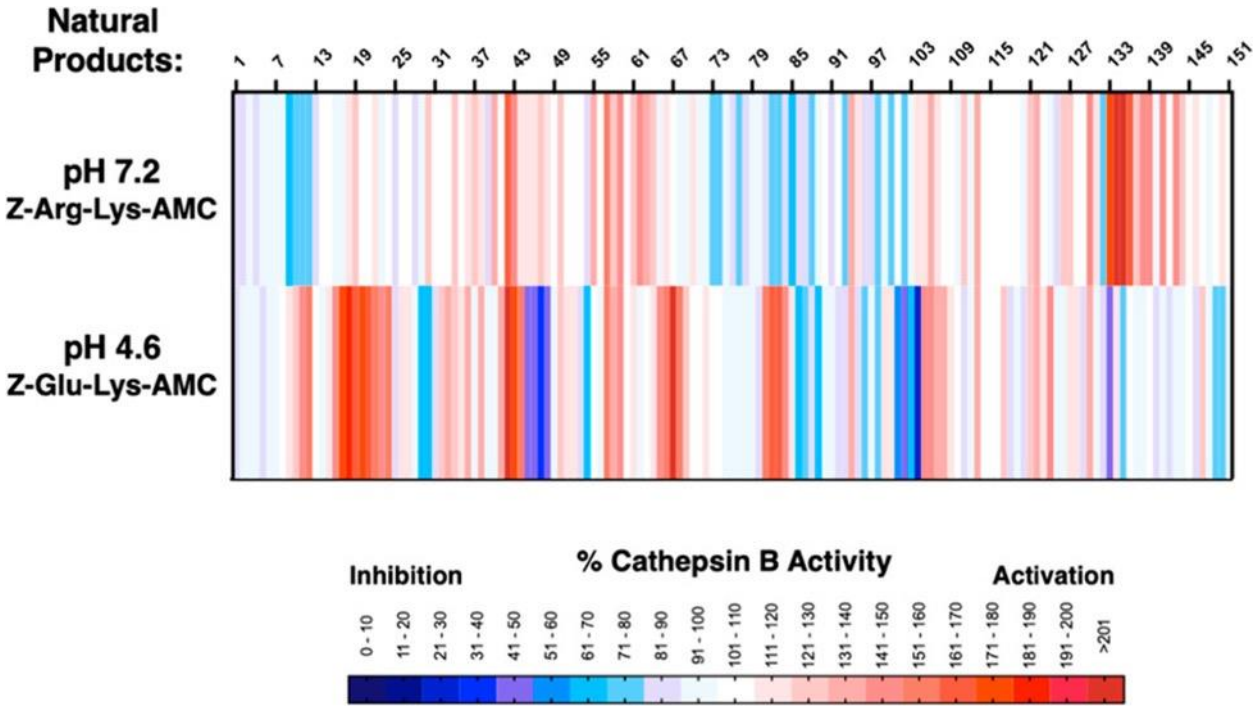

Figure 3.3 Heat map of the screening data illustrates pH-selective modulators of cathepsin B. NP molecules were preincubated with human cathepsin B (30 min) and then assessed for the modulation of proteolytic activity at pH 4.6 with the Z-E-K-AMC substrate and at pH 7.2 with the Z-R-K-AMC substrate. Modulators resulted from screening marine and plant natural products and synthetic compounds. Modulators of cathepsin B activity are illustrated in a heat map, which shows the inhibition (blue) and activation (red) by NPs (1–10 μM) compared to the controls (100%, no inhibitor).

3.2.3 GER-12 (Crossbyanol B) and GER-24 ((7*Z*,9*Z*,12*Z*)-Octadeca-7,9,12-trien-5-ynoic Acid) NP Inhibition of Cathepsin B at Acidic pH

To evaluate the seven inhibitors at the same concentration, inhibitors were tested at 5 μM since the initial inhibitor testing was performed in the micromolar range (shown in Table 3.1). Reassessment of the seven inhibitors (without preincubation) resulted in two compounds, GER-12 and GER-24, that demonstrated the inhibition of cathepsin B (Table 3.2). Therefore, continued studies examined GER-12 and GER-24 in concentration-dependent studies (Figures 3.4 and 3.5, respectively).

Table 3.2 Inhibitors with No Preincubation in Cathepsin B Assays at pH 4.6 with the Z-E-K-AMC Substrate[a]

inhibitor (5 μM)	% control cathepsin B activity
none	100
GER-12	28
GER-24	80
GER-163	103
GER-165	112
GER-169	99
GER-170	101
ST024730	110

[a]The indicated NP molecules were assessed at 5 μM, with no preincubation of inhibitor and cathepsin B enzyme, in assays using the substrate Z-E-K-AMC at pH 4.6.

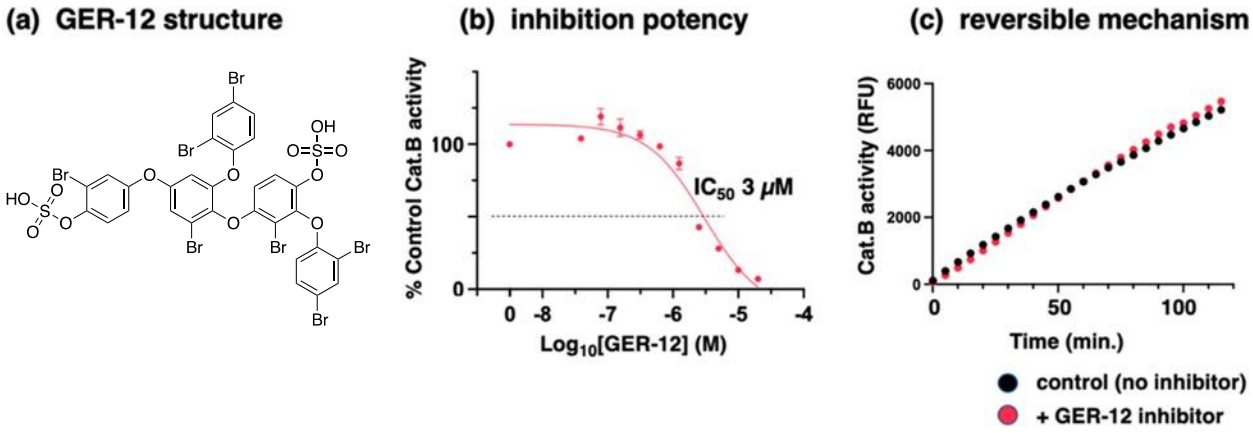

Figure 3.4 GER-12 (crossbyanol B) potency and reversible inhibition of cathepsin B. (a) The GER-12 NP structure, (b) the potency for inhibition illustrated by its IC_{50} value, and (c) the reversible mechanism of inhibition are illustrated. Potency was assessed at different concentrations of GER-12 to assess IC_{50} values for the inhibition of cathepsin B, and the reversible mechanism of GER-12 inhibition was determined by dilution experiments, as explained in the section Experimental Procedures.

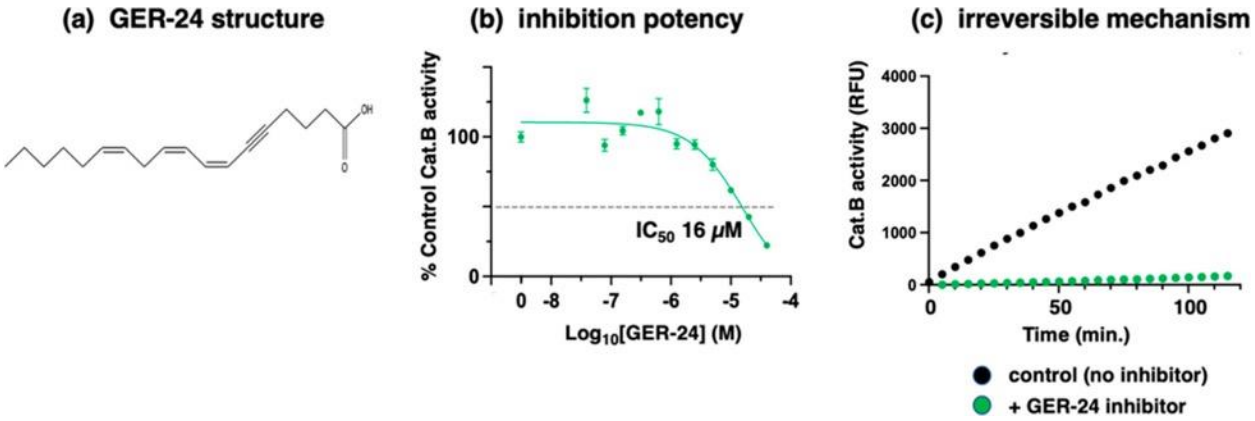

Figure 3.5 GER-24 ((7Z,9Z,12Z)-octadeca-7,9,12-trien-5-ynoic acid) potency and irreversible inhibition of cathepsin B. (a) The GER-24 NP structure, (b) the potency for inhibition illustrated by its IC_{50} value and (c) the irreversible mechanism of inhibition are illustrated. Potency was assessed at different concentrations of GER-12 for the inhibition of cathepsin B, as assessed by the IC_{50} value, and the irreversible mechanism of GER-12 inhibition was determined by dilution experiments, as explained in the section Experimental Procedures.

The potencies of the NPs were assessed by calculating the concentration of each compound that inhibited cathepsin B by 50% (IC_{50} value). The GER-12 inhibition of cathepsin B at pH 4.6 had an IC_{50} value of 3 μM (Figure 3.4b). The GER-24 inhibition of cathepsin at pH 4.6 had an IC_{50} value of 16 μM (Figure 3.5b). These results show the effective inhibition of cathepsin B at acidic pH by GER-12 and GER-24 at micromolar levels of inhibitors.

3.2.4 GER-12 Reversible Inhibition and GER-24 Irreversible Inhibition of Cathepsin B

The mechanism of GER-12 and GER-24 inhibition was assessed by preincubating cathepsin B (at 100× the enzyme concentration for the assay) for 30 min with the inhibitor (at 10× times its IC_{50}). A 100-fold dilution was then performed on the mixture, and the Z-E-K-AMC substrate was added to the mixture to the monitor the proteolytic activity over a time-course up to 120 min.

After GER-12 preincubation, the progress of cathepsin B activity in the time course was similar to that for the enzyme incubated alone (no inhibitor), demonstrating reversible inhibition by GER-12 (Figure 3.4c). Further assessment of the reversible inhibition showed that GER-12

inhibition of cathepsin B was not observed in the presence of the nonionic detergent triton X-100 (Figure 3.S1).

After GER-24 preincubation, cathepsin B inhibition occurred over the entire time course, which demonstrated the irreversible inhibition of cathepsin B by GER-24 (Figure 3.5c). These data demonstrate the different reversible and irreversible inhibition mechanisms of GER-12 and GER-24, respectively.

3.2.5 Kinetics of GER-12 and GER-24 Inhibition

Kinetics of GER-12's reversible inhibition of cathepsin B was assessed by Michael–Menten and inverse Lineweaver–Burk plots (Figure 3.S2). A K_i value of 1.4 μM was calculated for the noncompetitive inhibition of cathepsin B by GER-12. GER-24's irreversible inhibition of cathepsin B was observed to possess the kinetic constant k_{inact}/K_I of 4.2×10^5 μM^{-1} s^{-1} (Figure 3.S3).

3.2.6 GER-12 and GER-24 Inhibition of Cathepsin B Compared to Other Cysteine Cathepsins

GER-12 was evaluated for the inhibition of cathepsin B compared to members of the cysteine cathepsin family consisting of cathepsins C, H, K, L, S, V, and X. At 10 μM (pH 4.6), GER-12 inhibited cathepsin B up to 14% of the control with no inhibitor (100%) and inhibited cathepsins C, H, K, L, S, V, and X up to 26%, 8%, 21%, 89%, 13%, 3%, and 54% compared to control (Table 3.3). These data indicate that GER-12 inhibits several cysteine cathepsins in addition to cathepsin B.

Table 3.3 Evaluation of the GER-12 and GER-24 Inhibition of Cathepsin B Compared to Other Cysteine Cathepsin Proteases[a]

protease	GER-12 (10 μM) % control activity (100%, no inhibitor)	GER-24 (50 μM) % control activity (100%, no inhibitor)
cathepsin B	14	0
cathepsin C	26	65
cathepsin H	8	21
cathepsin K	21	7
cathepsin L	89	84
cathepsin S	13	0
cathepsin V	3	17
cathepsin X	53	67

[a]GER-12 and GER-24 inhibition (no preincubation) of cathepsin B and the cysteine cathepsins C, H, K, L, S, V, and X were compared. Assay conditions (no preincubation) for these human cysteine cathepsins are provided in the procedures.

At 50 μM (pH 4.6), GER-24 inhibited cathepsin B up to 0% of control (100%) and inhibited cathepsins C, H, K, L, S, V, and X up to 65% 21%, 7%, 84%, 0%, 17%, and 67% compared to the no-inhibitor control (100%) (Table 3.3). Thus, GER-24 at a high concentration of 50 μM inhibits cathepsin B and several cysteine cathepsin proteases.

These data show that the inhibition of cathepsin B by GER-12 and GER-24 occurs without selectivity, as shown by inhibition of other cysteine cathepsin proteases.

3.3 Discussion

Results of this study highlight the incorporation of biological pH conditions for screening NP modulators of cathepsin B at acidic pH compared to neutral pH conditions. The use of different pH screening conditions for cathepsin B resulted in the identification of different NP compounds that inhibited cathepsin B at lysosomal acidic pH 4.6 compared to cytosolic neutral pH 7.2. These findings indicate the importance of considering the distinct pH environments of the biological locations of enzyme targets in the design of screening conditions to identify NP or other types of chemical modulators. Most chemical library screens for enzyme modulators utilize the optimum in vitro enzymatic assay conditions, including pH. However, differential pH properties of

enzymes, such as those for cathepsin B, suggest that the target enzyme may be treated as distinct types of enzymes at different pH levels. Our previous finding of pH-selective modulators of cathepsin B may reflect the enzyme's pH-selective cleavage properties at acid and neutral pH conditions. (19) The discovery and development of modulators through chemical screening will benefit from specifying the pH condition of the enzyme target to address pH-specific cellular or physiological functions.

It is of interest that cathepsin B displays pH-dependent properties for inhibitors through compound screening at acidic pH 4.6 and neutral pH 7.2 conditions. Protease inhibitors often mimic peptide substrate-binding properties with the protease enzyme. The substrate profiling analysis of cathepsin B showed its pH-dependent preferences for amino acid residues adjacent to the P1–P1′ substrate cleavage sites. (19) Notably, glutamate (Glu) is the preferred P2 residue of cathepsin B at acidic pH 4.6, but the Glu residue is not preferred at pH 7.2. It is of interest that GER-24 possesses a functional group of −CH2–CH2–COOH that resembles the Glu side chain of substrates that interact with the S2 subsite (Glu-245) of the enzyme. (19) Thus, it is possible that the −CH2–CH2–COOH group of GER-24 may interact with cathepsin B at its S2 subsite. With respect to GER-12, its inhibitory activity was not observed in the presence of the detergent triton X-100, suggesting nonionic detergent-dependent interactions; however, a future structural analysis will be needed. Interactions of inhibitors with target proteases are best assessed by structural analysis via X-ray crystallography, which has, for example, been achieved for the selective CA-074 inhibitor of cathepsin B. (20−22) CA-074 interacts with the enzyme's active site region at the S2–S2′ subsites. It will be of interest to assess pH-selective inhibitor interactions with cathepsin B through future structural analyses.

Proteases such as cathepsin B may have dual functions within acidic lysosomes and extra-lysosomal neutral cellular compartments, including the cytosol, nuclei, and extracellular locations. (1,2,23) Cathepsin B, for example, displays distinct substrate and inhibitor specificity at acidic pH compared to neutral pH functions. (19,24) Therefore, it will be valuable to develop inhibitors of neutral pH cathepsin B to allow the assessment of its functions in extra-lysosomal locations, including cell death, inflammation, and cancer. Selective inhibitors of acidic cathepsin B functions will enhance the understanding the enzyme's role in protein health, namely proteostasis, which is important for cellular functions in health and disease. Furthermore, pH-selective activators may be utilized to gain an additional understanding of the function of cathepsin B.

Furthermore, the results of our NP screens for modulators of cathepsin B indicate that marine natural product molecules such as GER-12 (crossbyanol B from cyanobacteria) and GER-24 ((7Z,9Z,12Z)-octadeca-7,9,12-trien-5-ynoic acid from Rhodophyta) may possess pH-dependent modulating functions for target enzymes. This study opens avenues to assess natural products for the pH-selective inhibition or activation of proteases and enzymes. Therefore, natural product screening under different biological pH conditions, as demonstrated by this study, can be an important avenue to advance our understanding of the multiple roles of cathepsin B and enzymes in cellular compartments of differing pH conditions.

In summary, the results of this study indicate that using different pH conditions to screen NP chemical libraries can lead to the identification of pH-selective modulators of targeted protease enzymes in designated biological pH environments.

3.4 Experimental Procedures

Experimental procedures are summarized here. Detailed descriptions of protocols are provided in the Supporting Information.

3.4.1 Materials and Reagents

The sources of enzymes, peptide substrates, and reagents are provided in the Supporting Information.

3.4.2 Collection of Purified Marine and Plant Natural Products (NP)

Natural products have been collected and purified from multiple marine organisms of cyanobacteria, Rhodophyta, sponges, mollusk, Phaeophyceae, and plant sources. The list of NP molecules investigated is provided in Supporting Information Table 3.S1. Marine NP compound stocks were 1 mg/mL and were screened at a final concentration of 2 μg/mL. The plant NP compounds stocks were at 1 mM and were screened at a final concentration of 2 μM. The structures of the NP molecules are provided in Supporting Information Table 3.S2, which indicates diverse NP chemical structures. These molecules were utilized for screening in the cathepsin B assays.

3.4.4 NP Screening Conducted at pH 4.6 and pH 7.2 to Identify Modulators of Cathepsin B

Assays of cathepsin B (activated) with 151 pure marine natural products were conducted in triplicate with 5 mM DTT, 1 mM EDTA, 100 mM NaCl, and 1.5% DMSO using 0.2 ng/μL cathepsin B at pH 4.6 in 40 mM citrate phosphate buffer with 60 μM Z-Glu-Lys-AMC substrate and at pH 7.2 in 40 mM citrate phosphate buffer with 60 μM Z-Arg-Lys-AMC substrate. Each pure NP (151 compounds in total) was preincubated with the enzyme for 30 min at RT. To the mixture was then added the substrate, and the sample was incubated at RT for 30 min. Fluorescence was measured at 360 nm excitation and 460 nm emission. Cathepsin B activity in the absence and presence of each NP was assessed for significance using Student's *t* test with $p < 0.05$. As a positive inhibitor control, each screening plate included CA-074 (1 μM final concentration), a known selective inhibitor of cathepsin B; (21,22) CA-074 is a natural product originally isolated from *Aspergillus japonicus*. (25)

It is noted that the Z-Glu-Lys-AMC substrate at pH 4.6 and the Z-Arg-Lys-AMC substrate at pH 7.2 had similar K_m values of 460 and 429 μM, respectively. These similar K_m values of both substrates at a concentration of 60 μM in the screening assays represent equivalent substrate conditions.

3.4.4 Potency of NP Inhibition of Cathepsin B as Assessed by IC_{50} Values

GER-12 (crossbyanol B) and GER-24 ((7*Z*,9*Z*,12*Z*)-octadeca-7,9,12-trien-5-ynoic acid) at different concentrations were incubated with cathepsin B (activated) without preincubation in cathepsin B assay conditions (described above). IC_{50} values were calculated as the inhibitor concentration that reduced cathepsin B activity by 50%. Curve-fitting of the inhibition curves and the calculation of IC_{50} values were performed with Prism software (version 8). Confidence intervals of 95% were obtained for GER-24 and GER-12 at 7.9–36.5 and 2.1–4.4 μM, respectively, using a nonlinear regression curve fit model.

3.4.5 Assessment of Inhibitors for a Reversible or Irreversible Mechanism of Inhibition

Cathepsin B (100×) was preincubated with GER-12 or GER-24 at 10× the determined IC_{50} concentration for 30 min at room temperature (25 °C). Then, a 1:100 dilution of the mixture was performed. The Z-Glu-Lys-AMC substrate was added to the diluted mixture, and the fluorescence was monitored for proteolytic activity every minute for 2 h. The lack of inhibition of cathepsin B activity following dilution indicates a reversible inhibitory mechanism. The reduction of cathepsin B activity following dilution indicates an irreversible inhibitory mechanism.

3.4.6 Kinetics of the Reversible and Irreversible Inhibition of Cathepsin B

GER-12 reversible inhibition kinetics was assessed by Michaelis–Menten and Lineweaver–Burke inverse plots to determine the K_i value for the noncompetitive inhibition of cathepsin B by GER-12 using the equation ${}^{app}V_{max} = V_{max}(K_i /[I]_o + K_i))$. (26) The irreversible inhibition by GER-24 was assessed by determining the K_I value as we previously described. (19)

3.4.7 Evaluation of GER-12 and GER-24 for the Inhibition of Cathepsin B Compared to Other Cysteine Cathepsins

GER-12 at 10 μM and GER-24 at 50 μM were evaluated for the inhibition of cathepsin B compared to cathepsins C, H, K, L, S, V, and X. Assay conditions for these cathepsin proteases are described in the Supporting Information.

3.5 Supporting Information

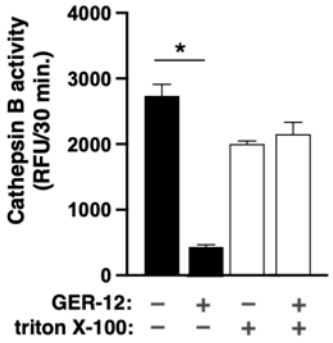

Figure 3.S1 Effect of triton X-100 on GER-12 inhibition of cathepsin B. GER-12 (10 μM final concentration) inhibition of cathepsin B was assessed in the absence and presence of 0.01% triton X-100. Error bars indicate standard deviation (n=3). Significance is indicated by *p<0.05 (by student's t-test)

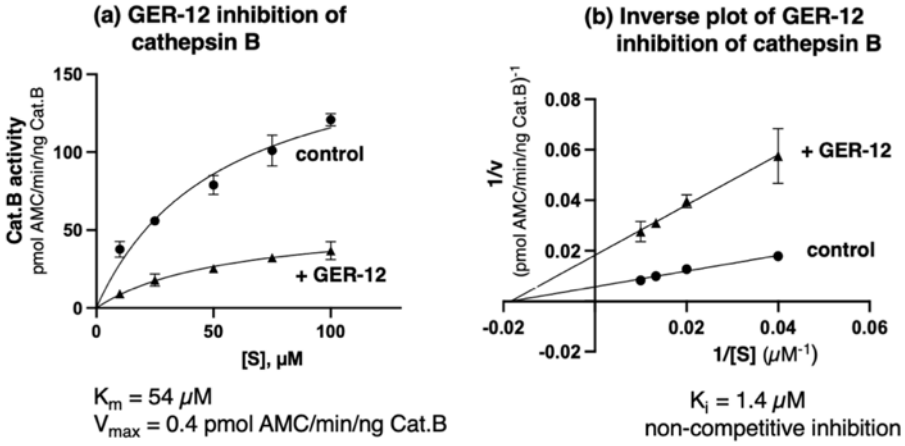

Figure 3.S2 GER-12 reversible kinetics for inhibition of cathepsin B. (a) GER-12 inhibition of cathepsin B activity. Cathepsin B activity was assayed with Z-Phe-Arg-AMC substrate over a range of concentrations in the absence and presence of the GER-12 inhibitor at 3 μM. The graph determined Km of 54 μM Z-Phe-Arg-AMC and Vmax of 0.4 pmol AMC/min/ng cathepsin B. Error bars indicate standard deviation. (b) Inverse plot of GER-12 inhibition of cathepsin B. Data for 1/[S] and 1/v was plotted in an inverse plot in Lineweaver-Burk format and the Ki was calculated as 1.4 μM. Error bars indicate standard deviation.

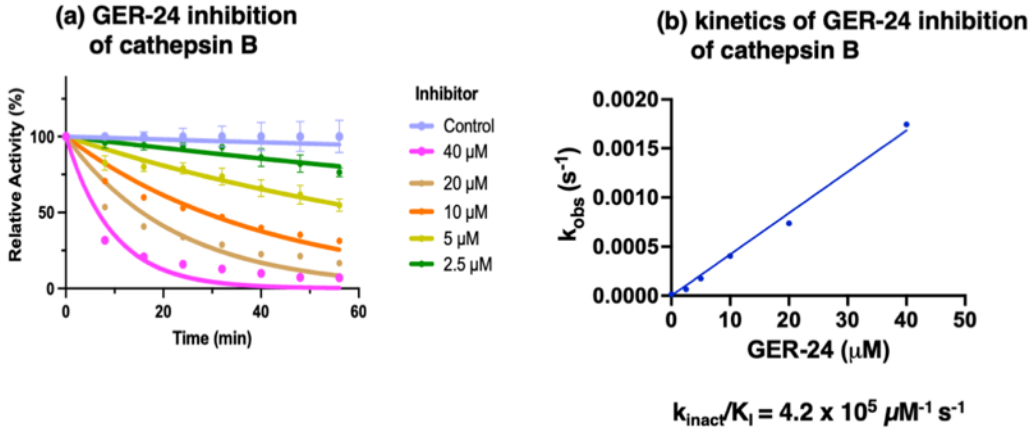

Figure 3.S3 GER-24 irreversible kinetics for inhibition of cathepsin B. (a) GER-24 inhibition of cathepsin B: inhibitor concentrations and time-course study. GER-24 inhibition of cathepsin B was assessed over a range of GER-24 concentrations in time-course studies. (b) GER-24 inhibition of cathepsin B and k_{obs} values. The k_{obs} values for inhibition of cathepsin B at different concentrations of GER-24 was plotted and K_{inact}/K_I was calculated as 4.2 x $10^5 \mu M^{-1} s^{-1}$.

3.6 Supplemental Experimental Procedures

3.6.1 Materials and reagents.

Recombinant human cysteine cathepsins B, L, S, V, C, H, and X, and thermolysin, were purchased from R & D Systems (Minneapolis, MN), and cathepsin K was purchased from Abcam (Cambridge, MA). Catalogue numbers are listed: cathepsin B (R & D #953-CY-010), cathepsin L (R & D #952-CY-010), cathepsin S (R & D #1183-CY-010), cathepsin V (R & D #1080-CY-010), cathepsin C (R&D #1071-CY-010), cathepsin H (R & D #75116-CY- 010), cathepsin X (R & D #934-CY-010), thermolysin (R & D #3097-ZN), and cathepsin K (ab157067). Assays utilized buffer components of citric acid monohydrate (Merck #1.00244.0500, Burlington, MA), sodium phosphate dibasic anhydrous (EMD #SX-072305, Burlington, MA), sodium acetate (Fisher Scientific #BP-333-500, Fair Lawn, NJ), dithiothreitol (DTT) (Promega #V351, Madison WI), sodium chloride (Fisher Chemical #S271-1, Pittsburgh, PA), and EDTA (Calbiochem #324503, Burlington, MA). Fluorogenic substrates of Z-Glu-Lys- AMC and Z-Arg-Lys-AMC were custom synthesized by Genscript (Piscataway, NJ). Purchase of Z-Phe-Arg-AMC (Anaspec #AS-24906,

Fremont, CA), Gly-Arg-AMC (Bachem #4002196, Torrance, CA), Arg-AMC (Bachem #I-1050, Torrance, CA), and MCA-Arg-Pro-Pro-Gly-Phe-Ser- Ala-Phe-Lys(Dnp)OH (CPC Scientific #AMYD-111A, San Jose, CA) provided substrates for the various cysteine cathepsin enzymes. CA-074 (Sigma/Millipore #205531, Burlington, MA) and phosphoramidon (R & D #6333) inhibitors were also purchased.

3.6.2 Activation of cathepsin B and other cysteine cathepsins.

Recombinant pro-cathepsin B was activated to its mature enzyme form by incubation in activation buffer of 20 mM Na-Acetate, pH 5.5, 5 mM DTT, 1 mM EDTA, and 100 mM NaCl at 37o C for 30 minutes. Cathepsin S, and V were activated in the same activation conditions as cathepsin B. Cathepsin H was activated with 50 μg/ml thermolysin in 50 mM MES pH 6.5, 10 mM CaCl2, 150 mM NaCl at room temperature for 3 hours followed by addition of phosphoramidon to 1 mM (per R&D Systems protocol). Cathepsin C was activated with 2 ng/μl cathepsin L, in conditions 25 mM MES pH 6, 5 mM DTT, 50 mM NaCl at room temperature for 60 min. Comparison of cathepsin B activity in the presence of each MNP was assessed by student's t-test with $p<0.05$ for significance.

3.6.3 Pure marine natural product (MNP) screen to identify modulators of cathepsin B conducted at pH 4.6 and pH 7.2.

Assays of cathepsin B activity with 151 pure marine natural products were conducted in conditions with 0.2 ng/μl cathepsin B, 60 μM Z-Glu-Lys-AMC, and Z-Arg-Lys-AMC in 40 mM citrate phosphate at pH 4.6 and pH 7.2 respectively, and Z-Phe-Arg-AMC at pH 4.6 and 7.2, 5 mM DTT, 1 mM EDTA, 100 mM NaCl, and 1.5% DMSO. Assays were performed in 96-well plates at room temperature (25o C) in a total volume of 100 μl in triplicates. Marine natural product compounds concentrations ranging from 1.6 to 12.6 μM, with the exception of two compounds S6 assayed around 35 μM and one compound at 60.2 μM, were added to enzyme in the absence of substrate and was incubated at room temperature (25^{o}C) for 30 minutes, followed by the addition

of substrate. Fluorescence was quantified at 30 minutes and 60 minutes after substrate was added, by a Biotek Synergy HTX microplate reader with excitation at 360 nm, and emission at 460 nm, gain 50, top optics and read height at 1 mm. Prism GraphPad software was used to analyze data. Comparison of cathepsin B activity in the absence and presence of each MNP was assessed by student's t-test with $p<0.05$ for significance.

3.6.4 Potency of MNP inhibition of cathepsin B assessed by IC50 values.

Evaluation of the effectiveness for GER-12, GER-24, as well as GER-163, GER-165, GER-169, GER-170, and ST024730 for inhibition of cathepsin B was conducted at pH 4.6. Marine natural product concentrations ranged from 0.039 to 40 μM. The inhibitors were added to the enzyme at the start of the incubation period, at room temperature, and thus there was no preincubation of cathepsin B with inhibitor. A vehicle control assay without inhibitor contained cathepsin B, Z-Glu-Lys-AMC substrate, and 2% v/v DMSO. Cathepsin B assays with marine natural products were conducted with 0.2 ng/μl cathepsin B, 40 μM Z-Glu-Lys-AMC, in 40 mM citrate phosphate at pH 4.6, 5 mM DTT, 1 mM EDTA, 100 mM NaCl, and 2% DMSO, in 96-well plates at RT (25o C) in a total volume of 100 μl in triplicate. IC50 values were calculated as the concentration of inhibitor that reduced cathepsin B by 50%.

3.6.5 Assessment of inhibitors for reversible or irreversible mechanism of inhibition.

Cathepsin B was preincubated with GER-12 or GER-24 at 10 times the determined IC50 concentration for 30 minutes at room temperature (25ºC), followed by a 1:10 dilution and addition of Z-Glu-Lys-AMC substrate and monitoring fluorescence for proteolytic activity every minute for 2 hours. Lack of inhibition of cathepsin B activity following dilution indicates reversible inhibitory mechanism. Reduction of cathepsin B activity following dilution indicates irreversible inhibitory mechanism.

3.6.6 Evaluation of GER-12 and GER-24 for inhibition of cathepsin B compared to other cysteine cathepsins.

GER-12 at 10 μM, and GER-24 at 50 μM, were evaluated for inhibition of cathepsin B compared to cathepsins C, H, K, L, S, V, and X. Inhibitor, cathepsin enzyme, and substrate were incubated in 40 mM citrate phosphate at pH 4.6, 5 mM DTT, 1 mM EDTA, 100 mM NaCl, and 2% DMSO, in 96-well plates at room temperature (25ºC) in a total volume of 100 μl in triplicate. Cathepsin K (0.07 ng/μl), cathepsin L(0.004 ng/μl), cathepsin S (0.6 ng/μl), and cathepsin V (0.08 ng/μl) were assayed with 40 μM Z-F-R-AMC substrate. Cathepsin H (1 ng/μl), cathepsin C (1 ng/μl), and cathepsin X (0.1 ng/μl) were assayed with substrates consisting of 40 μM Arg-AMC, Gly-Arg-AMC, and MCA-Arg-Pro-Pro-Gly-Phe-Ser-Ala-Phe-Lys(Dnp)OH, respectively. Inhibition was determined by comparing reduction of fluorescence values to the DMSO vehicle control as % control activity (no inhibitor).

Table 3.S1 Natural Product Compound Structures[a]

GER-1	GER-6	GER-7	GER-8	GER-11
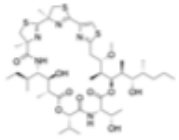	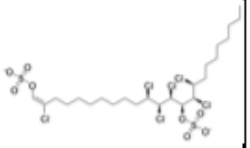	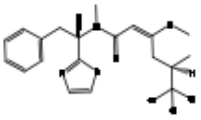	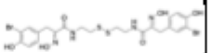	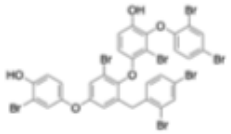
GER-12	GER-19	GER-20	GER-21	GER-24
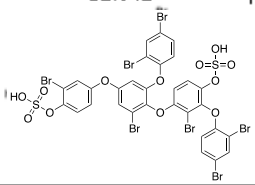	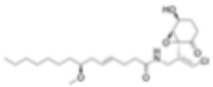	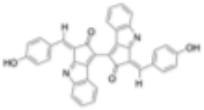	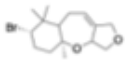	
GER-26	GER-29	GER-33	GER-35	GER-37
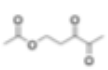	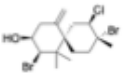	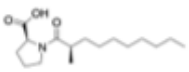	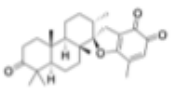	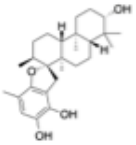
GER-38	GER-40	GER-43	GER-44	GER-46
	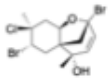	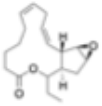	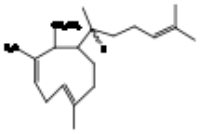	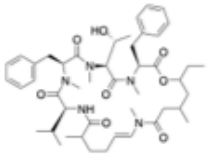
GER-48	GER-50	GER-54	GER-57	GER-61
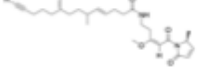	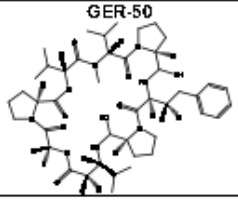	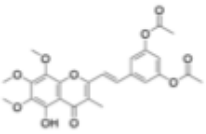	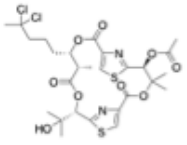	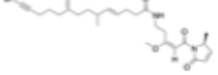
GER-62	GER-63	GER-69	GER-71	GER-72
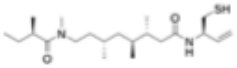	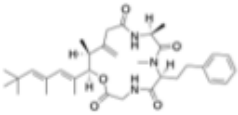	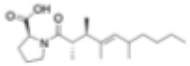	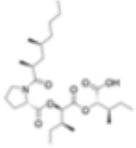	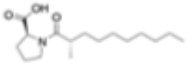
GER-73	GER-74	GER-76	GER-79	GER-82
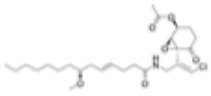	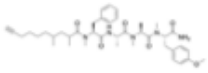	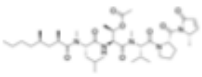	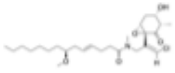	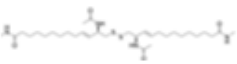

Table 3.S1 Natural Product Compound Structures[a] Continued

GER-83	GER-85	GER-86	GER-87	GER-88
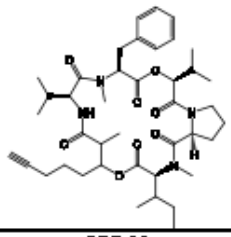	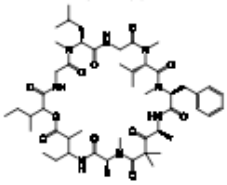	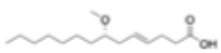	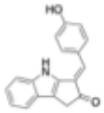	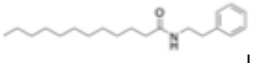
GER-89	GER-90	GER-91	GER-92	GER-93
	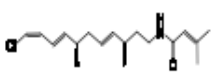		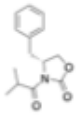	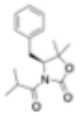
GER-94	GER-95	GER-96	GER-97	GER-98
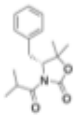	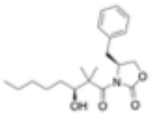	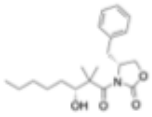	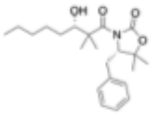	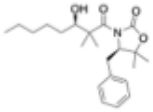
GER-99	GER-100	GER-101	GER-102	GER-103
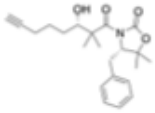	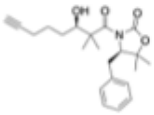		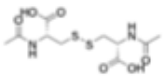	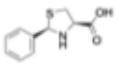
GER-104	GER-105	GER-106	GER-107	GER-108
	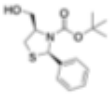	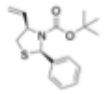	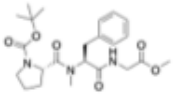	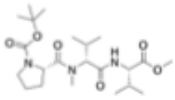
GER-109	GER-110	GER-111	GER-113	GER-114
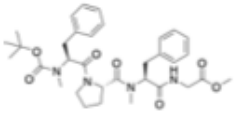	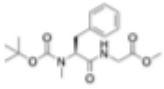	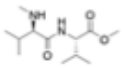	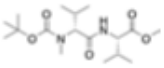	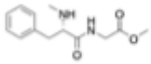
GER-117	GER-119	GER-120	GER-121	GER-122
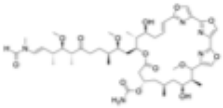	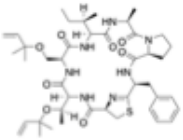	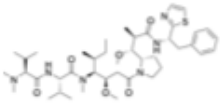	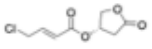	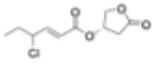
GER-125	GER-129	GER-130	GER-132	GER-133
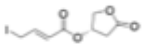	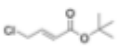	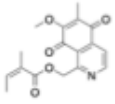	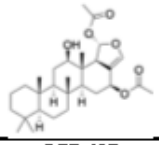	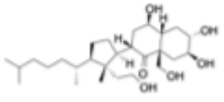
GER-134	GER-135	GER-136	GER-137	GER-138

Table 3.S1 Natural Product Compound Structures[a] Continued

GER-139	GER-140	GER-141	GER-144	GER-145
	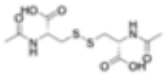	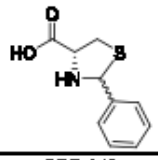	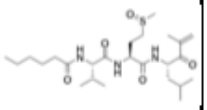	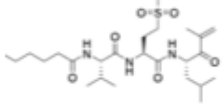
GER-146	GER-147	GER-148	GER-149	GER-151
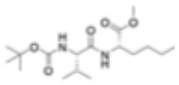	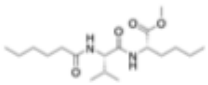	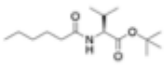	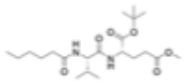	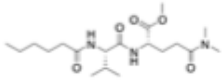
GER-152	GER-153	GER-154	GER-155	GER-156
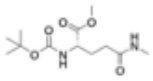	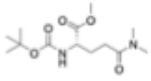	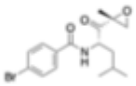	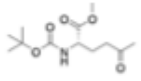	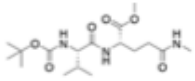
GER-157	GER-159	GER-160	GER-161	GER-162
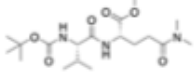	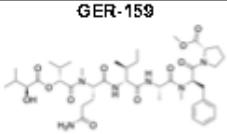	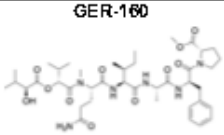	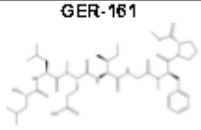	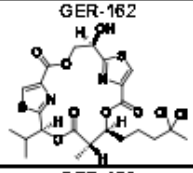
GER-163	GER-165	GER-166	GER-167	GER-168
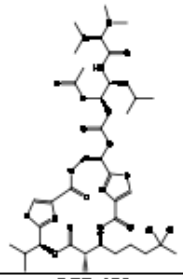	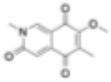	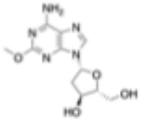		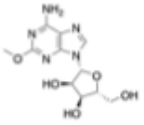
GER-169	GER-170	GER-171	GER-172 unknown structures under study	GER-173 unknown structures under study
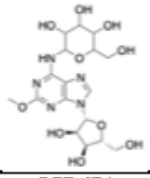	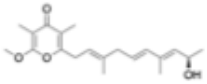	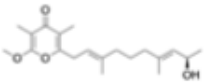		
GER-174	GER-175	ST002792	ST005095	ST005141
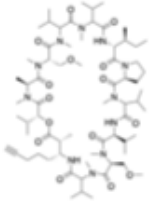		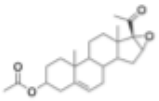	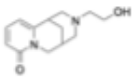	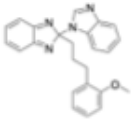
ST005173	ST005176	ST009496	ST009819	ST009844
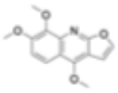	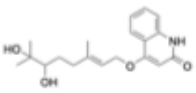	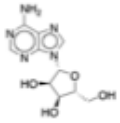	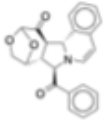	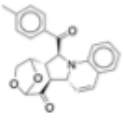

Table 3.S1 Natural Product Compound Structures[a] Continued

ST011914 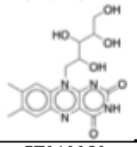	ST012030 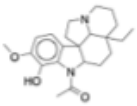	ST012797 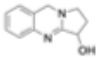	ST012920 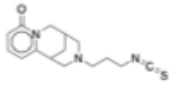	ST018409 
ST019369 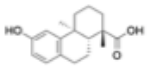	ST024700 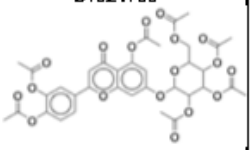	ST024702 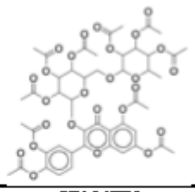	ST024706 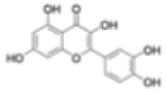	ST024711 
ST024730 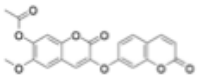	ST024752 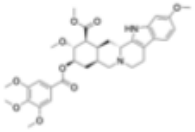	ST024772 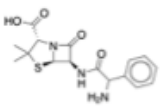	ST024783 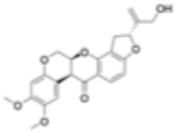	ST024789 
ST024792 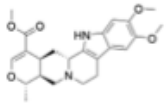	ST028625 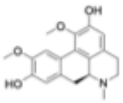	ST036759 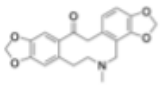	ST044225 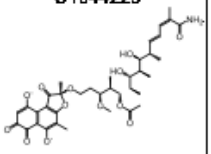	ST044516 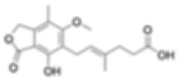
ST047929 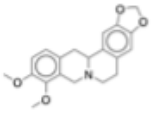	ST055629 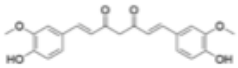	ST055760 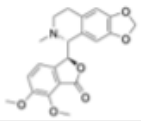	ST056188 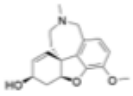	ST056282 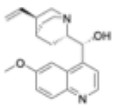
ST056285 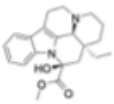	ST056292 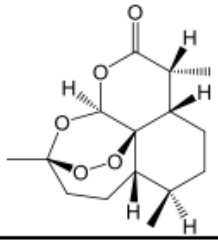	ST056294 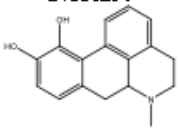	ST056297 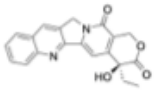	

[a]Structures of the pure natural product compounds of the library used for screening are shown in this Table S2. Note that the structures of GER-172 and GER-173 are currently unknown and are under study. All structures shown are as accurate according to available data at this time. A few structures are missing stereochemistry data at this time.

3.7 References

1. Turk, V.; Stoka, V.; Vasiljeva, O.; Renko, M.; Sun, T.; Turk, B.; Turk, D. Cysteine Cathepsins: From Structure, Function and Regulation to New Frontiers. *Biochim. Biophys. Acta, Proteins Proteomics* 2012, *1824* (1), 68–88.

2. Hook, V.; Yoon, M.; Mosier, C.; Ito, G.; Podvin, S.; Head, B. P.; Rissman, R.; O'Donoghue, A. J.; Hook, G. Cathepsin B in neurodegeneration of Alzheimer's disease, traumatic brain injury, and related brain disorders. Biochim. Biophys. Acta, Proteins Proteomics 1868, 1868, No. 140428.

3. Aggarwal, N.; Sloane, B. F. Cathepsin b: Multiple Roles in Cancer. *Proteomics: Clin. Appl.* 2014, *8* (5-6), 427–437.

4. Amaral, E. P.; Riteau, N.; Moayeri, M.; Maier, N.; Mayer-Barber, K. D.; Pereira, R. M.; Lage, S. L.; Kubler, A.; Bishai, W. R.; D'Império-Lima, M. R.; Sher, A.; Andrade, B. B. Lysosomal Cathepsin Release Is Required for NLRP3-Inflammasome Activation by Mycobacterium Tuberculosis in Infected Macrophages. *Front. Immunol.* 2018, *9*.

5. Rajamäki, K.; Lappalainen, J.; Öörni, K.; Välimäki, E.; Matikainen, S.; Kovanen, P. T.; Eklund, K. K. Cholesterol Crystals Activate the NLRP3 Inflammasome in Human Macrophages: A Novel Link between Cholesterol Metabolism and Inflammation. *PLoS ONE* 2010, *5* (7).

6. Hook, G.; Hook, V.; Kindy, M. The Cysteine Protease Inhibitor, E64D, Reduces Brain Amyloid-β and Improves Memory Deficits in Alzheimer's Disease Animal Models by Inhibiting Cathepsin B, but Not BACE1, β-Secretase Activity. *J. Alzheimer's Dis.* 2011, *26* (2), 387–408.

7. Kindy, M. S.; Yu, J.; Zhu, H.; El-Amouri, S. S.; Hook, V.; Hook, G. R. Deletion of the Cathepsin B Gene Improves Memory Deficits in a Transgenic Alzheimer's Disease Mouse Model Expressing ABPP Containing the Wild-Type β-Secretase Site Sequence. *J. Alzheimer's Dis.* 2012, *29* (4), 827–840.

8. Hook, G.; Yu, J.; Toneff, T.; Kindy, M.; Hook, V. Brain Pyroglutamate Amyloid-β Is Produced by Cathepsin B and Is Reduced by the Cysteine Protease Inhibitor E64d, Representing a Potential Alzheimer's Disease Therapeutic. *J. Alzheimer's Dis.* 2014, *41* (1), 129–149.

9. Hook, G.; Jacobsen, J. S.; Grabstein, K.; Kindy, M.; Hook, V. Cathepsin B Is a New Drug Target for Traumatic Brain Injury Therapeutics: Evidence for E64d as a Promising Lead Drug Candidate. *Front. Neurol.* 2015, *6*.

10. Sun, Y.; Rong, X.; Lu, W.; Peng, Y.; Li, J.; Xu, S.; Wang, L.; Wang, X. Translational Study of Alzheimer's Disease (AD) Biomarkers from Brain Tissues in ABPP/PS1 Mice and Serum of Ad Patients. *J. Alzheimer's Dis.* 2015, *45* (1), 269–282.

11. Assfalg-Machleidt, I.; Jochum, M.; Nast-Kolb, D.; Siebeck, M.; Billing, A.; Joka, T.; Rotze, G.; Valet, G.; Zauner, R.; Scheuber, H. P. Cathepsin B-Indicator for the Release of Lysosomal Cysteine Proteinases in Severe Trauma and Inflammation. *Biol. Chem. Hoppe-Seyler* 1990, *371*, 211–222.

12. Villa, F. A.; Gerwick, L. Marine Natural Product Drug Discovery: Leads for Treatment of Inflammation, Cancer, Infections, and Neurological Disorders. *Immunopharmacol. Immunotoxicol.* 2010, *32* (2), 228–237.

13. Che, C.-T.; Zhang, H. Plant Natural Products for Human Health. *Int. J. Mol. Sci.* 2019, *20* (4), 830.

14. Rauf, A.; Khalil, A. A.; Olatunde, A.; Khan, M.; Anwar, S.; Alafnan, A.; Rengasamy, K. R. R. Diversity, Molecular Mechanisms and Structure-Activity Relationships of Marine Protease Inhibitors—a Review. *Pharmacol. Res.* 2021, *166*, 105521.

15. Cid-Gallegos, M. S.; Corzo-Ríos, L. J.; Jiménez-Martínez, C.; Sánchez-Chino, X. M. Protease Inhibitors from Plants as Therapeutic Agents- A Review. *Plant Foods Hum. Nutr. (N. Y., NY, U. S.)* 2022, *77* (1), 20–29.

16. Miller, B.; Friedman, A. J.; Choi, H.; Hogan, J.; McCammon, J. A.; Hook, V.; Gerwick, W. H. The Marine Cyanobacterial Metabolite Gallinamide A Is a Potent and Selective Inhibitor of Human Cathepsin L. *J. Nat. Prod.* 2013, *77* (1), 92–99.

17. Ashhurst, A. S.; Tang, A. H.; Fajtová, P.; Yoon, M. C.; Aggarwal, A.; Bedding, M. J.; Stoye, A.; Beretta, L.; Pwee, D.; Drelich, A.; Skinner, D.; Li, L.; Meek, T. D.; McKerrow, J. H.; Hook, V.; Tseng, C.-T.; Larance, M.; Turville, S.; Gerwick, W. H.; O'Donoghue, A. J.; Payne, R. J. Potent Anti-SARS-Cov-2 Activity by the Natural Product Gallinamide A and Analogues via Inhibition of Cathepsin L. *J. Med. Chem.* 2021, *65* (4), 2956–2970.

18. Newman, D. J.; Cragg, G. M. Natural Products as Sources of New Drugs over the Nearly Four Decades from 01/1981 to 09/2019. *J. Nat. Prod.* 2020, *83* (3), 770–803.

19. Yoon, M. C.; Solania, A.; Jiang, Z.; Christy, M. P.; Podvin, S.; Mosier, C.; Lietz, C. B.; Ito, G.; Gerwick, W. H.; Wolan, D. W.; Hook, G.; O'Donoghue, A. J.; Hook, V. Selective Neutral pH Inhibitor of Cathepsin B Designed Based on Cleavage Preferences at Cytosolic and Lysosomal pH Conditions. *ACS Chem. Biol.* 2021, *16* (9), 1628–1643.

20. Yamamoto, A.; Tomoo, K.; Hara, T.; Murata, M.; Kitamura, K.; Ishida, T. Substrate Specificity of Bovine Cathepsin B and Its Inhibition by CA074, Based on Crystal Structure Refinement of the Complex. *J. Biochem.* 2000, *127* (4), 635–643.

21. Towatari, T.; Nikawa, T.; Murata, M.; Yokoo, C.; Tamai, M.; Hanada, K.; Katunuma, N. Novel Epoxysuccinyl Peptides a Selective Inhibitor of Cathepsin B, in Vivo. *FEBS Lett.* 1991, *280* (2), 311–315.

22. Murata, M.; Miyashita, S.; Yokoo, C.; Tamai, M.; Hanada, K.; Hatayama, K.; Towatari, T.; Nikawa, T.; Katunuma, N. Novel EPOXYSUCCINYL Peptides Selective Inhibitors of Cathepsin B, in Vitro. *FEBS Lett.* 1991, *280* (2), 307–310.

23. Ni, J.; Lan, F.; Xu, Y.; Nakanishi, H.; Li, X. Extralysosomal Cathepsin B in Central Nervous System: Mechanisms and Therapeutic Implications. *Brain Pathol.* 2022.

24. Yoon, M. C.; Christy, M. P.; Phan, V. V.; Gerwick, W. H.; Hook, G.; O'Donoghue, A. J.; Hook, V. Molecular Features of CA-074 Ph-Dependent Inhibition of Cathepsin B. *Biochemistry* 2022, *61* (4), 228–238.

25. Barrett, A. J.; Kembhavi, A. A.; Brown, M. A.; Kirschke, H.; Knight, C. G.; Tamai, M.; Hanada, K. L-*Trans*-Epoxysuccinyl-Leucylamido(4-Guanidino)Butane (E-64) and Its Analogues as Inhibitors of Cysteine Proteinases Including Cathepsins B, H and l. *Biochem. J.* 1982, *201* (1), 189–198.

26. Voet, D.; Voet, J. In *Biochemistry*; J. Wiley & Sons: New York, NY, 1995; pp 482–485.

Acknowledgements

Chapter 3, in full, is a reprint of the material as it appears in ACS Omega in American Chemical Society. Von V. Phan, Charles Mosier, Michael C. Yoon, Evgenia Glukhov, Conor R Caffrey, Anthony J O'Donoghue, William H. Gerwick, and Vivian Hook, American Chemical Society, 2022. The dissertation author was the primary researcher and author of this material.

Chapter 4 Distinct Cleavage Properties of Cathepsin B Compared to Cysteine Cathepsins Enable the Design and Validation of a Specific Substrate for Cathepsin B over a Broad pH Range

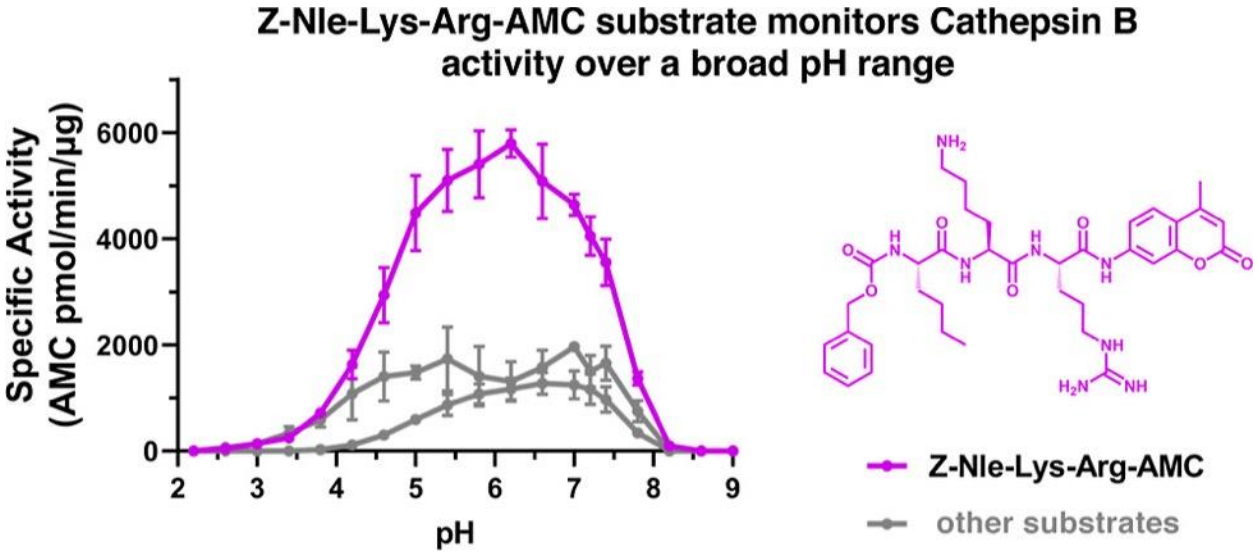

Figure 4.1 Chapter 4 Graphical Abstract. The biological and pathological functions of cathepsin B occur in acidic lysosomes and at the neutral pH of cytosol, nuclei, and extracellular locations. Importantly, cathepsin B displays different substrate cleavage properties at acidic pH compared to neutral pH conditions. It is, therefore, desirable to develop specific substrates for cathepsin B that measure its activity over broad pH ranges. Current substrates used to monitor cathepsin B activity consist of Z-Phe-Arg-AMC and Z-Arg-Arg-AMC, but they lack specificity since they are cleaved by other cysteine cathepsins. Furthermore, Z-Arg-Arg-AMC monitors cathepsin B activity at neutral pH and displays minimal activity at acidic pH. Therefore, the purpose of this study was to design and validate specific fluorogenic peptide substrates that can monitor cathepsin B activity over a broad pH range from acidic to neutral pH conditions. In-depth cleavage properties of cathepsin B were compared to those of the cysteine cathepsins K, L, S, V, and X via multiplex substrate profiling by mass spectrometry at pH 4.6 and pH 7.2. Analysis of the cleavage preferences predicted the tripeptide Z-Nle-Lys-Arg-AMC as a preferred substrate for cathepsin B. Significantly, Z-Nle-Lys-Arg-AMC displayed the advantageous properties of measuring high cathepsin B specific activity over acidic to neutral pHs and was specifically cleaved by cathepsin B over the other cysteine cathepsins. Z-Nle-Lys-Arg-AMC specifically monitored cathepsin B activity in neuronal and glial cells which were consistent with relative abundances of cathepsin B protein. These findings validate Z-Nle-Lys-Arg-AMC as a novel substrate that specifically monitors cathepsin B activity over a broad pH range.

4.1 Introduction

Cathepsin B is a lysosomal cysteine protease that participates in protein degradation to maintain cellular balance of functional protein pathways. (1−3) Cathepsin B belongs to the family of cysteine cathepsin proteases that together function in lysosomal protein homeostasis. (4,5) Cathepsin B and other cysteine cathepsin family members normally function within lysosomes at acidic pH 4.6. (6−8) However, in numerous human diseases of neurological disorders (9−20) combined with infectious diseases, inflammation, and related conditions, (21−26) cathepsin B leaks out of the lysosome into the cytosol of neutral pH 7.2. (27,28) Cathepsin B retains its enzymatic activity at cytosolic neutral pH and activates cell death (29−32) and inflammatory (33−36) pathways that result in disease pathogenesis. In addition to the significant cellular function of cathepsin B at the neutral pH of the cytosol, cathepsin B is also present at neutral pH cellular locations of the nucleus (37,38) as well as extracellular locations, especially in human diseases such as Alzheimer's disease (39,40) and cancer. (41−43)

The prominent biological functions of cathepsin B at distinct acidic and neutral pH environments of tissues (44−46) indicate the need to specifically monitor cathepsin B activity over a broad pH range, without detecting other cysteine cathepsins. Currently, no such substrates exist because Z-Phe-Arg-AMC that is routinely used to assay cathepsin B in the field also monitors cathepsin L and other cysteine protease activities. (44,45,47−50) Furthermore, Z-Arg-Arg-AMC has been found as a specific substrate for cathepsin B over other cysteine cathepsins, (44,48) but this substrate preferentially monitors the neutral pH activity of cathepsin B rather than the enzyme's acidic activity. (44) Therefore, the purpose of this study was to rationally design selective peptide-AMC substrates that specifically monitor cathepsin B activity with high specific activity at both acidic and neutral pH conditions, without cleavage by other cysteine cathepsins.

The strategy of this study was to design specific substrates for cathepsin B based on its unique pH-dependent cleavage properties at acidic pH 4.6 compared to those at neutral pH 7.2. Cleavage properties of cathepsin B were determined by multiplex substrate profiling mass spectrometry (MSP-MS) that utilizes a defined peptide library designed to contain all known amino acids adjacent to protease cleavage sites. (51) These substrate properties of cathepsin B were compared to those of other cysteine cathepsins L, K, S, V, and X at acidic and neutral pH conditions. The unique cleavage properties of cathepsin B allowed design of Z-peptide-AMC substrates for assessment of broad pH monitoring of cathepsin B activity, with specificity shown by a lack of cleavage by other cysteine cathepsins.

Results identified Z-Nle-Lys-Arg-AMC that monitors high specific activity of cathepsin B at acidic to neutral pHs, and this substrate is specific for cathepsin B over other cysteine cathepsins L, K, S, and V. Kinetic studies demonstrated greater catalytic efficiency of Z-Nle-Lys-Arg-AMC for analysis of acidic and neutral pH cathepsin B activity compared to the Z-Arg-Arg-AMC substrate, currently used in the field as a specific cathepsin B substrate. (44,48) Furthermore, the novel Z-Nle-Lys-Arg-AMC substrate was demonstrated to specifically measure cathepsin B activity in neuronal and glial cells that contain varying levels of cathepsin B and other cathepsins (determined by proteomics assessment). Overall, the novel Z-Nle-Lys-Arg-AMC substrate advantageously monitors specific cathepsin B activity over a broad pH range of acidic to neutral pH conditions and, thus, will be useful for the assessment of cathepsin B activity at physiological pH conditions.

4.2 Results

4.2.1 Analysis of Cathepsin B Substrates Z-Phe-Arg-AMC and Z-Arg-Arg-AMC for Cleavage by Cysteine Cathepsins Demonstrate Lack of Specificity

We compared the specific activity of human cathepsin B with the fluorogenic substrates Z-Phe-Arg-AMC and Z-Arg-Arg-AMC with that of other cysteine cathepsins (Table 4.1). Both of

these substrates were cleaved by cathepsin B and other cysteine cathepsins L, K, S, and V, indicating that these substrates are not specific for cathepsin B. These assays also demonstrated that cathepsins B, K, and S were active at both acidic and neutral pHs of 4.6 and 7.2, respectively, but cathepsins L and V displayed activity only at acidic pH 4.6 and not at pH 7.2. These data are consistent with others with respect to the pH properties of these cathepsins. (44,45,47−50) Significantly, these findings confirm the lack of specificity of Z-Phe-Arg-AMC and Z-Arg-Arg-AMC substrates for cathepsin B.

Comparison of Z-Arg-Arg-AMC cleavage by cathepsin B at acidic lysosomal pH 4.6 and at neutral pH 7.2 of the cytosol showed that this substrate displays pH-dependent cleavage properties. Z-Arg-Arg-AMC is readily cleaved by cathepsin B at neutral pH, but this substrate has poor cleavage activity at acidic pH that is one-third of the specific activity at neutral pH.

The lack of specificity of Z-Phe-Arg-AMC and Z-Arg-Arg-AMC for cathepsin B compared to other cysteine cathepsins, and preference of Z-Arg-Arg-AMC to monitor neutral pH cathepsin B, indicates the need for the development of specific substrates of cathepsin B operating over a broad pH range.

4.2.2 Cathepsin B Displays Distinct Cleavage Properties Compared to Other Cysteine Cathepsins Revealed by MSP-MS

The substrate cleavage properties of human cathepsin B were compared to that of the cysteine cathepsins K, L, V, S, and X by MSP-MS analysis. MSP-MS was conducted by incubation of each protease with a library of 228 14-mer peptides at acidic pH 4.6 and neutral pH 7.2, and cleavage products were identified and analyzed using LC–MS/MS. The peptide library used for MSP-MS analysis was designed to contain all known protease cleavage sites with respect to amino acid residues at cleavage sites combined with neighboring residues. (51) These cysteine proteases cleaved peptides at both pH 4.6 and pH 7.2 in the MSP-MS study, with the exception of cathepsin

X that generated a low number of cleavage products at only pH 4.6 (shown by volcano plots in Supporting Information Figure 4.S1).

MSP-MS analysis of cleavage site locations within the 14-mer peptides showed that cathepsin B differs in its exopeptidase and endopeptidase cleavages compared to the other cysteine cathepsins. Cathepsin B displayed major dipeptidyl carboxypeptidase (DPCP) cleavages occurring between residues 12 and 13 of the peptide substrates, as well as lower endopeptidase cleavages occurring within the 14-mer substrates (Figure 4.2a). The dual DPCP and endopeptidase data of cathepsin B activity is consistent with other studies. (4,5,44) These DPCP and endopeptidase activities of cathepsin B distinguish it from the cathepsins K, L, S, and V, which displayed endopeptidase activities and no carboxypeptidase activity (Figure 4.2b–e). Cathepsin X displayed endopeptidase and monopeptidyl carboxypeptidase cleavage (Figure 4.2f) (with a low number of five peptides cleaved), which differ from that of cathepsin B.

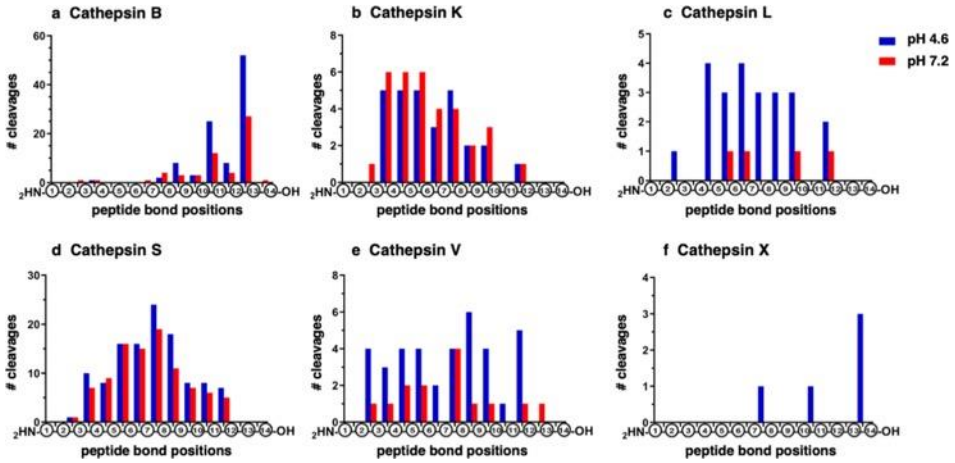

Figure 4.2 Exopeptidase and endopeptidase cleavages by cathepsin B compared to other cysteine cathepsins assessed by MSP-MS. The proteolytic cleavage properties of cathepsin B and cysteine cathepsins K, L, S, V, and X were assessed at pH 4.6 and pH 7.2 by substrate profiling with the peptide library in MSP-MS assays. MSP-MS analyses were conducted for cathepsins B, K, L, S, V, and X as shown in panels (a–f), respectively. After incubation of each protease with the peptide library for 15 min, with the exception that cathepsin X was incubated with the library for 60 min, cleavage products were identified by nano-LC–MS/MS as described in the methods. The number of cleavages at each peptide bond, numbers 1 to 13, is illustrated for the cysteine cathepsins B, K, L, S, V, and X.

The substrate cleavage specificity of cathepsin B was compared to that of the other cysteine cathepsins by assessing preferred residues at the P4–P4′ positions surrounding the P1–P1′ cleavage site using z-scores and iceLogo (Supporting Information Figures 4.S2 and 4.S3). Heat maps of z-scores illustrated the preferred residues (green shade) and non-preferred residues (yellow shade) at each of the P4 to P4′ positions. All amino acids were assessed with the exception of methionine and cysteine; norleucine (n) was used as a sulfur-free isostere of methionine.

Comparison of the heat maps at pH 4.6 and pH 7.2 for cathepsins B, K, S, and V showed differing patterns for each of these proteases at the acidic and neutral pH conditions (Supporting Information Figures 4.S2 and 4.S3). We focused on the preferred residues at positions P3 to P1 for cathepsin B (Figure 4.3) that can be utilized for designing specific Z-peptide-AMC fluorogenic substrates spanning acidic and neutral pH activities of cathepsin B.

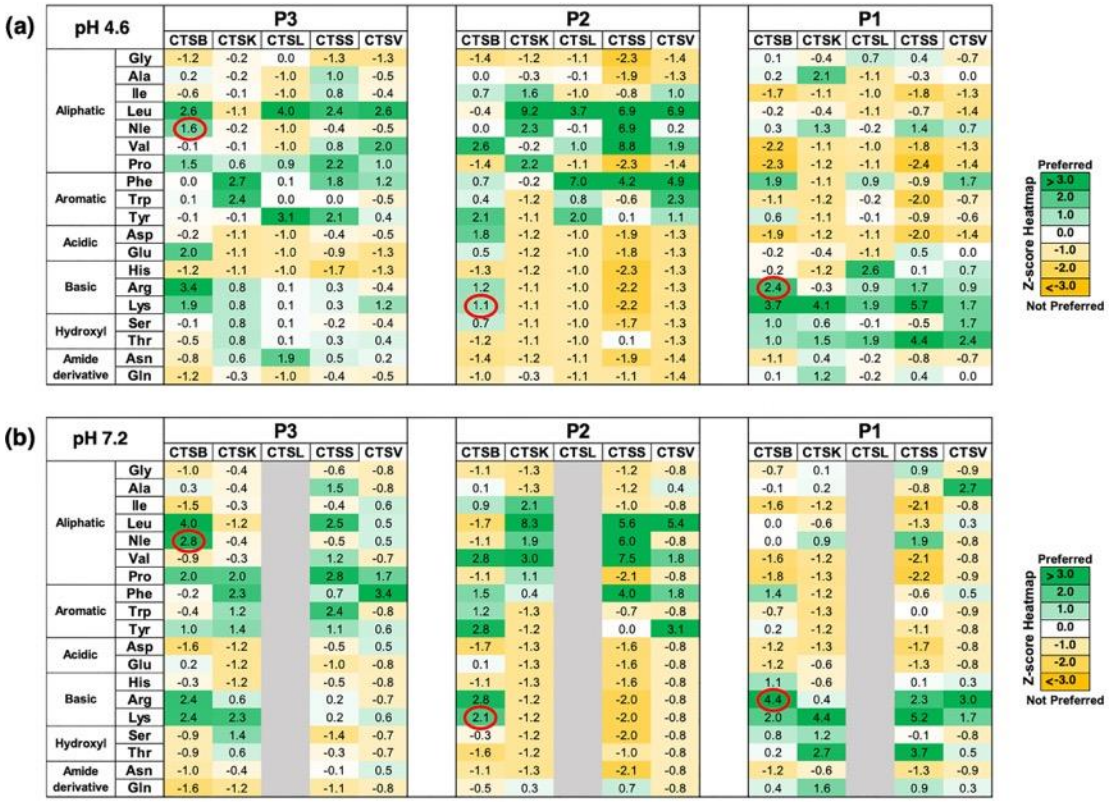

Figure 4.3 Assessment of distinct cathepsin B preferred residues at P1 to P3 positions adjacent to P1–P1′ cleavage sites compared to other cysteine cathepsins. The preferred residues of human cathepsin B at P1 to P3 positions were compared to that of cathepsins K, L, S, and V at pH 4.6 (panel a) and pH 7.2 (panel b) shown in heat maps of *z*-scores. Preferred residues are indicated by positive scores (green shades), and non-preferred residues are indicated by negative scores (yellow shades). The residues circled in red indicate unique residues preferred by cathepsin B over the other cathepsins at the P1 to P3 positions. The *z*-scores represent comparisons of the frequencies of amino acids at each of these positions (relative to the cleavage sites) of our MSP-MS experimental with the "reference data set" that covers all 2964 possible cleavage sites of the peptide library. The *z*-scores were, thus, calculated using the equation $(X - \mu)/\sigma$, where X represents the frequency of a specific amino acid in the "experimental data set", μ denotes the frequency of that amino acid at a particular position in the "reference data set", and σ signifies the standard deviation. Positive *z*-scores indicate preferred residues and negative scores indicate not-preferred residues, shown in the heat map as green to yellow shading for high to low *z*-scores.

For cathepsin B, we sought to identify amino acids that were preferred by cathepsin B at both pH 4.6 and pH 7.2 (Figure 4.3). At P3, P2, and P1, the enzyme displayed preferences for basic residues (Arg and Lys). In addition, norleucine (Nle) and Leu were preferred at P3, and Val was preferred at P2. Cathepsins K, S, L, and V had different P3 and P2 preferences compared to cathepsin B. In particular, Nle at the P3 position, and Arg and Lys at P2 were not preferred by

cathepsins K, S, L, and V (Figure 4.3). Val at P2 was preferred by cathepsin K, S, L, and V at one or both pH conditions and, therefore, was not selective for cathepsin B. At the P1 position, cathepsins K, L, and S preferred Lys over Arg, while cathepsin V preferred Lys over Arg at pH 4.6 and the opposite at pH 7.2. Compilation of the preferred P3, P2, and P1 residues for the five enzymes revealed the distinct preferences of cathepsin B for Nle at the P3 position, Lys or Arg at P2, and Arg at P1. These cleavage properties suggested that a fluorogenic peptide consisting of tripeptides Z-Nle-Lys-Arg-AMC or Z-Nle-Arg-Arg-AMC would be selectively cleaved by cathepsin B at both pH 4.6 and pH 7.2 relative to the other four cysteine cathepsin enzymes.

4.2.3 Design and Validation of Z-Nle-Arg-Lys-AMC as a Specific Cathepsin B Substrate for Acidic and Neutral pH Conditions

We synthesized Z-Nle-Lys-Arg-AMC and Z-Nle-Arg-Arg-AMC and quantified cathepsin B activity at acidic and neutral pH conditions (Figure 4.4). The specific activity of cathepsin B for cleaving Z-Nle-Lys-Arg-AMC was higher than all other substrates at both pHs. The Z-Nle-Arg-Arg-AMC substrate displayed about 30% and 50% less activity at pH 4.6 and pH 7.2, respectively, compared to Z-Nle-Lys-Arg-AMC. The Z-Nle-Lys-Arg-AMC substrate monitored higher cathepsin B specific activity compared to the commonly used cathepsin B substrates of Z-Phe-Arg-AMC and Z-Arg-Arg-AMC.

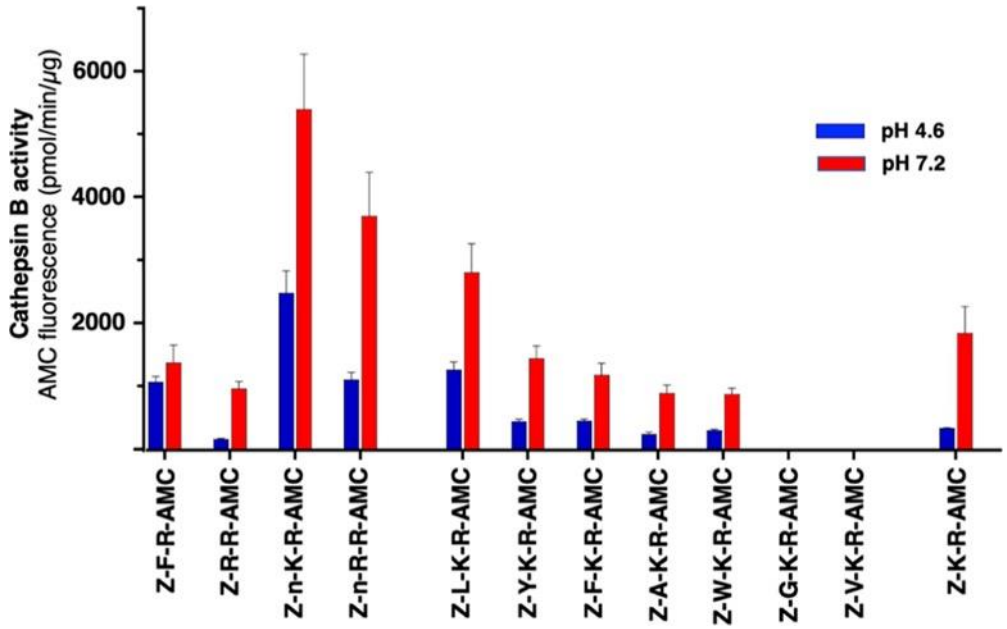

Figure 4.4 Z-Nle-Lys-Arg-AMC monitors high cathepsin B specific activity at pH 4.6 and pH 7.2 compared to related tripeptide and dipeptide substrates. Z-Nle-Lys-Arg-AMC (Z-n-K-R-AMC) and the indicated tripeptide and dipeptide fluorogenic substrates (at 40 μM) were compared for proteolysis by cathepsin B at pH 4.6 (blue bars) and pH 7.2 (red bars). One-letter codes for amino acids are shown for the peptidic substrates. Proteolytic activity of cathepsin B is shown as the mean ± SD (n = 4).

Modifications of the P3 residues of variant tripeptide sequences of Z-Nle-Lys-Arg-AMC were assessed (Figure 4.4). Substitution of Leu for Nle at the P3 position generated the substrate Z-Leu-Lys-Arg-AMC, which showed less activity than Z-Nle-Lys-Arg-AMC. When the P3 residue was modified to Tyr, Phe, Ala, or Trp, the resultant substrates displayed decreased activities at both acid and neutral pHs. When the P3 residue was changed to Gly or Val, no cathepsin B activity was observed, correlating with Gly and Val having negative z-scores in the MSP-MS data.

Assessment of the dibasic substrate of Z-Lys-Arg-AMC that lacks a P3 amino acid but has the most favorable P2 and P1 residues had lower activity than Z-Nle-Lys-Arg-AMC but higher activity than substrates that have an unfavorable amino acid at the P3 position.

Overall, analysis of Z-Nle-Lys-Arg-AMC and related peptide-AMC substrates demonstrated that the optimized residues at P3, P2, and P1 positions provided design and validation of the high specific activity of the novel Z-Nle-Lys-Arg-AMC substrate of cathepsin B.

4.2.4 Z-Nle-Lys-Arg-AMC Substrate Monitors Cathepsin B Activity over a Broad pH Range

The pH properties of Z-Nle-Lys-Arg-AMC were assessed and compared to the established substrates Z-Arg-Arg-AMC and Z-Phe-Arg-AMC (Figure 4.5). Z-Nle-Lys-Arg-AMC showed a broad optimum pH range of pH 4.5 to pH 7.5 that represented 50% of the maximal activity observed at pH 5.5–6.5, which was above the activity measurements monitored by the other two Z-Arg-Arg-AMC and Z-Phe-Arg-AMC substrates. The structure of Z-Nle-Lys-Arg-AMC illustrates its side chains of the tripeptide residues of this high activity substrate (Figure 4.5a). Kinetic assessment by kcat/Km values showed the high catalytic efficiency of cathepsin B activity monitored with Z-Nle-Lys-Arg-AMC and lower catalytic efficiency with Z-Arg-Arg-AMC at both pH 7.2 and pH 4.6 (Figure 4.5b and Supporting Information Table 4.S1). Z-Phe-Arg-AMC displayed high kcat/Km values similar to Z-Nle-Lys-Arg at pH 7.2 and had higher catalytic efficiency at pH 4.6.

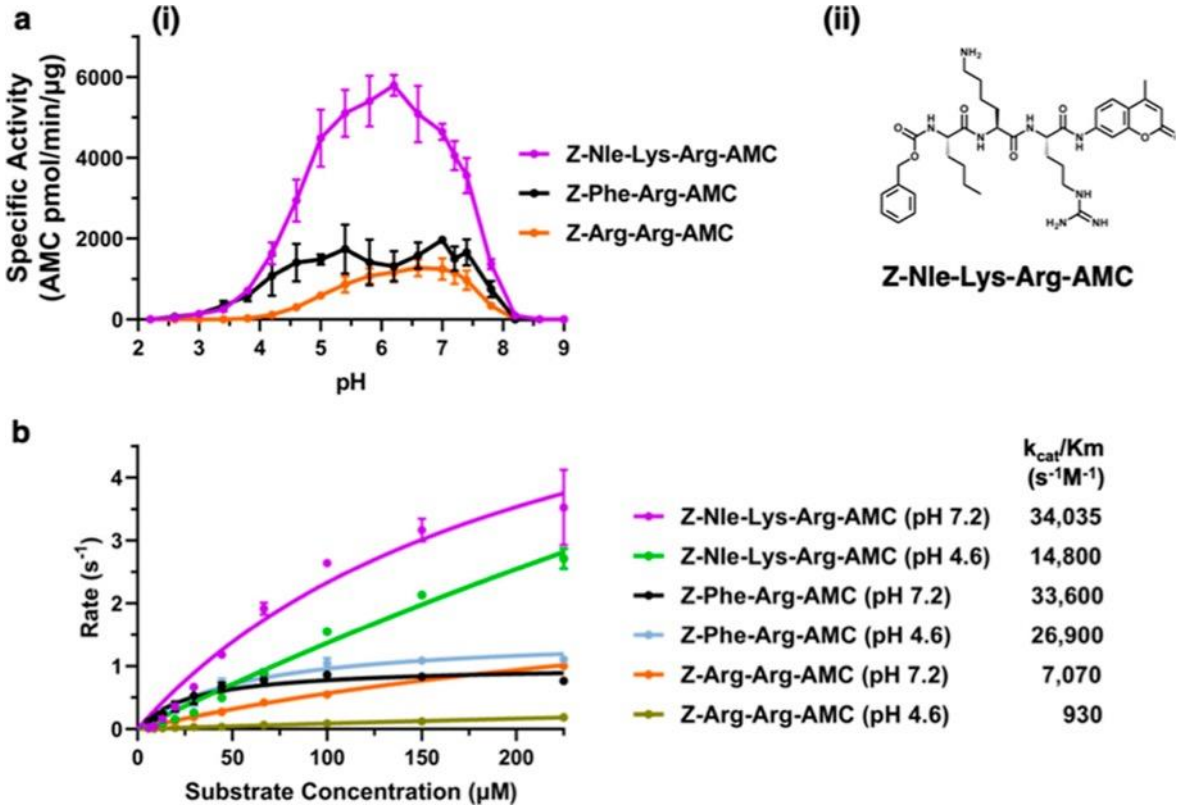

Figure 4.5 Cathepsin B cleaves Z-Nle-Lys-Arg-AMC over a broad pH range. (a) pH profile of human cathepsin B activity with Z-Nle-Lys-Arg-AMC compared to Z-Arg-Arg-AMC and Z-Phe-Arg-AMC substrates. (i) Cathepsin B pH profiles with three different substrates (40 µM) were assessed at pH 2 to 9. Data points are shown as the mean ± SD (n = 3). (ii) Structure of Z-Nle-Lys-Arg-AMC is shown. This substrate provides the highest specific activity for cathepsin B activity. (b) Kinetic k_{cat}/K_m values for cathepsin B activity with the substrates Z-Nle-Lys-Arg-AMC, Z-Arg-Arg-AMC, and Z-Phe-Arg-AMC. k_{cat}/K_m values for each of the substrates at pH 4.6 and pH 7.2 were calculated for cathepsin B by plotting the rate of AMC product formation of the y-axis with its respective substrate concentration of the x-axis as described in the methods.

4.2.5 Z-Nle-Lys-Arg-AMC Specifically Monitors Cathepsin B Activity Compared to Other Cysteine Cathepsins

Z-Nle-Lys-Arg-AMC specifically detected cathepsin B activity and not cathepsins L, K, S, V, and X activities evaluated at pHs 4.6, 5.5, and 7.2 (Figure 4.6 and Supporting Information Figure 4.S4). In contrast, Z-Arg-Arg-AMC was not specific for cathepsin B since this substrate was cleaved by cathepsins L and V. The Z-Phe-Arg-AMC substrate was cleaved by cathepsin L

with greater activity than that for cathepsin B; this substrate was also cleaved by cathepsins K and V. These data demonstrate Z-Nle-Lys-Arg-AMC as a specific substrate for cathepsin B.

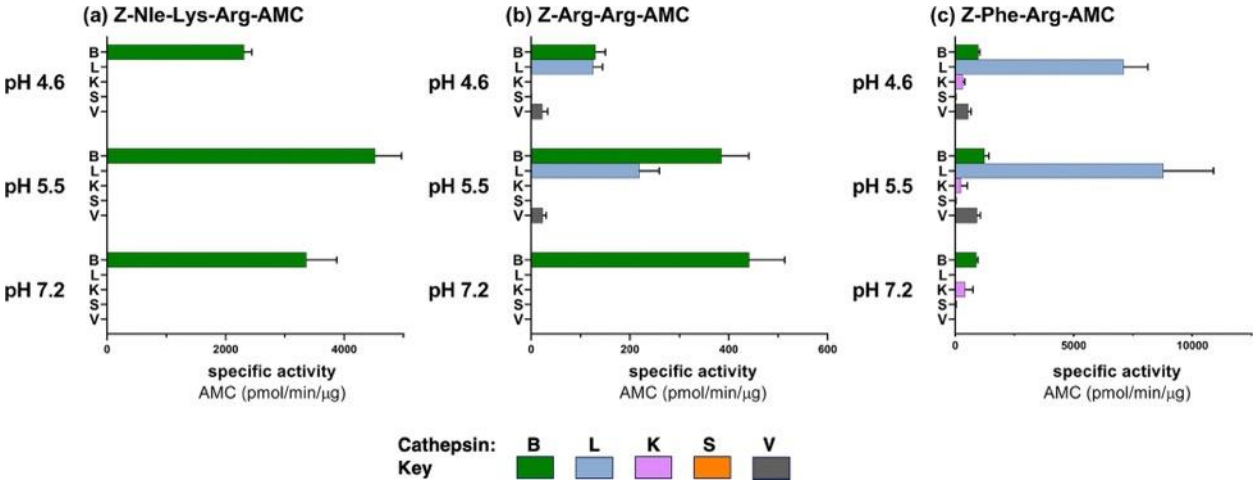

Figure 4.6 Z-Nle-Lys-Arg-AMC displays specificity for cathepsin B over other cysteine cathepsins L, K, S, and V. (a) Z-Nle-Lys-Arg-AMC: cathepsin B specific activity for cleavage of Z-Nle-Lys-Arg-AMC was compared to that of cathepsins L, K, S, and V at pHs 7.2, 5.5, and 4.6. (b) Z-Arg-Arg-AMC: cathepsin B specific activity for cleavage of Z-Arg-Arg-AMC was compared to that of cathepsins L, K, S, and V at pHs 7.2, 5.5, and 4.6. (c) Z-Phe-Arg-AMC: cathepsin B specific activity for cleavage of Z-Phe-Arg-AMC was compared to that of cathepsins L, K, S, and V at pHs 7.2, 5.5, and 4.6. All data are shown as the mean ± SD (n = 3).

4.2.6 Specific Cathepsin B Activity in Neuronal and Glial Cells Assessed by the Z-Nle-Lys-Arg-AMC Substrate

To evaluate the novel substrate Z-Nle-Lys-Arg-AMC in a complex biological sample that contains other proteases and proteins, the assay of cathepsin B activity in homogenates of human neuroblastoma cells (SHSY-5Y and SK-N-MC neuroblastoma) and mouse microglial cells (BV2 microglia) compared the use of the Z-Nle-Lys-Arg-AMC substrate to that of Z-Arg-Arg-AMC and Z-Phe-Arg-AMC substrates. Cathepsin B activity was assessed as CA-074 sensitive activity (Figure 4.7), ensuring that the observed activity was inhibited by the specific CA-074 inhibitor of cathepsin B. (58,59) For the three cell types, the highest specific activity of cathepsin B was observed at pH 5.5 compared to pH 4.6 and pH 7.2 (Supporting Information Figure 4.S5). Cathepsin B is present in situ within the pH 5.5 environment of secretory vesicles that produce

peptide neurotransmitters. (60) The two neuroblastoma cell lines showed similar specific activities of cathepsin B. The microglial cells displayed high cathepsin B specific activity that was 2 to 4 times higher than that of the neuroblastoma cells depending on the pH. Notably, the Z-Arg-Arg-AMC substrate detected none or little activity at pH 4.6 in the three cell types, whereas the Z-Nle-Lys-Arg-AMC substrate detected robust cathepsin B activity.

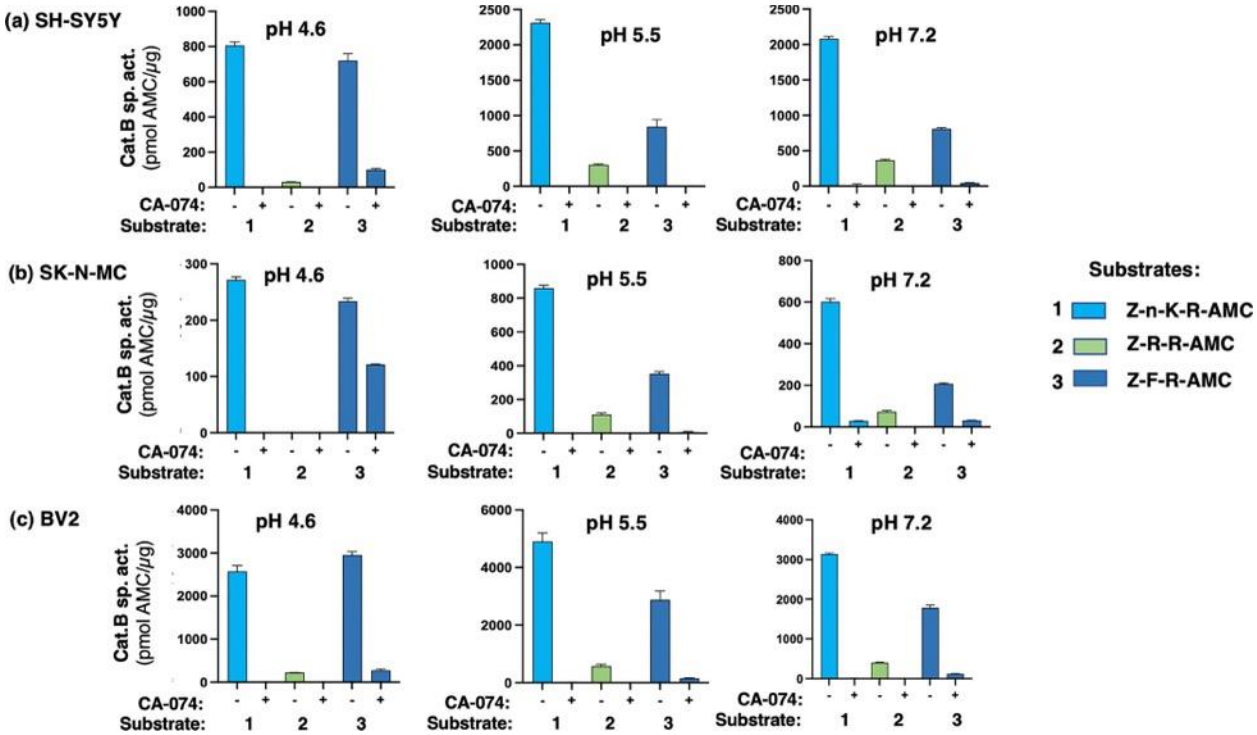

Figure 4.7 Cathepsin B assessed as CA-074-sensitive activity in neuroblastoma and microglial cells assessed with Z-Nle-Lys-Arg-AMC compared to Z-Arg-Arg-AMC and Z-Phe-Arg-AMC. Proteolytic activity of cathepsin B and other cysteine cathepsins were measured by fluorogenic assays of cell homogenates incubated with Z-Nle-Lys-Arg-AMC, Z-Arg-Arg-AMC, and Z-Phe-Arg-AMC substrates (60 μM for each substrate) at pHs 4.6, 5.5, and 7.2 with or without pre-incubation with CA-074, a potent and selective cathepsin B inhibitor. Cells assessed consisted of (a) human neuroblastoma SH-SY5Y, (b) human neuroblastoma SK-N-MC, and (c) mouse microglia BV2. Results display specific activity in the absence and presence of CA-074 which indicates cathepsin B specific activity. Data show cathepsin B activity as pmol AMC/μg enzyme protein (30 min incubation) as the mean ± SD (n = 3).

To assess the prediction that mouse cathepsin B resembles human cathepsin B for substrate preferences as demonstrated by the cellular assays, purified recombinant mouse cathepsin B was

evaluated with the Z-Nle-Lys-Arg-AMC and Z-Arg-Arg-AMC substrates, as well as the Z-Phe-Arg-AMC substrate at pHs 4.6, 5.5, and 7.2 (Supporting Information Figure 4.S6). The highest specific activity of mouse cathepsin B was observed with Z-Nle-Lys-Arg-AMC among the three substrates. Z-Arg-Arg-AMC-cleaving activity of cathepsin B was low. A moderate specific activity was observed with Z-Phe-Arg-AMC. These activities of mouse cathepsin B with the three substrates were represented by kcat/Km kinetic values, showing high catalytic efficiency for the Z-Nle-Lys-Arg-AMC substrate, modest catalytic efficiency for Z-Phe-Arg-AMC, and low catalytic efficiency for the Z-Arg-Arg-AMC substrate (Supporting Information Figure 4.S6). These findings demonstrate Z-Nle-Lys-Arg-AMC as an excellent substrate for mouse cathepsin B as well as for human cathepsin B.

4.2.7 Higher Abundance of Cathepsin B Protein in Microglia Compared to Neuroblastoma Cells Represented by Cathepsin B Activities

To assess whether the higher cathepsin B specific activity in microglia compared to that in neuroblastoma cells may be related to the greater levels of cathepsin B protein, the relative levels of cathepsin B protein in these cells were evaluated by proteomics MS (Table 4.2). Label-free proteomics identified and quantitated the relative levels of cysteine cathepsins. The level of cathepsin B in microglial cells was about 3-fold greater than in the two neuroblastoma cell types, thus, correlating with the observation of an average of about 3 times greater cathepsin B activity in microglia compared to neuroblastoma cells.

Table 4.1 Cysteine Cathepsins in Neuroblastoma and Microglial Cells Assessed by Proteomics[a]

cell type	cysteine cathepsin	identification by nano-LC–MS/MS	quantifiable, peak area × 10^6
neuroblastoma SH-SY5Y (human)	cathepsin B	+	8.97 ± 2.69
	cathepsin C	+	(not quantifiable)
neuroblastoma SK-N-MC (human)	cathepsin B	+	6.11 ± 3.84
	cathepsin C	+	(not quantifiable)
microglia BV2 (mouse)	cathepsin B	+	28.08 ± 10.47
	cathepsin C	+	1.07 ± 0.46
	cathepsin K	+	17.51 ± 5.48
	cathepsin L	+	7.62 ± 2.11
	cathepsin X	+	21.80 ± 3.66

[a]Cysteine cathepsin proteins present in neuroblastoma SH-SY5Y and SK-N-MC cells, and in microglia BV2 cells, were assessed by quantitative label-free proteomics. Proteomics identified the cathepsins, and relative quantitation is provided for those that met the criteria for quantification (described in Materials and Experimental Details).

It is interesting to observe that the microglial cells contained higher levels of multiple cysteine cathepsins compared to the neuroblastoma cells. The microglial cells contained robust levels of cathepsins B, D, and X, along with cathepsins A, K, L, and C. In the SH-SY5Y neuroblastoma cells, only two cathepsins, B and D, were detected; in the SKNMC neuroblastoma cells, cathepsins B and D were abundant and low levels of cathepsin C were detected.

These findings illustrate the cell type-specific differences in the expression levels of cathepsin B and related cysteine cathepsins. Notably, our newly developed substrate, Z-Nle-Lys-Arg-AMC, effectively detects the relative levels of cathepsin B activity. These results contribute to defining the variability of cathepsin B activity among different cell types and highlight the utility of Z-Nle-Lys-Arg-AMC as a tool for assessing cathepsin B specific activity in biological systems.

4.3 Discussion

The prominent functions of cathepsin B in health and disease occur in acidic lysosomes and at the neutral pH of cytosol, nuclei, and extracellular locations. Notably, cathepsin B displays

different substrate cleavage properties at the acidic pH compared to neutral pH conditions. (45−47) It is, therefore, necessary to develop specific substrates for cathepsin B that specifically measure its proteolytic activity over broad pH ranges. Evaluation by this study of current substrates used to monitor cathepsin B activity, consisting of Z-Phe-Arg-AMC and Z-Arg-Arg-AMC, found that they lack specificity since they are cleaved by other cysteine cathepsins; furthermore, Z-Arg-Arg-AMC does not optimally assess cathepsin B activity at acidic pH. Therefore, the purpose of this study was to conduct in-depth substrate cleavage profiles of cathepsin B compared to other cysteine cathepsins K, L, S, V, and X for designing specific fluorogenic substrates that can monitor cathepsin B proteolytic activity at acidic to neutral pH conditions. Cleavage profiles of these proteases were assessed by MSP-MS that analyzed cleavages of peptide library components at pH 4.6 and pH 7.2. Analysis of the preferred and non-preferred residues at the P3, P2, and P1 positions adjacent to the P1–P1′ cleavage sites predicted the tripeptide Z-Nle-Lys-Arg-AMC as a preferred substrate for cathepsin B. Significantly, Z-Nle-Lys-Arg-AMC displayed the advantageous properties of measuring high cathepsin B specific activity over acidic to neutral pHs and was specific for cathepsin B over other cysteine cathepsins. Z-Nle-Lys-Arg-AMC specifically measured cathepsin B activity in neuronal and glial cells which were consistent with relative abundances of cathepsin B protein. These findings validate Z-Nle-Lys-Arg-AMC as a novel substrate that specifically monitors cathepsin B activity over a broad pH range.

Substrate cleavage profiling analysis of cathepsin B and cysteine cathepsins conducted by MSP-MS, at pH 4.6 and pH 7.2, revealed each protease's distinct pattern of preferred amino acids at P4 to P4′ positions of the P1–P1′ cleavage sites of the peptide library. We focused on the P3 to P1 residue preferences for designing Z-peptide-AMC substrates that utilize non-prime site residues of cleavage sites. Comparisons showed that cathepsin B displayed unique preferences over other

cysteine cathepsins, consisting of Nle at the P3 position, Lys at the P2 position, and Arg at the P3 position at both acidic and neutral pHs. This evaluation formed the basis for the design of Z-Nle-Lys-Arg-AMC as a specific cathepsin B substrate. Indeed, the assessment of Z-Nle-Lys-Arg-AMC with a series of Z-peptide-AMC substrates indicated that Nle was important over other substitutions consisting of Leu, Tyr, Phe, Ala, Trp, Gly, or Val. Dipeptides containing dibasic sequence combinations of Lys and Arg were poor compared to Z-Nle-Lys-Arg-AMC as the substrate. The pH profile of Z-Nle-Lys-Arg-AMC detected cathepsin B of high specific activity at pH 4.5 to pH 7.5, which covers the biological pH range of cathepsin B within acidic lysosomes to modestly acidic secretory vesicles and the neutral cytosol, nuclei, and extracellular locations.

The high catalytic activity and specificity of Z-Nle-Lys-Arg-AMC were based on the preference of cathepsin B for P3 and P2 residues adjacent to the P1–P1′ cleavage site. When compared to the Z-dipeptide-AMC substrates, the Z-tripeptide-AMC variants with inclusion of Nle as the P3 residue enhances cathepsin B specificity and catalytic efficiency, as shown by the higher specific activities for Z-Nle-Lys-Arg-AMC and Z-Nle-Arg-Arg-AMC compared to their dipeptide variants Z-Lys-Arg-AMC and Z-Arg-Arg-AMC, respectively. Notably, Val or Gly at P3 prevented any turnover of the substrate, suggesting that the P3 residue interacting with the enzyme S3 pocket plays a key role in substrate binding even when favorable amino acids are present at other positions. Additionally, at the P2 position, cathepsin B preferred Lys and Arg basic residues residues at both acidic pH 4.6 and neutral pH 7.2.

In neuronal and glial cells, cathepsin B activity was measured with high specific activity with the novel substrate Z-Nle-Lys-Arg-AMC. Cathepsin B activity was confirmed by inhibition by CA-074, a specific inhibitor of cathepsin B, (52,53) indicating CA-074-sensitive activity. While Z-Nle-Lys-Arg-AMC was highly sensitive for monitoring cathepsin B activity, Z-Arg-Arg-AMC

could monitor only low cathepsin B activity. The Z-Phe-Arg-AMC substrate detected cathepsin B as well as other cysteine cathepsin activity and, thus, was not specific for cathepsin B.

Z-Nle-Lys-Arg-AMC holds promise for evaluation of cathepsin B in various cellular and disease conditions. For example, cathepsin B is secreted by cancer cells into the tumor microenvironment (41−43) where cathepsin B activity can be monitored by Z-Nle-Lys-Arg-AMC. Furthermore, bacterial infection promoted cellular cathepsin B activity at a neutral pH environment (61) and, thus, the Z-Nle-Lys-Arg-AMC can be valuable for monitoring cathepsin B at neutral pH cellular environments in infectious diseases. The sensitivity of this substrate is particularly advantageous for detecting low concentrations of cathepsin B in diverse biological and pathological systems that would otherwise not be detected with the traditionally used substrates. Therefore, use of this substrate may enable a more comprehensive understanding of the role of cathepsin B in human diseases and biological systems.

Findings of this study show that the novel Z-Nle-Lys-Arg-AMC substrate is specific for cathepsin B over other cysteine cathepsins and is a sensitive substrate to monitor cathepsin B activity over a broad pH range from acidic to neutral conditions. This substrate is advantageous over other routinely used substrates for cathepsin B which are non-specific or unable to detect the enzyme's activity at low to high pH conditions. Z-Nle-Lys-Arg-AMC detects cathepsin B in human and mouse species cell types and thus will be useful for clinical cathepsin B biomarker studies as well as for mouse models of human disease conditions.

4.4 Materials and Experimental Details

4.4.1 Materials: Cathepsin B and Cysteine Cathepsins, Substrates, MSP-MS Library and Nano-LC–MS/MS, Cell Culture, and Proteomics

Cathepsin B and cysteine cathepsins (human, recombinant), were obtained from R&D Systems (Minneapolis, MN) or Abcam (Cambridge, MA). Proteases obtained for this study were procathepsin B (R&D Systems, #953-CY-010), active cathepsin L (R&D Systems, #952-CY-010),

active cathepsin K (Abcam, #ab157067), procathepsin S (R&D Systems, #1183-CY-010), procathepsin V (R&D Systems, #1080-CY-010), and procathepsin X (R&D, #934-CY). Mouse cathepsin B was obtained from R&D Systems (R&D Systems, #965-CY-010). The UniProt identification numbers for the human cathepsin proteases studied are P07858 for cathepsin B, P07711 for cathepsin L, P43235 for cathepsin K, P25774 for cathepsin L, 060911 for cathepsin V, and Q9UBR2 for cathepsin X (also known as cathepsin Z). The Uniprot identification for mouse cathepsin B is P10605.

The substrates Z-KR-AMC, Z-GKR-AMC, Z-VKR-AMC, Z-YKR-AMC, Z-FKR-AMC, Z-WKR-AMC, Z-LKR-AMC, Z-AKR-AMC, Z-nRR-AMC, and Z-nKR-AMC ("n" represents norleucine) were custom-synthesized by GenScript (Piscataway, NJ). Z-RR-AMC was purchased from Bachem (#4004789) (Torrance, CA). Z-FR-AMC was purchased from Anaspec (#AS-24096) (Fremont, CA).

The design and synthesis of the 228 14-mer peptide library used for MSP-MS assays are described in ref (51). MSP-MS assays utilized low-binding 600 μL microtubes (Corning, Reynosa, MX), dithiothreitol (DTT) (#V351, Promega, Madison, WI), urea (#U2222, Teknova, Hollister, CA), HPLC-grade water (#W6-4, Fisher Scientific), citric acid monohydrate (#1.00244.0500, Merck, Burlington, MA), sodium phosphate dibasic anhydrous (#SX-072305, EMD, Burlington, MA), sodium acetate (#BP-333-500, Fisher Scientific, Fair Lawn, NJ), EDTA (#324503, Calbiochem, Burlington, MA), sodium chloride (#S271-1, Fisher Chemical, Pittsburgh, PA), acetonitrile (#A955-4, Fisher Chemical, Pittsburgh, PA), formic acid (FA) (#A117-50, Fisher Chemical, Pittsburgh, PA), trifluoroacetic acid (TFA) (#A116-50, Fisher Chemical, Pittsburgh, PA), C18 LTS Tips (#PT-LC18-960, Rainin, Oakland, CA), C18 for SPE stage-tips (#2215-C18,

3M Co., Maplewood, MN), and BEH C18 packing material (#186004661, Waters Corp., Milford, MA).

Cell culture of human neuroblastoma (SHSY-5Y and SK-N-MC) and mouse microglia (BV2) utilized reagents consisting of RPMI 1640, MEMa, F-12K, heat-inactivated fetal bovine serum, and phosphate-buffered saline (PBS) (catalog numbers: 11875093, 12561056, 30-2004, and 10082147, 10010023, respectively, from Gibco, Grand Island, NY). For proteomics, cells were homogenized in a buffer containing a cocktail of protease inhibitors of pepstatin A, leupeptin, chymostatin, and AEBSF (catalog numbers: 516481, 108976, 230790, and 101500, respectively, from Millipore Burlington, MA), and E64c (catalog number: N-1655 from Bachem, Torrance, CA).

Proteomics of cells utilized trypsin/Lys-C (V5037, Promega Madison WI), Empore C18 (octadecyl) (2215, from 3M, St, Paul, MN), and peptide assay (23,275, Pierce Waltham, MA) for sample preparation, combined with nano-LC–MS/MS reagents of trifluoroacetic acid, formic acid, Optima LC–MS water, Optima LC–MS acetonitrile (A116, 85178, W65, and A955, respectively, from Fisher Scientific, Waltham, MA). LC columns utilized were a pricofrit self-pack column of 360 μm OD, 75 μm ID, and 15 μm tip (PF360-75-15-N from New Objective, Littleton, MA) and an Acquity UPLC BEH C18 (130 Å, 1.7 μm) (186004661, from Waters Corp. Milford, MA).

4.4.2 Activation of Cathepsin B and Cysteine Cathepsin Proteases

Recombinant human procathepsins B, V, and S were activated by incubation at 37 °C for 30 min in the 20 mM Na-acetate pH 5.5, 100 mM NaCl, 5 mM DTT, 1 mM EDTA activation buffer. Recombinant human procathepsin X was activated by incubation at room temperature for 5 min in the 20 mM citrate phosphate pH 3.5, 100 mM NaCl, and 5 mM DTT activation buffer.

4.4.3 Cathepsin B Activity with Z-Arg-Arg-AMC and Z-Phe-Arg-AMC Substrates at pH 4.6 and 7.2

Cathepsin B (0.04 ng/μL) activity was assessed with Z-Arg-Arg-AMC and Z-Phe-Arg-AMC substrates (40 μM final concentration) in 40 mM citrate phosphate buffer pH 4.6 or Tris–HCl pH 7.2 in 1 mM EDTA, 100 mM NaCl, and 5 mM DTT with incubation at room temperature (25 °C) in triplicate, and AMC fluorescence readings per second (RFU/s) (excitation 360 nm, emission 460 nm) were recorded over a period of 30 min by a BioTek Synergy HTX plate reader (Software version 3.08.01). Enzyme initial velocity was calculated using the highest slope recorded for 10 consecutive fluorescent readings within the initial 30 min. The mean and standard deviation (SD) were determined from triplicates. RFU/s were converted to pmol/min/μg (specific activity) using AMC standard curves. All data were plotted, calculated, and analyzed using GraphPad Prism (version 9.4.1).

Table 4.2 Z-Phe-Arg-AMC and Z-Arg-Arg-AMC Substrates of Cathepsin B Are Cleaved by Several Cysteine Cathepsins[a]

protease	substrate			
	Z-Phe-Arg-AMC		Z-Arg-Arg-AMC	
	pH 4.6	pH 7.2	pH 4.6	pH 7.2
cathepsin B	974	895	130	441
cathepsin L	7099	0	125	0
cathepsin K	332	420	0	0
cathepsin S	21	29	0	0
cathepsin V	546	0	23	0

[a]The specific activity for cathepsins B, L, K, S, and V were determined for each substrate Z-Phe-Arg-AMC and Z-Arg-Arg-AMC (40 μM) at pH 4.6 and pH 7.2 as described in the Materials and Experimental Details.

4.4.4 Protease Substrate Cleavage Profiling by MSP-MS

4.4.4.1 Peptide Library for Substrate Profiling by MS

MSP-MS was performed for cathepsins B, L, K, S, and V at pH 4.6 and 7.2 by methods that we have described previously. (51) Cathepsin X was performed only at pH 4.6. In a total volume of 22 μL, cathepsin B (0.1 ng/μL), cathepsin L (0.04 ng/μL), cathepsin K (0.07 ng/μL), cathepsin S (1.2 ng/μL), cathepsin V (0.16 ng/μL), and cathepsin X (0.09 ng/μL) were incubated with a mixture of 228 14-mer peptides (0.5 μM for each peptide) in 50 mM citrate phosphate at pH 4.6 or pH 7.2, 100 mM NaCl, 5 mM DTT, 1 mM EDTA assay buffer for 15 and 60 min at 25 °C. 10 μL was removed at 15 and 60 min to be combined with 60 μL of 8 M urea. A control assay used inactivated cathepsins by incubating it with 8 M urea for 60 min at 25 °C, prior to addition of the peptide library in the assay buffer. Assays were conducted in quadruplicate. Samples were acidified by addition of 40 μL of 2% TFA and desalted using custom-made C18 spin tips. The collected liquid samples were dried completely in a vacuum centrifuge and then stored at −70 °C. For LC–MS/MS analysis, dried samples were resuspended in 40 μL of 0.1% TFA, and 4 μL was injected into the Thermo Fisher Scientific Q-Exactive mass spectrometer with an Ultimate 3000 HPLC. Peptides were separated by reverse-phase chromatography using a C18 column at (65 °C), which was done as we have previously described. (50,51)

4.4.4.2 PEAKS Bioinformatics Analysis

PEAKS (v 8.5) software (Bioinformatics Solutions Inc.) was used for MS/MS data analysis. The 228 14-mer library sequence was used as the database for MS data searching and matching, and as a control it was also searched with a decoy consisting of the 228 14-mer library sequences in a reverse order. A precursor tolerance of 0.01 Da and 20 ppm for MS2 fragments was used. Data were filtered to 0.9% peptide sequence false discovery rates determined from hits from decoys. Label-free quantification (LFQ) was used for peptide quantification, and the data was

normalized by LOESS-G normalization method using Normalyzer tool version 1.1.1. (52) Outliers from groups of replicates were removed by Dixon's Q test. (53) Missing and zero values were treated the same and replaced with imputed values determined from randomized normally distributed numbers within the range of the smallest 5% dataset ± SD. The control 0 min values in MSP-MS obtained for cathepsins B, L, K, S, V, and X at pH 4.6 were also analyzed by PEAKS (for n = 20). To determine if the peptide intensity data in at least one of the groups of the 0, 15, and 60 min timepoints were statistically significant, ANOVA testing with multiple testing correction was used; those with $q < 0.05$ were considered for further analysis. Cleaved peptide products at the 15 or 60 min timepoints were defined as having intensity scores of 8-fold or more with $p < 0.05$ by the two-tailed homoscedastic t-test.

4.4.4.3 Cleavage Site Analysis by iceLogo

Evaluation of the frequencies of the P4 to P4′ amino acids adjacent to the cleavage sites was conducted using the iceLogo software 1.3.8, where the "experimental data set" consists of the detected cleavage sites defined earlier and the "reference data set" that consists of all possible cleavages within the MSP-MS library of 228 14-mer peptides. *z*-scores were calculated by the equation $(X - \mu)/\sigma$, where X is the frequency of the amino acid occurring in the "experimental data set" at a specific position relative to the cleavage site (e.g., P3, P2, and P1), μ is the frequency of the amino acid at a specific position in the "reference data set", and σ is the SD. *z*-scores were utilized to generate iceLogo illustrations of the relative frequencies of amino acid residues at each of the P3 to P1 positions of the cleaved peptides where heights of the single letter amino acids represent "percent difference", defined as the difference in the frequency for an amino acid appearing in the "experimental data set" relative to the "reference data set". Amino acids shown above the midline have positive *z*-scores, indicating preferred amino acids, and amino acids shown

below the midline have negative *z*-scores, indicating not preferred amino acids, illustrated using $p < 0.30$ cutoff criteria in the iceLogo software with $p < 0.05$ labeled in purple.

4.4.5 Analysis of pH-Dependent Cathepsin B Activity with Fluorogenic Substrates Designed from MSP-MS Data

For comparison of cathepsin B activity at pH 4.6, pH 5.5, and pH 7.2 with multiple fluorogenic substrates, cathepsin B (0.04 ng/μL) was incubated with 40 μM substrates consisting of Z-Lys-Arg-AMC, Z-Phe-Arg-AMC, Z-Arg-Arg-AMC, Z-Gly-Lys-Arg-AMC, Z-Val-Lys-Arg-AMC, Z-Tyr-Lys-Arg-AMC, Z-Phe-Lys-Arg-AMC, Z-Trp-Lys-Arg-AMC, Z-Leu-Lys-Arg-AMC, Z-Ala-Lys-Arg-AMC, Z-Nle-Arg-Arg-AMC, and Z-Nle-Lys-Arg-AMC. AMC product formation (RFU/s) monitored in 40 mM citrate phosphate, pH 4.6 and pH 7.2, 1 mM EDTA, 100 mM NaCl, and 5 mM DTT was determined from the average of RFU/s triplicates at each pH condition.

For analysis of pH-dependent activity of cathepsin B (0.04 ng/μL), proteolytic activity was monitored over the pH range of pH 2.2–9.0 in 40 mM citrate phosphate (pH 2.2 to pH 6.6) and 40 mM Tris–HCl (pH 7.0 to 9.0), 1 mM EDTA, 100 mM NaCl, and 5 mM DTT, with preincubation in each pH buffer for 10 min prior to initiating the assay by addition of Z-Nle-Lys-Arg-AMC, Z-Arg-Arg-AMC, or Z-Phe-Arg-AMC to a final concentration of 40 μM to generate the pH curve data.

For evaluation of cathepsin B and cysteine cathepsins for substrate selectivity, each cathepsin was incubated with 40 μM substrates consisting of Z-Phe-Arg-AMC, Z-Arg-Arg-AMC, and Z-Nle-Lys-Arg-AMC, and the activity was monitored in 40 mM citrate phosphate (pH 4.6, pH 5.5 and pH 7.2), 1 mM EDTA, 100 mM NaCl, and 5 mM DTT for cathepsin B (0.04 ng/μL), cathepsin K (0.03 ng/μL), cathepsin L (0.03 ng/μL), cathepsin S (0.14 ng/μL), cathepsin V (0.04 ng/μL), and cathepsin X (0.20 ng/μL). Since cathepsin X cannot cleave any of the AMC substrates,

MCA-RPPGFSAFK(Dnp)-OH (R&D Systems #ES005) was used to verify that cathepsin X was active.

4.4.6 Kinetic Parameters of Cathepsin B Assessed by k_{cat} and K_m Values with Fluorogenic Substrates

The kinetic parameters of k_{cat} and K_m for Z-Nle-Lys-Arg-AMC, Z-Arg-Arg-AMC, and Z-Phe-Arg-AMC substrates were determined at pH 4.6 and pH 7.2, using substrate concentrations of 225–5.9 μM with 0.04 ng/μL cathepsin B. RFU values were converted to s^{-1} using AMC standard curves. The k_{cat} and K_m values were obtained from curve fitting the converted RFU data using GraphPad Prism9 software to the equation $v_0 = (V_{max}[S])/(K_m + [S])$, where v_0 is the initial velocity of the enzyme with its corresponding [S] substrate concentration and V_{max} is the maximum enzyme velocity at saturated [S]. $V_{max} = k_{cat}[E]_T$, where $[E]_T$ is the total cathepsin B concentration used in the assay. K_m is the x-axis value [S], where $y = V_{max}/2$. SD values for k_{cat} and K_m were determined from curving fitting the v_0 and [S] data from triplicates.

4.4.7 Neuronal and Microglial Cell Culture

Human neuroblastoma SH-SY5Y (54) and SK-N-MC (55) cells and embryonic mouse microglia BV2 (gifted by Christopher Glass, Ph.D, UC San Diego) were grown in 5% CO_2 at 37 °C under sterile conditions. Growth media conditions were 10% heat-inactivated fetal bovine serum (Life Technologies, Carlsbad, CA) and media consisting of 90% MEMa (Life Technologies) for SK-N-MC cells, 45% Ham's F12-K (ATCC, Manassas, VA), and 45% MEMa (Life Technologies) for SH-SY5Y and 90% RPMI (Life Technologies) for BV2.

4.4.8 Cathepsin B Activity in Human Neuroblastoma and Mouse Microglia

Characterization of the Z-Nle-Lys-Arg-AMC substrate in proteolytic activity assays for specific cathepsin B activity of cell homogenates (prepared in 0.32 M sucrose) was conducted at

40 mM citrate phosphate pH 4.6, 5.5, and 7.2, 5 mM DTT, 1 mM EDTA, 100 mM NaCl, 1.2% DMSO, and homogenates of human neuroblastoma cell lines, SHSY-5Y and SK-N-MC, and mouse microglia cell line, BV2. A concentration of 60 μM Z-Nle-Lys-Arg-AMC, Z-Arg-Arg-AMC, and Z-Phe-Arg-AMC substrates was used in the proteolytic activity assays. Cell homogenates were diluted 1:10 prior to addition to assays. Homogenate protein concentrations were measured by the Biorad protein assay kit (Biorad #5000113, Hercules, CA). The cathepsin B specific inhibitor, CA-074, was used to specifically inhibit cathepsin B activity at concentrations of 1 μM at pH 4.6 and 5.5 and 10 μM at pH 7.2. Assays were performed in 96-well plates at room temperature (25 °C) in a total volume of 100 μL with triplicates. Cell homogenates were incubated with CA-074 or inhibitor controls at RT for 30 min in the absence of substrate, followed by addition of the substrate and incubation at 37 °C. Fluorescence was quantified at 15, 30, and 60 min after substrate was added, by a Biotek Synergy HTX microplate reader with excitation at 360 nm, emission at 460 nm, gain 50, top optics, and read height at 1 mm. Prism GraphPad software was used to analyze data.

4.4.9 Proteomics Identification and Quantitation of Cysteine Cathepsins in Neuronal and Microglial Cells

Analysis of neuronal and microglial cells by proteomics MS utilized protocols that we have previously described elsewhere. (56,57) To summarize, approximately 10^8 cells were collected from 90% confluent flasks with PBS washing and centrifugation at 500*g*. Cell pellets were lysed by dounce homogenization in ice-cold 100 mM Tris pH 7.4, 50 mM NaCl, 1 mM EDTA, and protease inhibitors [10 μM pepstatin A, 10 μM leupeptin, 10 μM chymostatin, 100 μM AEBSF (Millipore, Burlington, MA), and 10 μM E64c (Bachem, Torrance, KA)]. Tryptic digests for proteomics analyses were prepared from 200 mg of total cellular protein as described previously, (59) with two biological flask replicates per cell line and triplicate technical replicate injections

per biological replicate. Tryptic peptides were diluted to 0.5 mg/mL in 2% acetonitrile, 0.1% trifluoroacetic acid, and 2 μg total amount injected by nano-LC–MS/MS on a Dionex UltiMate 3000 nano LC and Q-Exactive mass spectrometer (Thermo Fisher Scientific). Spectra were acquired as described previously. (59) For protein identification and quantitation, spectra were queried against a custom database consisting of the protein sequences of 15 human cathepsins (SH-SY5Y and SK-N-MC) or 15 mouse cathepsins (BV2) with PEAKS v. 8.5 using decoy-fusion and LFQ methods (Bioinformatics Solutions Inc., Waterloo, ON), with search parameters described previously. (59) Proteins were considered identified if present in at least 2 of 3 technical replicates and at least 1 biological replicate. Proteins were considered quantifiable based on the same criteria as for identification. Peak intensity areas of quantifiable data are expressed as mean ± SD.

4.5 Supporting Information

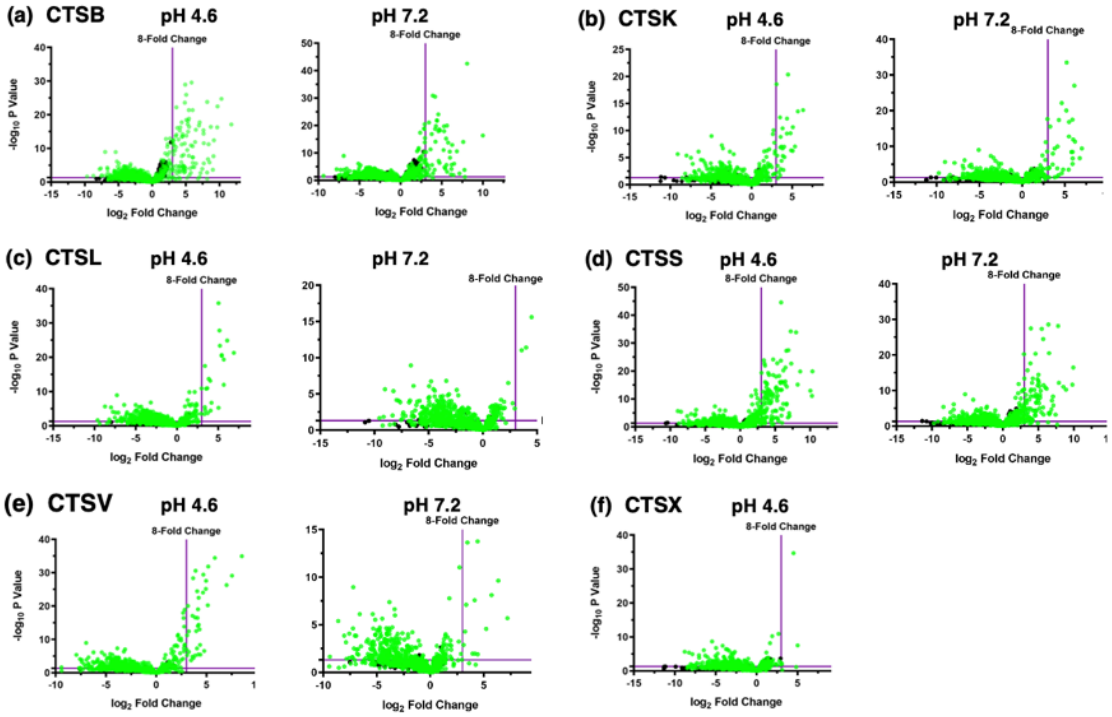

Figure 4.S1 Cathepsins B, K, L, S, V, and X cleavage profiling analyzed by MSP-MS. Volcano plots of cathepsin B (panel a), cathepsin K (panel b), cathepsin L (panel c), cathepsin S (panel d), cathepsin V (panel e), and cathepsin X (panel f) peptide cleavages from MSP-MS data show the log2 ratios of relative quantities of peptide products generated by each of these cathepsins compared to no enzyme activity controls, illustrated by $-\log_{10}$ p values. Peptide products generated with at least an 8-fold change above controls and with $p < 0.05$ were analyzed for the frequencies of amino acid residues at the P4−P4′ positions of the P1−↓P1′ cleavage site in the heatmaps and iceLogos depicted in Figures 4.2 and 4.3.

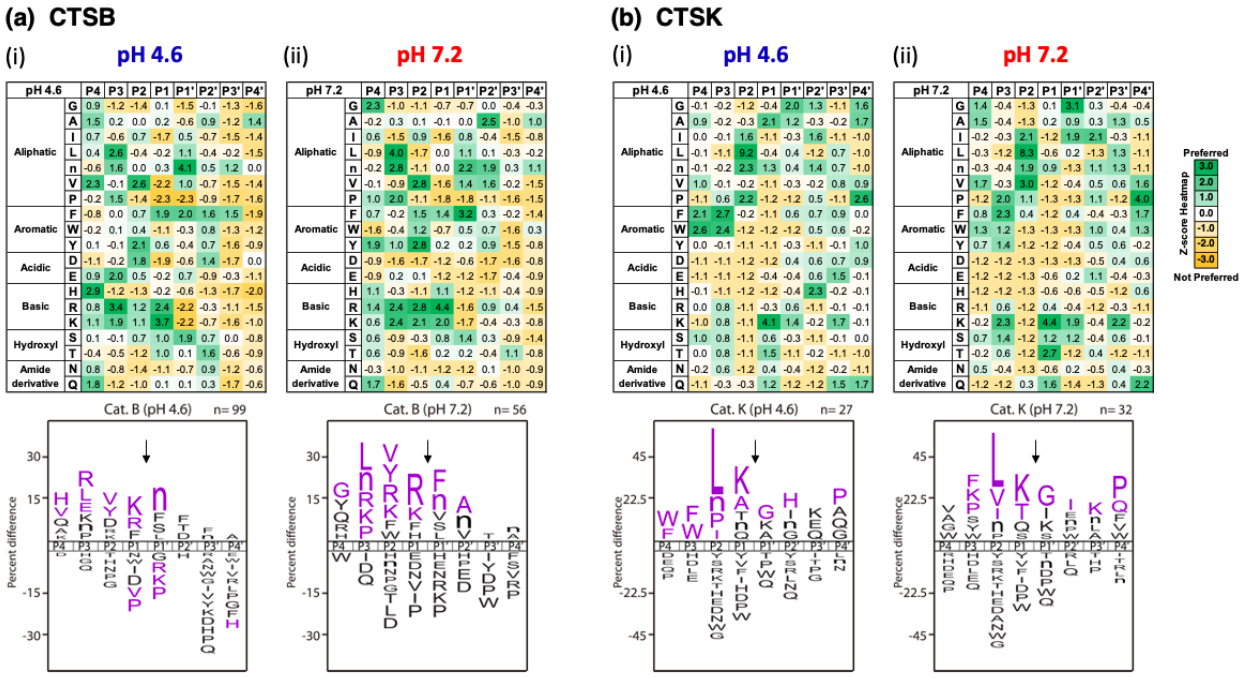

Figure 4.S2 Cathepsin B and cathepsin K cleavage profiles at pH 4.6 and pH 7.2 assessed for preferred residues at P4 to P4' positions adjacent to P1-P1' cleavage sites. (a) Cathepsin B cleavage profiles at pH 4.6 and pH 7.2. The preference of cathepsin B cleavages for amino acid residues at each of the P4 to P4' positions adjacent to the P1-P1' cleavage site was deduced from MSP-MS data cleavage profiling data. Z-scores provided quantitation of preferred (green shades) and non-preferred (yellow shades) residues illustrated in a heat map. The z-scores were utilized for iceLogo illustration of the primary preferred residues at the P4 to P4' positions shown above the mid-line, with non-preferred residues shown below the mid-line. The purple letters indicate significance of $p < 0.05$, and the black letters indicate $p < 0.3$. (b) Cathepsin K cleavage profiles at pH 4.6 and pH 7.2. The preference of cathepsin K cleavages for residues at P4 to P4' positions was defined from MSP-MS data, indicated by z-scores shown in a heat map for preferred residues (green shades) and non-preferred residues (yellow shades). The primary preferred residues, based on z-scores, were plotted in iceLogo illustrations. The purple letters indicate significance of $p < 0.05$, and the black letters indicate $p < 0.3$.

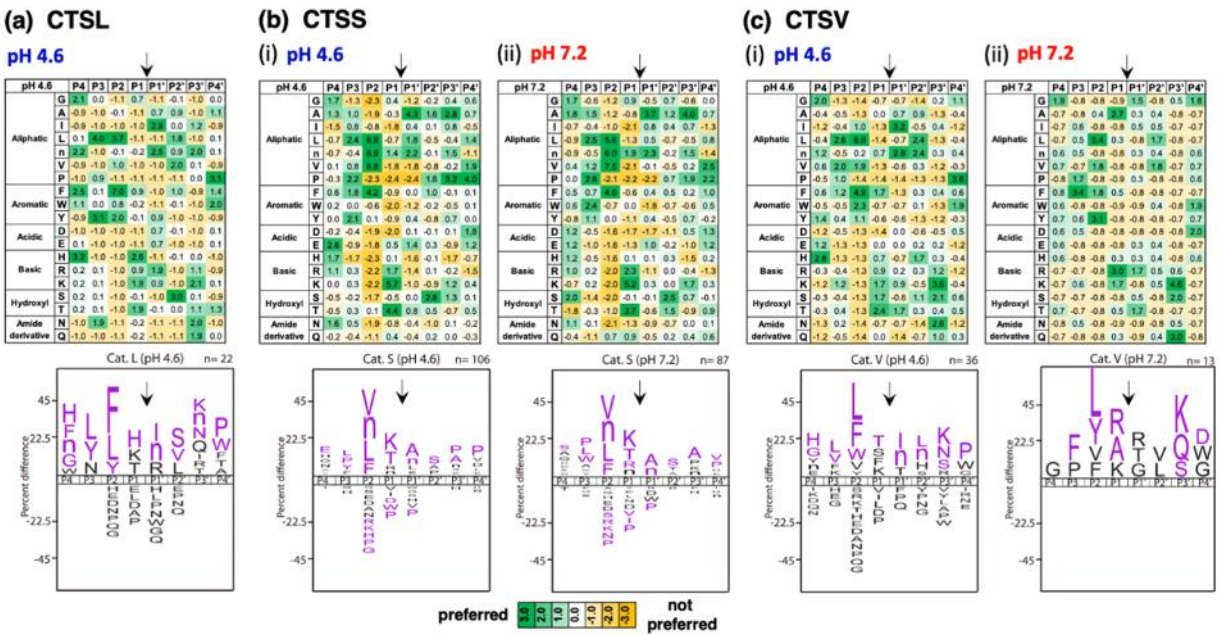

Figure 4.S3 Cathepsins L, S, and V cleavage profiles at pH 4.6 and pH 7.2 assessed for preferred residues at P4 to P4' positions. The preferences of each cathepsin protease for residues at P4 to P4' positions were defined by MSP-MS data, and indicated z-scores for preferred residues (green shades) and non-preferred residues (yellow shades). IceLogo illustrated the main preferred residues (above the line) and preferred residues with significance of $p < 0.05$ are shown in purple letters.

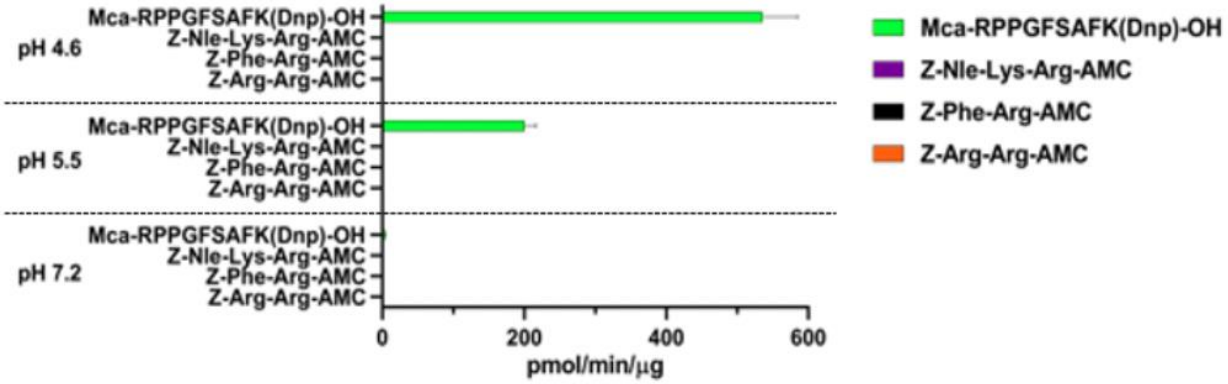

Figure 4.S4 Evaluation of cathepsin X to cleave Z-peptide-AMC substrates of Z-Nle-Lys-Arg-AMC, Z-Phe-Arg-AMC, and Z-Arg-Arg-AMC. Cathepsin X activity is illustrated with its standard substrate Mca-RPPGFSAFK(Dnp)-OH, showing activity at pH 4.6 and pH 5.5 (but not at pH 7.2). Cathepsin X was assessed for proteolytic cleavage of the Z-Nle-Lys-Arg-AMC, Z-Phe-Arg-AMC, or Z-Arg-Arg-AMC substrates (40 µM substrate concentrations) at the three pHs tested of pH 4.6, 5.5, and 7.2. Cathepsin X did not display cleavage of these fluorogenic substrates.

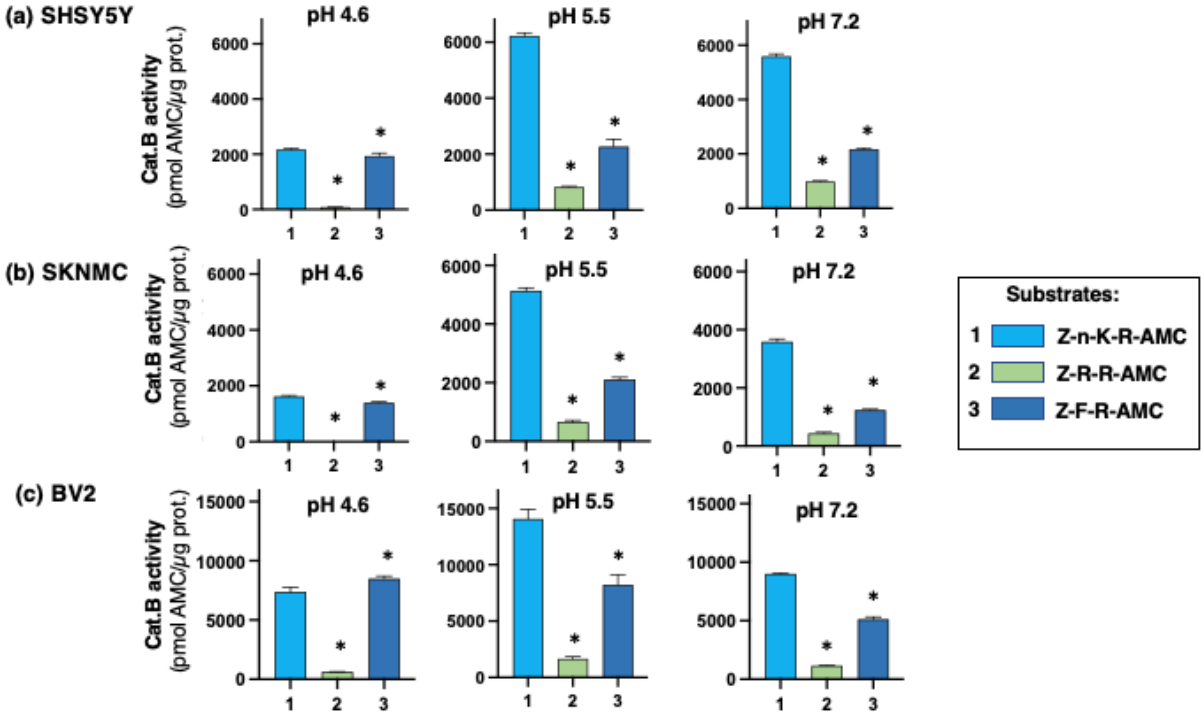

Figure 4.S5 Specific cathepsin B activity monitored with novel Z-Nle-Lys-Arg-AMC substrate in human neuroblastoma and mouse microglia cells. Cathepsin B activity in cell homogenates from human neuroblastoma SHSY-5Y cells (panel a), human neuroblastoma SK-N-MC cells (panel b), and mouse microglia BV2 cells (panel c) was assessed with the substrates Z-Nle-Lys-Arg-AMC, Z-Arg-Arg-AMC, and Z-Phe-Arg-AMC (60 μM) at pH 4.6, 5.5, and 7.2. Data show cathepsin B activity as pmol AMC/μg enzyme protein (30 min incubation) as the mean + SD (n=3). Significance is indicated by *$p < 0.05$ (student's t-test) comparing proteolytic activity with the of substrates Z-Arg-Arg-AMC and Z-Phe-Arg-AMC compared to Z-Nle-Lys-Arg-AMC.

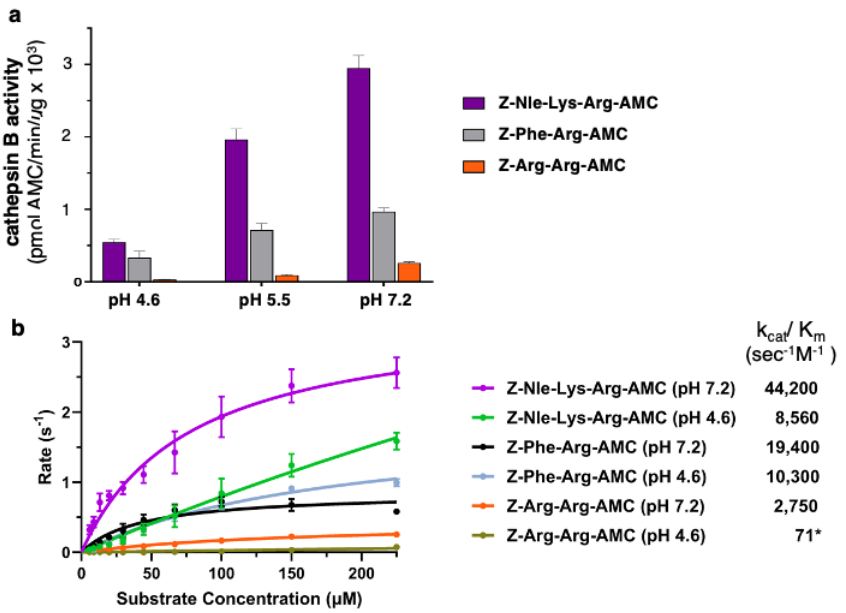

Figure 4.S6 Mouse cathepsin B displays pH-dependent activity with the substrates Z-Nle-Arg-Lys-AMC, Z-Arg-Arg-AMC, and Z-Phe-Arg-AMC. (a) pH-dependence of mouse cathepsin B activity with Z-Nle-Lys-Arg-AMC compared to Z-Arg- Arg-AMC and Z-Phe-Arg-AMC substrates. Cathepsin B specific activity with the three different substrates (40 µM) were assessed at pH 4.6, 5.5, and 7.2. Data points are shown as the mean ± SD (n = 3). (b) Kinetic kcat/Km values for cathepsin B activity with the substrates Z-Nle-Lys-Arg, Z-Arg-Arg- AMC and Z-Phe-Arg-AMC. k_{cat}/Km values for each of the substrates at pH 4.6 and pH 7.2 were calculated for mouse cathepsin B as described in the methods. (The asterisk indicates that the k_{cat} /K_m was determined from the linear slope of the curve since the curve did not plateau out.

Table 4.S1 Kinetic values of human cathepsin B assessed with substrates Z-Nle-Lys-Arg-AMC, Z-Arg-Arg-AMC, and Z-Phe-Arg AMC at pH 4.6 and 7.2.

Z-Nle-Lys-Arg-AMC

	z-nKR-AMC (pH 4.6)	z-nKR-AMC (pH 7.2)
k_{cat} (s^{-1})	18.5 ± 8.5	7.4 ± 1.0
K_m (µM)	1254 ± 649	216 ± 50
k_{cat}/K_m ($s^{-1}M^{-1}$)	14761	34035

Z-Arg-Arg-AMC

	z-RR-AMC (pH 4.6)	z-RR-AMC (pH 7.2)
k_{cat} (s^{-1})	n.d.*	2.8 ± 0.2
K_m (µM)	n.d.*	395 ± 42
k_{cat}/K_m ($s^{-1}M^{-1}$)	930*	7065

Z-Phe-Arg-AMC

	z-FR-AMC (pH 4.6)	z-FR-AMC (pH 7.2)
k_{cat} (s^{-1})	1.5 ± 0.1	1.0 ± 0.1
K_m (µM)	55.2 ± 7.4	29.9 ± 5.0
k_{cat}/K_m ($s^{-1}M^{-1}$)	26885	33645

Kinetic values were determined from three independent determinations assessed for Michaelis-Menten kinetics with standard deviation (conducted using GraphPad Prism). n.d. = not determined.

4.6 References

1. De Duve C, Wattiaux R. (1966) Functions of lysosomes. *Annu Rev Physiol. 28,* 435-92.

2. Xu H, Ren D. (2015) Lysosomal physiology. *Annu Rev Physiol. 77*, 57-80.

3. Lawrence RE, Zoncu R. (2019) The lysosome as a cellular centre for signaling, metabolism and quality control. *Nat Cell Biol. 21*, 133-142.

4. Turk V, Stoka V, Vasiljeva O, Renko M, Sun T, Turk B, Turk D. (2012) Cysteine cathepsins: from structure, function and regulation to new frontiers, *Biochim Biophys Acta*. *1824*, 68-88.

5. Barrett AJ, Rawlings ND, and Woessner JF. (2004). *Handbook of Proteolytic Enzymes*, 2nd edition, Elsevier Academic Press, Amsterdam.

6. Mindell JA. (2012) Lysosomal acidification mechanisms, *Annu Rev Physiol. 74*, 69-86.

7. Ishida Y, Nayak S, Mindell JA, Grabe M. (2013) A model of lysosomal pH regulation, *J Gen Physiol. 141*, 705-20.

8. Ohkuma S, Poole B. (1978) Fluorescence probe measurement of the intralysosomal pH in living cells and the perturbation of pH by various agents, *Proc Natl Acad Sci USA 75*, 3327-31.

9. Hook G, Reinheckel T, Ni J, Wu Z, Kindy M, Peters C, Hook V. (2022) Cathepsin B Gene Knockout Improves Behavioral Deficits and Reduces Pathology in Models of Neurologic Disorders, *Pharmacol Rev. 74*, 600-629.

10. Nakanishi H. (2020) Microglial cathepsin B as a key driver of inflammatory brain diseases and brain aging, *Neural Regen Res.15*, 25-29.

11. Ditaranto K, Tekirian TL, Yang AJ. (2001) Lysosomal membrane damage in soluble Abeta-mediated cell death in Alzheimer's disease, *Neurobiol Dis. 8*, 19-31.

12. Umeda T, Tomiyama T, Sakama N, Tanaka S, Lambert MP, Klein WL, Mori H. (2011) Intraneuronal amyloid β oligomers cause cell death via endoplasmic reticulum stress, endosomal/lysosomal leakage, and mitochondrial dysfunction in vivo, *J Neurosci Res. 89*, 1031-42.

13. Lafrenaye AD, McGinn MJ, Povlishock JT. (2012) Increased intracranial pressure after diffuse traumatic brain injury exacerbates neuronal somatic membrane poration but not axonal injury: evidence for primary intracranial pressure-induced neuronal perturbation, *J Cereb Blood Flow Metab. 32*, 1919-32.

14. Hernandez ML, Marone M, Gorse KM, Lafrenaye AD. Cathepsin B Relocalization in Late Membrane Disrupted Neurons Following Diffuse Brain Injury in Rats. ASN Neuro. 2022 Jan-Dec;14:17590914221099112. PMCID: PMC9069603.

15. Luo CL, Chen XP, Li LL, Li QQ, Li BX, Xue AM, Xu HF, Dai DK, Shen YW, Tao LY, Zhao ZQ. (2013) Poloxamer 188 attenuates in vitro traumatic brain injury-induced mitochondrial and lysosomal membrane permeabilization damage in cultured primary neurons, *J Neurotrauma 30*, 597-607.

16. Windelborn JA, Lipton P. (2008) Lysosomal release of cathepsins causes ischemic damage in the rat hippocampal slice and depends on NMDA-mediated calcium influx, arachidonic acid metabolism, and free radical production, *J Neurochem. 106*, 56-69.

17. Kilinc M, Gürsoy-Ozdemir Y, Gürer G, Erdener SE, Erdemli E, Can A, Dalkara T. (2010) Lysosomal rupture, necroapoptotic interactions and potential crosstalk between cysteine proteases in neurons shortly after focal ischemia, *Neurobiol Dis. 40*, 293-302.

18. Dong H, Qin Y, Huang Y, Ji D, Wu F. (2019) Poloxamer 188 rescues MPTP-induced lysosomal membrane integrity impairment in cellular and mouse models of Parkinson's disease, *Neurochem Int. 126*, 178-186.

19. Freeman D, Cedillos R, Choyke S, Lukic Z, McGuire K, Marvin S, Burrage AM, Sudholt S, Rana A, O'Connor C, Wiethoff CM, Campbell EM. (2013) Alpha-synuclein induces lysosomal rupture and cathepsin dependent reactive oxygen species following endocytosis, *PLoS One 8*, e62143.

20. Amritraj A, Peake K, Kodam A, Salio C, Merighi A, Vance JE, Kar S. (2009) Increased activity and altered subcellular distribution of lysosomal enzymes determine neuronal vulnerability in Niemann-Pick type C1-deficient mice, *Am J Pathol 175*, 2540-56.

21. Fujisawa A, Kambe N, Saito M, Nishikomori R, Tanizaki H, Kanazawa N, Adachi S, Heike T, Sagara J, Suda T, Nakahata T, Miyachi Y. (2007) Disease-associated mutations in CIAS1 induce cathepsin B-dependent rapid cell death of human THP-1 monocytic cells, *Blood 109*, 2903-11.

22. Rajamäki K, Lappalainen J, Oörni K, Välimäki E, Matikainen S, Kovanen PT, Eklund KK. (2010) Cholesterol crystals activate the NLRP3 inflammasome in human macrophages: a novel link between cholesterol metabolism and inflammation, *PLoS One 5*, e11765.

23. Gonzalez EA, Martins GR, Tavares AMV, Viegas M, Poletto E, Giugliani R, Matte U, Baldo G. (2018) Cathepsin B inhibition attenuates cardiovascular pathology in mucopolysaccharidosis I mice, *Life Sci 196*, 102-109.

24. Saluja A, Dudeja V, Dawra R, Sah RP. (2019) Early Intra-Acinar Events in Pathogenesis of Pancreatitis, *Gastroenterology 156*, 1979-1993.

25. Amaral EP, Riteau N, Moayeri M, Maier N, Mayer-Barber KD, Pereira RM, Lage SL, Kubler A, Bishai WR, D'Império-Lima MR, Sher A, Andrade BB. (2018) Lysosomal Cathepsin Release Is Required for NLRP3-Inflammasome Activation by *Mycobacterium tuberculosis* in Infected Macrophages, *Front Immunol 9*, 1427.

26. Morchang A, Panaampon J, Suttitheptumrong A, Yasamut U, Noisakran S, Yenchitsomanus PT, Limjindaporn T. (2013) Role of cathepsin B in dengue virus-mediated apoptosis, *Biochem Biophys Res Commun 438*, 20-5.

27. Bright GR, Fisher GW, Rogowska J, Taylor DL. (1987) Fluorescence ratio imaging microscopy: temporal and spatial measurements of cytoplasmic pH, *J Cell Biol. 104*, 1019-33.

28. Madshus IH. (988) Regulation of intracellular pH in eukaryotic cells. *Biochem J. 1988* 250, 1-8.

29. de Castro,MA, Bunt G, Wouters FS. (2016) Cathepsin B launches an apoptotic exit effort upon cell death-associated disruption of lysosomes, *Cell Death Discov 2*, 16012.

30. Droga-Mazovec G, Bojic L, Petelin A, Ivanova S, Romih R, Repnik U, Salvesen GS, Stoka V, Turk V, Turk B. (2008) Cysteine cathepsins trigger caspase-dependent cell death through cleavage of bid and antiapoptotic Bcl-2 homologues, *J Biol Chem 283*, 19140-50.

31. Kavčič N, Pegan K, Turk B. (2017) Lysosomes in programmed cell death pathways: from initiators to amplifiers. *Biol Chem 398*, 289-301.

32. Wei MC, Lindsten T, Mootha VK, Weiler S, Gross A, Ashiya M, Thompson CB, Korsmeyer SJ. (2000) tBID, a membrane-targeted death ligand, oligomerizes BAK to release cytochrome c, *Genes Dev 14*, 2060-71.

33. Campden RI, Zhang Y. (2019) The role of lysosomal cysteine cathepsins in NLRP3 inflammasome activation, *Arch Biochem Biophys 670*, 32-42.

34. Bai H, Yang B, Yu W, Xiao Y, Yu D, Zhang Q. (2018) Cathepsin B links oxidative stress to the activation of NLRP3 inflammasome, *Exp Cell Res 362*, 180-187.

35. Lian D, Lai J, Wu Y, Wang L, Chen Y, Zhang Y, Boini KM, Huang Y, Chen Y. (2018) Cathepsin B-mediated NLRP3 inflammasome formation and activation in angiotensin II - Induced hypertensive mice: role of macrophage digestion dysfunction, *Cell Physiol Biochem 50*, 1585-1600.

36. Amaral EP, Riteau N, Moayeri M, Maier N, Mayer-Barber KD, Pereira RM, Lage SL, Kubler A, Bishai WR, D'Império-Lima MR, Sher A, Andrade BB. (2018) Lysosomal cathepsin release is required for NLRP3-inflammasome activation by mycobacterium tuberculosis in infected macrophages. *Front Immunol 9*, 1427.

37. Tedelind S, Poliakova K, Valeta A, Hunegnaw R, Yemanaberhan EL, Heldin NE, Kurebayashi J, Weber E, Kopitar-Jerala N, Turk, B, Bogyo M, Brix K. (2010) Nuclear cysteine cathepsin variants in thyroid carcinoma cells, *Biol Chem 391*, 923-35.

38. Hämälistö S, Stahl JL, Favaro E, Yang Q, Liu B, Christoffersen L, Loos B, Boldú C, Joyce JA, Reinheckel T, Barisic M, Jäättelä M. (2020) Spatially and temporally defined lysosomal leakage facilitates mitotic chromosome segregation, *Nat Commun 11*, 229.

39. Cataldo AM, Thayer CY, Bird ED, Wheelock TR, Nixon RA. (1990) Lysosomal proteinase antigens are prominently localized within senile plaques of Alzheimer's disease: evidence for a neuronal origin. *Brain Res. 513,* 181-92.

40. Cataldo AM, Hamilton DJ, Nixon RA. (1994) Lysosomal abnormalities in degenerating neurons link neuronal compromise to senile plaque development in Alzheimer disease. *Brain Res. 640,* 68-80.

41. Giusti I, D'Ascenzo S, Millimaggi D, Taraboletti G, Carta G, Franceschini N, Pavan A, Dolo V. (2008) Cathepsin B mediates the pH-dependent proinvasive activity of tumor-shed microvesicles. *Neoplasia 10,* 481-8.

42. Victor BC, Anbalagan A, Mohamed MM., Sloane, B.F., Cavallo-Medved ,D. (2011) Inhibition of cathepsin B activity attenuates extracellular matrix degradation and inflammatory breast cancer invasion. *Breast Cancer Res 13,* R115.

43. Aggarwal N, Sloane BF. (2014) Cathepsin B: multiple roles in cancer, *Proteomics Clin Appl 8,* 427-37.

44. Yoon MC, Solania A, Jiang Z, Christy MP, Podvin S, Mosier C, Lietz CB, Ito G, Gerwick WH, Wolan DW, Hook G, O'Donoghue AJ, Hook V. (2021) Selective Neutral pH Inhibitor of Cathepsin B Designed Based on Cleavage Preferences at Cytosolic and Lysosomal pH Conditions. *ACS Chem Biol. 16,* 1628-1643.

45. Yoon MC, Christy MP, Phan VV, Gerwick WH, Hook G, O'Donoghue AJ, Hook V. (2022) Molecular Features of CA-074 pH-Dependent Inhibition of Cathepsin B. *Biochemistry 61*, 228-238.

46. Turk B, Dolenc I, Zerovnik E, Turk D, Gubensek F, Turk V (1994). Human cathepsin B is a metastable enzyme stabilized by specific ionic interactions associated with the active site. *Biochemistry* 33, 14800-6.

47. Caglic D, Kosec G, Bojic L, Reinheckel T, Turk V, Turk B. (2009) Murine and human cathepsin B exhibit similar properties: possible implications for drug discovery. *Biol Chem. 390,* 175-9.

48. Poreba M, Groborz K, Vizovisek M, Maruggi M, Turk D, Turk B, Powis G, Drag M, Salvesen GS. (2019) Fluorescent probes towards selective cathepsin B detection and visualization in cancer cells and patient samples. *Chem Sci. 10,* 8461-8477.

49. Turk B, Dolenc I, Turk V, Bieth JG. (1993) Kinetics of the pH-induced inactivation of human cathepsin L. Biochemistry 32, 375-80.

50. Turk B, Dolenc I, Lenarcic B, Krizaj I, Turk V, Bieth JG, Björk I. (1999) Acidic pH as a physiological regulator of human cathepsin L activity. Eur J Biochem 259(3), 926-32.

51. O'Donoghue AJ, Eroy-Reveles AA, Knudsen GM, Ingram J, Zhou M, Statnekov JB, Greninger AL, Hostetter DR, Qu G, Maltby DA, Anderson MO, Derisi JL, McKerrow JH,

Burlingame AL, Craik CS. (2012) Global identification of peptidase specificity by multiplex substrate profiling. *Nat Methods. 9*, 1095-100.

52. Chawade A, Alexandersson E, Levander F. (2014) Normalyzer: a tool for rapid evaluation of normalization methods for omics data sets. J Proteome Res. 13, 3114-20.

53. Rorabacher, DB. (1991) Statistical treatment for rejection of deviant values: critical values of Dixon's Q parameter and related subrange ratios at the 95% confidence level. Anal. Chem. 63, 139-146.

54. Biedler JL, Roffler-Tarlov S, Schachner M, Freedman LS. (1978) Multiple neurotransmitter synthesis by human neuroblastoma cell lines and clones. Cancer Res. 38, 3751-7. PMID: 29704.

55. Helson L, Das SK, Hajdu SI. (1975) Human neuroblastoma in nude mice. Cancer Res. 1975 Sep;35(9):2594-9. PMID: 167965.

56. Podvin S, Jones A, Liu Q, Aulston B, Ransom L, Ames J, Shen G, Lietz CB, Jiang Z, O'Donoghue AJ, Winston C, Ikezu T, Rissman RA, Yuan S, Hook V. (2020) Dysregulation of Exosome Cargo by Mutant Tau Expressed in Human-induced Pluripotent Stem Cell (iPSC) Neurons Revealed by Proteomics Analyses. *Mol Cell Proteomics 19*, 1017-1034.

57. Podvin S, Jones A, Liu Q, Aulston B, Mosier C, Ames J, Winston C, Lietz CB, Jiang Z, O'Donoghue AJ, Ikezu T, Rissman RA, Yuan SH, Hook V. (2021) Mutant Presenilin 1 Dysregulates Exosomal Proteome Cargo Produced by Human-Induced Pluripotent Stem Cell Neurons. ACS Omega 6, 13033-13056.

58. Towatari T, Nikawa T, Murata M, Yokoo C, Tamai M, Hanada K, and Katunuma N. (1991) Novel epoxysuccinyl peptides. A selective inhibitor of cathepsin B, in vivo, *FEBS. Lett*. 280, 311-5.

59. Murata M, Miyashita S, Yokoo C, Tamai M, Hanada K, Hatayama K, Towatari T, Nikawa T, and Katunuma N. (1991) Novel epoxysuccinyl peptides. Selective inhibitors of cathepsin B, in vitro, *FEBS. Lett.* 280, 307-10.

60. Jiang Z, Lietz CB, Podvin S, Yoon MC, Toneff T, Hook V, O'Donoghue AJ. (2021) Differential Neuropeptidomes of Dense Core Secretory Vesicles (DCSV) Produced at Intravesicular and Extracellular pH Conditions by Proteolytic Processing. ACS Chem Neurosci. 12, 2385-2398.

61. Sanman LE, van der Linden WA, Verdoes M, Bogyo M. (2016) Bifunctional Probes of Cathepsin Protease Activity and pH Reveal Alterations in Endolysosomal pH during Bacterial Infection. Cell Chem Biol 23, 793-804.

Acknowledgements

Chapter 4, in full, is a reprint of the material as it appears in Biochemistry in American Chemical Society. Michael C. Yoon, Von V. Phan, Sonia Podvin, Charles Mosier, Anthony J O'Donoghue, and Vivian Hook, American Chemical Society, 2023. The dissertation author was a co-author of this material.

Chapter 5 Involvement of Cytosolic Cathepsin B in Cell Death Induced by Low Nutrient Stress in Microglia Cells

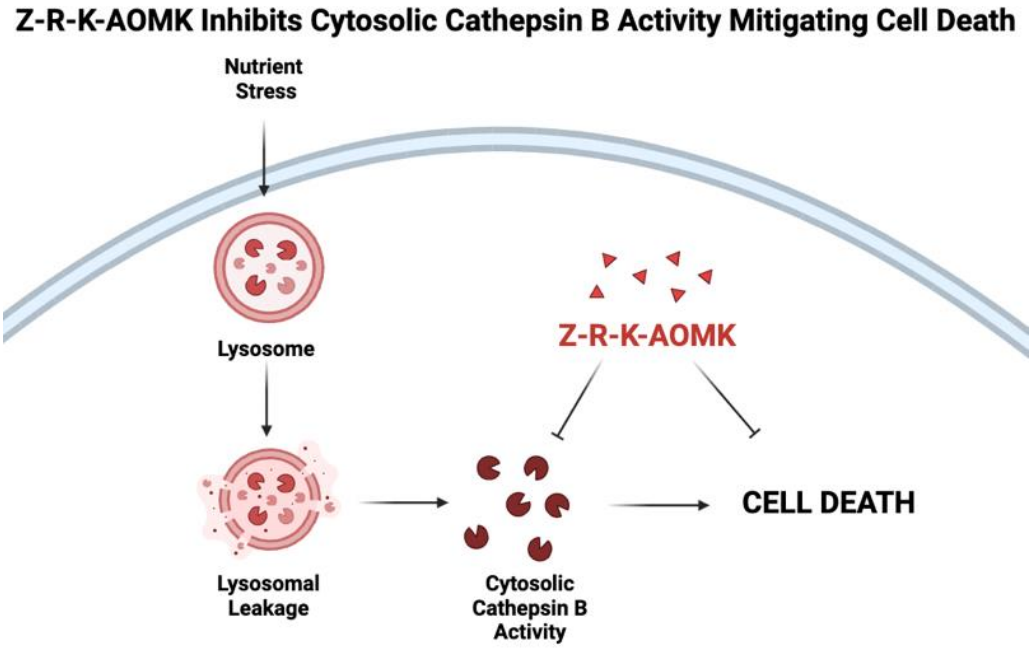

Figure 5.1 Chapter 5 Abstract. Cathepsin B's involvement in neurological conditions like Alzheimer's disease (AD) and traumatic brain injury (TBI) stems from its ability to move from lysosomes to the cytosol, where it activates pathways linked to cell death and inflammation, worsening disease progression. Our study utilizes nutrient stress, commonly seen in neurological disorders, as a model for AD and TBI. Nutrient stress induces mitochondrial dysfunction, leading to metabolic disruptions that cause lysosomal leakage, cathepsin B translocation, and activation, exacerbating neuropathology. Our study aims to elucidate the mechanisms underlying cathepsin B activation during stress and evaluate the efficacy of the novel inhibitor Z-R-K-AOMK in mitigating its activity. We found that Z-R-K-AOMK effectively inhibits mouse cathepsin B activity, exhibiting a preference for neutral pH environments. Under nutrient stress, characterized by low fetal bovine serum (FBS) conditions, we observed increased cell death and cathepsin B activity. Incubation with Z-R-K-AOMK significantly reduced cell death and cathepsin B activity, highlighting its therapeutic potential. Fractionation of subcellular organelles revealed an induction of cytosolic cathepsin B activity under low nutrient conditions, incubation with Z-R-K-AOMK significantly reduced cytosolic cathepsin B activity corroborating our hypothesis. In conclusion, our study underscores the pathogenic role of cathepsin B in stress-induced cell death in neurological diseases. Targeting cytosolic cathepsin B with Z-R-K-AOMK emerges as a promising therapeutic strategy, though further investigations into cathepsin B inhibition, cell death mechanisms, and cellular localization are warranted to develop effective treatments for these conditions.

5.1 Introduction

Cathepsin B, an essential lysosomal cysteine protease, plays a fundamental role in protein degradation essential for maintaining cellular homeostasis. (1-3) Significantly, cathepsin B is a bioactive protease that produces biologically active proteins and peptides. (3) These molecules intricately modulate various normal biological processes and are implicated in the pathogenesis of numerous human diseases. While typically localized and functional within the acidic environment of the lysosome at pH 4.6 (4-5), in numerous neurologic conditions, cathepsin B translocate from the lysosome to the cytosol at neutral pH 7.2, retaining its proteolytic activity. (1, 6-9) The biologically active peptides produced by cytosolic cathepsin B activate cell death (10-12) and inflammatory pathways (13-14) leading to neurodegeneration and neuroinflammation that contribute to disease pathogenesis of many neurological disorders, including Alzheimer's disease (AD), traumatic brain injury (TBI), inflammatory neurological diseases, aging, and more. (15)

Cathepsin B has emerged as a novel therapeutic target in AD and TBI, attributed to its involvement in lysosomal leakage and the distinct pathogenic properties of cytosolic cathepsin B. (16) Research indicates that cathepsin B contributes to the underlying mechanisms driving the neuropathogenesis of AD and TBI. In AD mouse models, increased expression of cathepsin B is observed, and knockout (KO) of the gene leads to improvements in memory deficits and reduction of Aβ. (17) Similarly, studies employing controlled cortical impact (CCI) mouse models of TBI reveal elevated expression and activity of cathepsin B, with KO of the gene reducing TBI-induced dysfunctions and blocking increased production of proapoptotic Bax. (16, 18) Previous work from our lab demonstrated that chemical inhibition of cathepsin B by E64d improves behavioral dysfunctions and neuropathology in AD and TBI mouse models. (19) However, E64d, a pan-cysteine protease inhibitor, lacks selectivity for cytosolic cathepsin B over lysosomal cathepsin B or other lysosomal cysteine cathepsins.

To explore the specific role of cytosolic cathepsin B in AD and TBI pathogenesis, the development of a selective inhibitor was essential. Given the drastic difference in pH between the cytosolic neutral pH 7.2 and lysosomal acidic pH 4.6, a pH-selective inhibitor, Z-R-K-AOMK, was designed to capitalize on the differences. (20) This inhibitor leverages differences in conformation or ionization states, thereby increasing potency for cathepsin B in neutral pH environments compared to acidic pH environments. By exploiting the pH disparity and cleavage properties between cathepsin B in the cytosol and the lysosome, the goal of developing pH-selective inhibitors was to selectively and specifically inhibit neutral, cytosolic cathepsin B without affecting acidic, lysosomal cathepsin B or other lysosomal cysteine cathepsins. Studies assessing cathepsin B activity with a diverse set of peptides in different pH environments have revealed distinct cleavage selectivity. (20-21) The present study aims to utilize the neutral pH-selective inhibitor, Z-R-K-AOMK, and pH differences in the cytosol and lysosome to investigate the impact of lysosomal leakage of cathepsin B into the cytosol and evaluate whether inhibiting cathepsin B activity in the cytosol can mitigate cell death associated with AD and TBI.

Among AD, TBI, and the various neurologic diseases, there is a common occurrence of nutrient stress. Cell death results in large part from low nutrient stress. Metabolic disturbances, encompassing sugars, lipids, proteins, and iron often manifest following TBI, (22) and often seen are dysfunctions in glucose uptake and utilization (23-24), leading to systemic metabolic changes. (25) Similar dysfunctions in glucose uptake and utilization are evident in AD, exacerbating energy deficiencies within the central nervous system. (26) Glucose transport and metabolism decrease with age, and in some cases of AD, glucose hypometabolism precedes decades before the cognitive decline. These effects provide a feedforward loop where cell death and inflammation trigger dysfunctional energy metabolism, that further exacerbates neurodegeneration. (27) Mitochondrial

dysfunctions from metabolic dysfunction are commonly linked with lysosomal dysfunction. The lysosome serves a role in nutrient sensing, utilization, and recycling, and compromising lysosomal function can lead to severe metabolic and neurologic impact, contributing to disease pathology. (28) In light of these observations, nutrient deprivation is utilized in this study as a stressor, modeling AD and TBI. Nutrient stress induces lysosomal membrane permeabilization (29), which in turn causes cathepsin B translocation from the lysosome to the cytosol, activating cell death and inflammatory pathways, thereby exacerbating the pathological cascade seen in AD and TBI, and various other neurological disorders.

To delve deeper into the mechanisms by which nutrient deprivation triggers cathepsin B activity in the cytosol, this study employs the neutral pH-selective inhibitor, Z-R-K-AOMK (20), in conjunction with nutrient deprivation in mouse microglia BV2 cells. The aim is to investigate the impact of leakage of cathepsin B from lysosomes into the cytosol, and to assess whether inhibiting cathepsin B activity in the cytosol can attenuate cell death associated with AD and TBI. Understanding the mechanisms by which cytosolic cathepsin B exerts its detrimental effects on neuronal viability is crucial for developing targeted therapeutic interventions. By elucidating the intricate pathways involved in cathepsin B-mediated neurodegeneration, researchers can identify novel drug targets and strategies aimed at preserving neuronal function and halting disease progression.

5.2 Results

5.2.1 Z-R-K-AOMK effectively inhibits mouse cathepsin at neutral cytosolic pH

The effectiveness of Z-R-K-AOMK inhibition of mouse cathepsin B was evaluated at both pH 4.6 and 7.2 (Figure 5.2). At a cytosolic pH of 7.2, Z-R-K-AOMK proved to be a potent inhibitor, displaying an IC_{50} value of 25 nM (IC_{50}, concentration of inhibitor for 50% inhibition). However, under lysosomal conditions with a pH of 4.6, the inhibitor exhibited reduced potency,

as evidenced by an IC_{50} value of 2,500 nM. These findings indicate a significant 100-fold difference in potency between neutral pH 7.2 and acidic pH 4.6, underscoring the pH-dependent inhibitory characteristics of Z-R-K-AOMK against mouse cathepsin B.

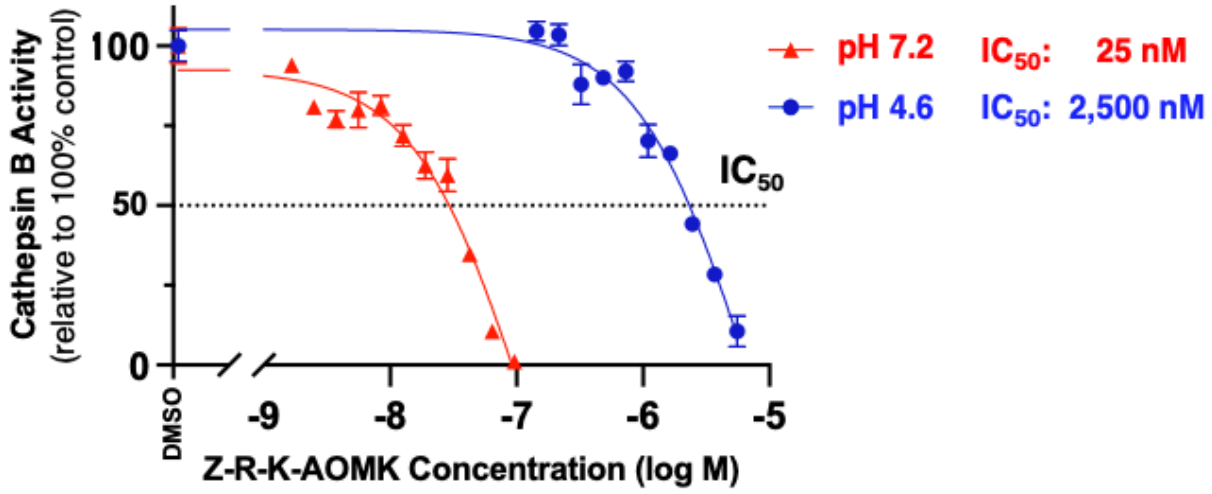

Figure 5.2 Z-R-K-AOMK pH-dependent inhibition of mouse cathepsin B under acidic and neutral pH conditions. Potencies of Z-R-K-AOMK inhibition of mouse cathepsin B were assessed at pH 4.6 and pH 7.2 over a range of concentrations of Z-R-K-AOMK. Inhibitory potencies were assessed by IC_{50} values, representing inhibitor concentrations that reduced cathepsin B activity by 50%. Poor pH-dependent inhibition was displayed at pH 4.6, while potent pH-dependent inhibition was displayed at pH 7.2.

5.2.2 Cell death and cathepsin B activity are induced by low nutrient stress, a prevalent stressor in AD and TBI

We examined cell death (Figure 5.3a) and cathepsin B activity (Figure 5.3b) in embryonic mouse microglia BV2 cells under normal nutrient (10% FBS) and low nutrient stress (0% FBS) conditions. Cell death was evaluated through LDH activity in the cell culture media, while cathepsin B activity was assessed using a fluorogenic substrate in cell homogenates. The results illustrate that cell death increases under low nutrient conditions, as evidenced by the 223.58% increase in media LDH activity between the normal and stressed conditions (Figure 5.3a). Notably, treatment with the Z-R-K-AOMK inhibitor mitigates this increase in media LDH activity at 0%

FBS, decreasing LDH activity by 45.96%, suggesting a reduction in cell death upon inhibitor incubation. Furthermore, the data demonstrates a significant decrease in cathepsin B activity in BV2 cell homogenate upon treatment with the Z-R-K-AOMK inhibitor, observed across both 10% and 0% FBS conditions, with a reduction of cathepsin B activity of 72.22% and 90.08% respectively (Figure 5.3b).

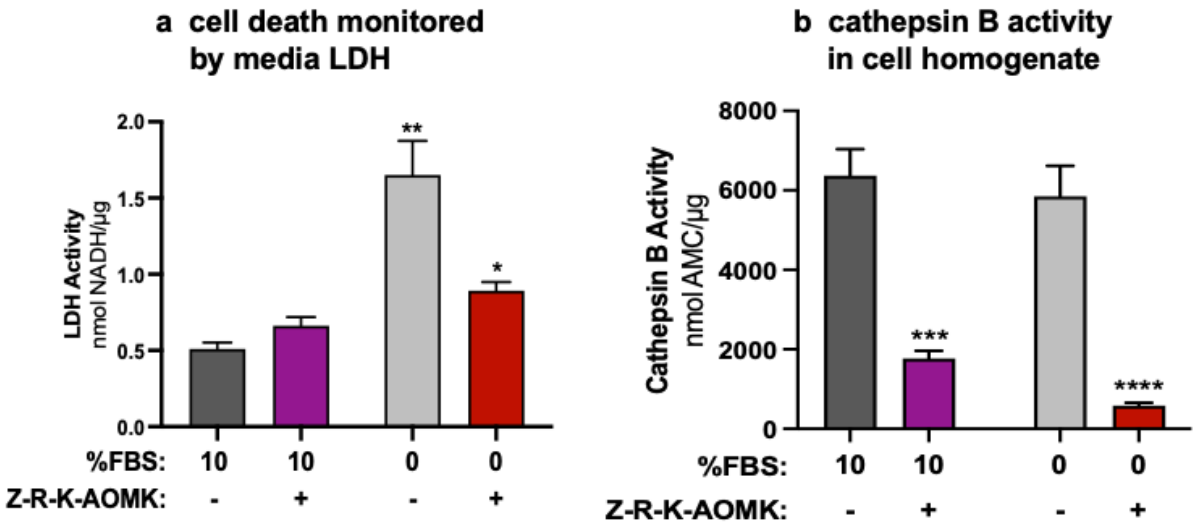

Figure 5.3 Mouse microglia BV2 cells display increased cell death and cathepsin B activity under stressed conditions, reduced by Z-R-K-AOMK inhibitor. (a) Cell death in normal nutrient, 10% FBS, and low nutrient, 0% FBS, conditions with and without Z-R-K-AOMK incubation, monitored by media LDH. Data show LDH activity in cell culture media as nmol NADH/µg total homogenate protein as the mean ± SEM (n=3). Significance is indicated by * $p<0.05$ (student's t-test), compared to 0% FBS without Z-R-K-AOMK, 45.96%decrease in LDH activity. ** $p<0.005$ (student's t-test), compared to 10% FBS without Z-R-K-AOMK, 223.58% increase in LDH activity. (b) Cathepsin B activity in cell homogenate from mouse microglia BV2 cells were assessed with substrate Z-Nle-Lys-Arg-AMC (60 µM) at pH 5.5. Data show cathepsin B activity as nmol AMC/µg enzyme protein (30 min incubation) as the mean ± SEM (n=3). Significance is indicated by *** $p<0.0005$, compared to 10% FBS without Z-R-K-AOMK, 72.22% inhibition of activity. **** $p<0.00005$, compared to 0% FBS without Z-R-K-AOMK, 90.08% inhibition of activity.

5.2.3 Cytosol and lysosome isolation by density gradient fractionation

Subcellular organelle compartments from mouse microglia BV2 cells in normal nutrient and low nutrient conditions, with and without Z-R-K-AOMK incubation were meticulously

isolated through density centrifugation, following the outlined protocol in the methods section. Initially, BV2 cellular homogenate underwent two rounds of centrifugation to effectively separate cellular debris, nuclei, and mitochondria from the cytosol and lysosomes (Figure 5.4). Subsequently, the resulting supernatant, termed S2, underwent ultracentrifugation within a sucrose gradient comprising concentrations of 0.32, 0.8, 1.5, and 2.2 M sucrose. Expectedly, cytosolic compartments should emerge at the uppermost layer, characterized by a sucrose concentration of 0.32 M, while lysosomes are anticipated to appear within the intermediate layers, typically spanning between 0.8 and 1.5 M sucrose. Following the centrifugation process, twenty distinct fractions were meticulously collected and subjected to further analysis, as elaborated in subsequent sections.

5.2.4 Cathepsin B activity assessed in cytosol and lysosome gradient fractions from cells treated with stress and Z-R-K-AOMK inhibitor

We investigated the cathepsin B activity and LDH activity within the fraction samples obtained from the organelle isolation process through density gradient fractionation of microglia BV2 cells under low nutrient stress (0% FBS) and normal nutrient (10% FBS) conditions (Figure 5.5). In the fractions derived from the stressed condition, discernible peaks in cathepsin B activity were evident in fractions F1-3 and F8-12 (Figure 5.5a.i), indicative of cathepsin B activity within the anticipated layers corresponding to the cytosol and lysosomes, respectively (Figure 5.4). Conversely, within the fractions from the normal nutrient condition, similar peaks were observed in fractions F1-3 and F8-12, resembling the pattern observed under the low nutrient condition. However, noteworthy differences emerged, particularly in the cytosolic fractions where cathepsin B activity appeared notably increased in the stressed condition compared to the normal condition (Figure 5.5a.ii).

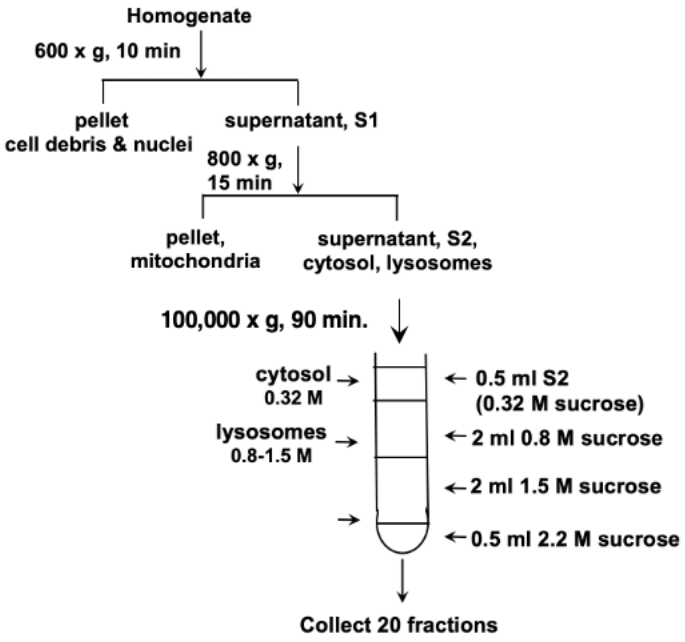

Figure 5.4 Cellular cytosol and lysosome fractions separated by density gradient. Subcellular fractions of cellular cytosol and lysosomes were obtained through density gradient fractionation. Mouse microglia BV2 cell homogenate underwent sequential centrifugation steps at 600 x g for 10 minutes to isolate supernatant S1, followed by centrifugation of S1 at 800 x g for 15 minutes to obtain supernatant S2. The resulting supernatant S2 underwent ultracentrifugation at 100,000 x g for 90 minutes in a sucrose gradient. Fractions of 200 µl were collected from the top after ultracentrifugation. Differential centrifugation and sucrose gradient separation facilitated the isolation of subcellular compartments based on differences in density.

LDH activity was employed as a cytosolic marker. In the low nutrient stress condition, LDH activity was confined to fractions F1-3 (Figure 5.5b.i), suggesting these fractions as the cytosolic compartments. This observation was consistent in the normal condition, where LDH activity persisted solely within fractions F1-3 (Figure 5.5b.ii). Given that cathepsin B activity is characteristic of lysosomal proteases that may translocate into the cytosol under certain conditions, the exclusive presence of LDH activity in fractions F1-3 indicates them as the cytosolic fractions. Consequently, the remaining fractions harboring cathepsin B activity, namely F8-12, are presumed to represent the lysosomal fractions.

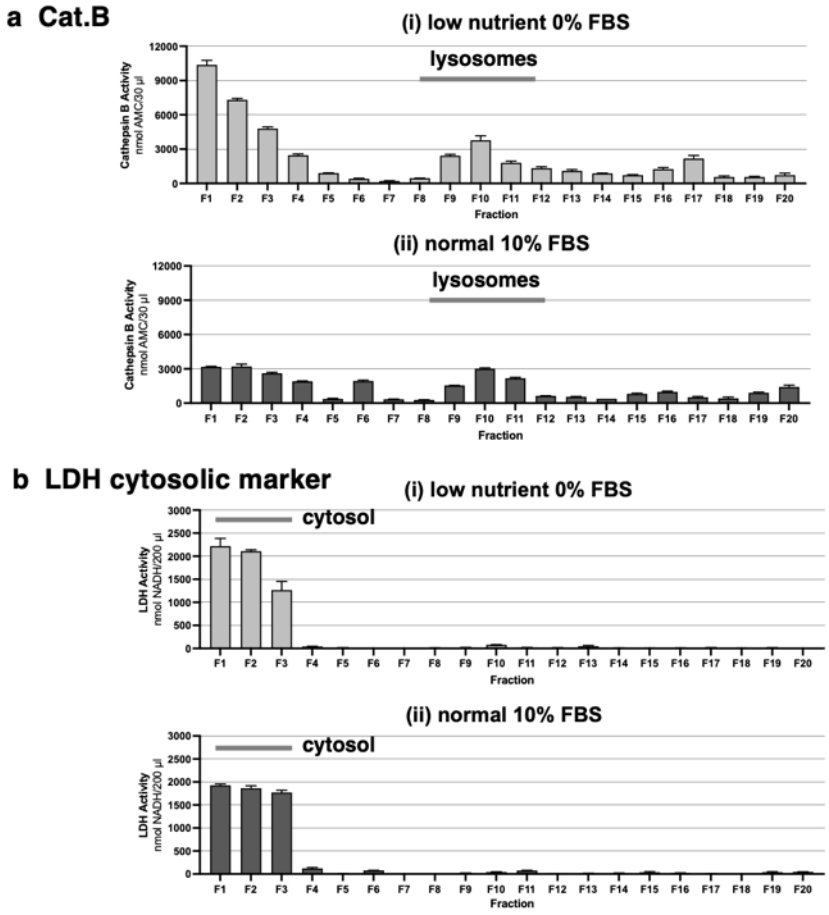

Figure 5.5 Cathepsin B and LDH activity in fractions separated by density gradient. (a) Cathepsin B activity was evaluated in fractions obtained from mouse microglia BV2 cells under low-nutrient (0% FBS) and normal-nutrient (10% FBS) conditions using substrate Z-Nle-Lys-Arg-AMC (60 µM) at pH 5.5. The data represent cathepsin B activity as nmol AMC/µg enzyme protein after a 30-minute incubation period, presented as the mean ± SEM (n=3). (b) LDH activity, serving as a cytosolic marker, was measured in fractions collected from mouse microglia BV2 cells under low-nutrient (0% FBS) and normal-nutrient (10% FBS) conditions. LDH activity in cell culture media is expressed as nmol NADH/µg total homogenate protein, represented as the mean ± SEM (n=3).

5.2.5 Cathepsin B activity in cytosol is induced by stress and inhibited by Z-R-K-AOMK

The impact of low nutrient stress and incubation with the Z-R-K-AOMK inhibitor on cathepsin B activity within the cytosol and lysosomes of mouse microglia BV2 cells was investigated. Under the 10% FBS condition, the Z-R-K-AOMK inhibitor demonstrated a 34.75% inhibition of cathepsin B activity in the cytosol (Figure 5.6a) and a 46.09% inhibition in the lysosome (Figure 5.6b). Conversely, at the 0% FBS condition, the inhibitor exhibited a similar

effect, inhibiting cathepsin B activity by 72.39% in the cytosol and 63.89% in the lysosome (Figure 5.6a and Figure 5.6b). Notably, cathepsin B activity was increased by 109.79% between the 10% FBS and 0% FBS conditions within the cytosol (Figure 5.6a), while no significant changes were observed in the lysosome (Figure 5.6b). This observation suggests that low nutrient conditions induce cathepsin B activity in the cytosol, which is effectively inhibited by incubation with the Z-R-K-AOMK inhibitor.

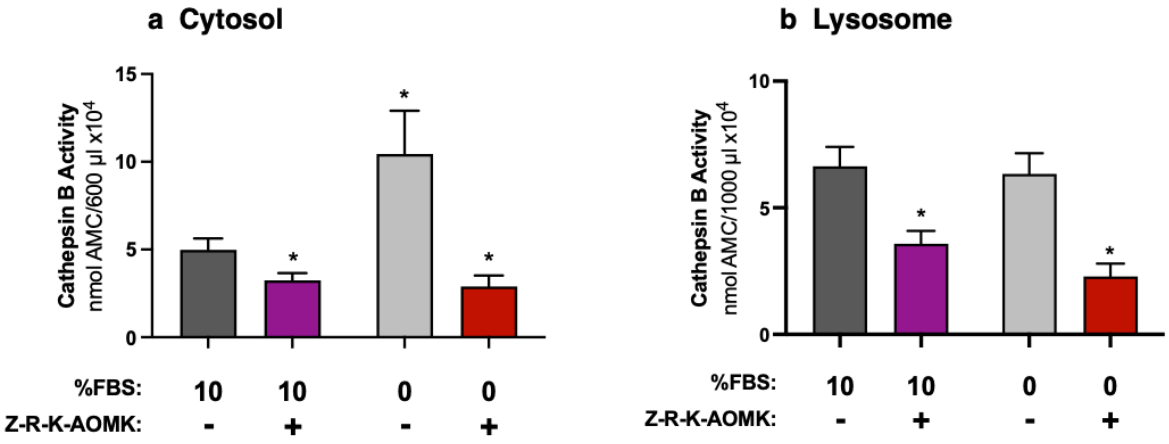

Figure 5.6 Cathepsin B activity in the cytosol is induced by stress and inhibited by Z-R-K-AOMK. (a) Cathepsin B activity in cytosol from mouse microglia BV2 cells in normal nutrient and low nutrient conditions, incubated with 2 µM Z-R-K-AOMK, were assessed with substrate Z-Nle-Lys-Arg-AMC (60 µM) at pH 5.5. Data show cathepsin B activity as nmol AMC/600 µl of cytosolic fractions $x10^4$ (60 min incubation) as the mean ± SEM (n=3). Significance is indicated by * $p<0.05$ at 10% FBS Z-R-K-AOMK inhibited Cathepsin B activity by 34.75%. At 0% FBS, Z-R-K-AOMK inhibited Cathepsin B Activity by 72.39%, * $p<0.05$. Cathepsin B Activity increased by 109.79% between 10% and 0% FBS, * $p<0.05$. (b) Cathepsin B activity in lysosome from mouse microglia BV2 cells in normal nutrient and low nutrient conditions, incubated with 2 µM Z-R-K-AOMK, were assessed with substrate Z-Nle-Lys-Arg-AMC (60 µM) at pH 5.5. Data show cathepsin B activity as nmol AMC/1000 µl of lysosomal fractions $x10^4$ (60 min incubation) as the mean ± SEM (n=3). Significance is indicated by * $p<0.05$ at 10% FBS, Z-R-K-AOMK inhibited Cathepsin B activity by 46.09%, * $p<0.05$. At 0% FBS, Z-R-K-AOMK inhibited Cathepsin B Activity by 63.89%, * $p<0.05$.

5.3 Discussion

The role of cathepsin B in human physiology and neurological diseases is noteworthy, as products of cathepsin B proteolytic activity activate many biological pathways. Under stressful

conditions, lysosomal leakage prompts the translocation of cathepsin B from the lysosomal milieu into the cytosol, where it retains its proteolytic activity, consequently activating biological responses that may exacerbate cell stress, including cell death. (10-13) Cathepsin B in the cytosol is involved in multiple kinds of programmed cell death, including apoptosis, pyroptosis, ferroptosis, necroptosis, and autophagy. (10-14) It is therefore necessary to evaluate the pathogenic role of cathepsin B in conditions that are relevant to neurological disease. This study aims to evaluate the impact of lysosomal leakage and cytosolic cathepsin B, a prevalent occurrence in many neurological diseases, and assess the effects of inhibiting cathepsin B on neurodegeneration. Specifically, the study seeks to ascertain whether cytosolic cathepsin B contributes to cell death induced in stressful conditions and whether inhibition of cytosolic cathepsin B can ameliorate cell death. Employing a novel inhibitor, Z-R-K-AOMK, specifically designed for cathepsin B and selective to neutral pH, this study delves into the analysis of cathepsin B activity within different subcellular organelles of mouse microglia BV2 cells, focusing on the cytosol and lysosome, in conditions of nutrient deprivation, a common stressor in AD and TBI, and Z-R-K-AOMK application. Remarkably, the study reveals that low-nutrient conditions exacerbate cell death, while inhibition of cytosolic cathepsin B attenuates cell death induced by nutrient deprivation. These findings underscore the pathogenic involvement of cytosolic cathepsin B in cell death, shedding light on potential therapeutic strategies for mitigating neurodegeneration in neurological diseases.

The study investigates the efficacy of the inhibitor Z-R-K-AOMK in inhibiting mouse cathepsin B, revealing its preference for inhibition at neutral pH 7.2 over acidic pH 4.6, mirroring previous findings on human cathepsin B. (20) Notably, under cytosolic conditions of pH 7.2, Z-R-K-AOMK exhibits an IC_{50} value that is 100-fold more potent compared to lysosomal pH 4.6.

Previous research suggests that the P1 position (according to Schecter-Berger nomenclature) (30) of cathepsin B favors basic residues such as Arginine and Lysine. Furthermore, it was observed that basic residues are also preferred in the S2 substrate positions, likely due to interaction with the positively charged Glu245 residue at acidic pH. (20-21) Interestingly, both murine and human cathepsin B exhibit similar preferences, emphasizing the consistency of properties across species, (31) and it is evident in the current study that the inhibitor retains the pH-dependent inhibition of potency on cathepsin B. These findings affirm that the inhibitor retains its pH-dependent potency against mouse cathepsin B, suggesting its potential utility in inhibiting mouse cathepsin B in neutral pH environments.

The study investigated the impact of low nutrient stress on cell death in mouse microglia BV2 cells, dysfunctions in access to nutrient is common in many neurologic disorders, including AD and TBI and often exacerbate dysfunctions. Our studies utilize 10% Fetal Bovine Serum (FBS) representing normal nutrient conditions and 0% FBS representing low nutrient conditions as a model of stress in AD and TBI. Remarkably, our findings demonstrate that low nutrient stress significantly elevates lactate dehydrogenase (LDH) activity in cell culture media compared to normal nutrient conditions (Figure 5.3a). LDH activity in the media serves as a reliable indicator of cell death, as LDH, typically confined to the cytosol, is released into the media upon cellular lysis and demise. The observed increase in LDH activity between normal and low nutrient conditions unequivocally underscores the induction of cell death by low nutrient stress. Furthermore, our study reveals a noteworthy reduction in media LDH activity following incubation of BV2 cells with the pH-selective inhibitor Z-R-K-AOMK, indicating a significant decrease in cell death consequent to inhibitor treatment. Examination of cathepsin B activity upon Z-R-K-AOMK incubation demonstrates a substantial decrease under both normal and low nutrient

conditions (Figure 5.3b). Intriguingly, the data indicate more pronounced inhibition of cathepsin B activity under low nutrient conditions, suggesting enhanced efficacy of Z-R-K-AOMK in mitigating cathepsin B-mediated cell death during our stress induced model. These findings lend support to the notion of cathepsin B's pathogenic role, prompting further inquiry into the translocation of cathepsin B from the lysosome to the cytosol, where cytosolic cathepsin B activates cell death pathways. Additionally, the study aims to ascertain whether Z-R-K-AOMK effectively inhibits cytosolic cathepsin B, thereby providing valuable insights into potential therapeutic avenues for alleviating cell death associated with neurodegeneration.

In our study, we employed sucrose density ultracentrifugation to fractionate subcellular organelles in mouse microglia BV2 cell homogenate, aiming to investigate the effects of low nutrient stress model for AD and TBI, and Z-R-K-AOMK incubation on specific organelles, specifically the cytosol and lysosome. The homogenate underwent separation based on density, following the described methods, where fractions were collected from least dense to most dense. Previous research has established the cytosol's location in the uppermost, least dense layers, while lysosomes were typically found in the intermediate layers. As LDH serves as a cytosolic marker, being an enzyme localized in the cytosol, our findings indicate that the first three fractions harbor LDH activity, likely representing our cytosolic compartments. Cathepsin B, a lysosomal protease known to translocate to the cytosol under certain conditions, was observed in the fractions perceived as cytosolic and in the intermediate fractions, which were identified as lysosomal based on prior research. Notably, cathepsin B activity was found to be elevated in the cytosolic fractions under stressed conditions (0% FBS) compared to normal conditions (10% FBS), suggesting that low nutrient stress induces cathepsin B activity in the cytosol, commonly known in the field.

Additionally, we observed dispersed cathepsin B activity, possibly attributable to variations in lysosomal sizes and densities. (32)

In our investigation, we analyzed cathepsin B activity within compartments designated as cytosolic (fractions F1-3) or lysosomal (fractions F8-12), based on data from the previous section, to assess the impact of stress and simultaneous Z-R-K-AOMK incubation. Notably, we observed an increase in cytosolic cathepsin B activity under low nutrient stress conditions compared to normal nutrient conditions. Importantly, this increase in cytosolic cathepsin B activity induced by low nutrient stress was effectively inhibited by Z-R-K-AOMK. These findings align with our hypothesis that cytosolic cathepsin B is induced by stress and that inhibition of cytosolic cathepsin B can mitigate cell death. An unexpected observation emerged regarding the inhibition of lysosomal cathepsin B activity by the Z-R-K-AOMK inhibitor. Despite being a pH-selective inhibitor with more potent inhibitory activity for cathepsin B at neutral cytosolic pH environments compared to acidic lysosomal pH environments, our data revealed inhibition of cathepsin B activity in lysosomal compartments with Z-R-K-AOMK at 2 μM—a concentration lower than the indicated 2.5 μM IC_{50} value determined for Z-R-K-AOMK on mouse cathepsin B at pH 4.6. This observation may be elucidated by the prolonged incubation period of BV2 cells with the inhibitor, lasting 24 hours. This extended timeframe likely allows the irreversible inhibitor to effectively inhibit Cathepsin B activity at acidic lysosomal pH, albeit less potently than at neutral pH, thus accounting for this discrepancy.

In conclusion, our study highlights the critical role of cathepsin B in cellular homeostasis and its implications in AD, TBI, and other neurological diseases. Cathepsin B, a lysosomal protease, exhibits heightened activity in the cytosol during stressed conditions, contributing to cell death and inflammatory responses observed in various neurological disorders. Our findings

underscore the potential of cytosolic cathepsin B inhibition as a therapeutic strategy to mitigate cell death. Moreover, our investigation into the inhibitory properties of Z-R-K-AOMK, a pH-selective inhibitor, provides valuable insights into its effectiveness in modulating cathepsin B activity. Utilizing sucrose density ultracentrifugation, we elucidated the spatial distribution of cathepsin B activity within cytosolic and lysosomal fractions, confirming its induction in the cytosol under low nutrient conditions. The inhibition of cytosolic cathepsin B activity by Z-R-K-AOMK further corroborates its role in mediating cell death during nutrient stress. Overall, our study offers an understanding of the molecular mechanisms underlying stress-induced cell death, highlighting the therapeutic potential of targeting cathepsin B in neurological disorders. Further research into the interplay between cathepsin B inhibition, cell death, and cellular localization may unveil novel avenues for therapeutic intervention in neurological diseases.

5.4 Materials and Experimental Details

5.4.1 Cathepsin B Activity in Recombinant Mouse Cathepsin B Assay

Mouse recombinant cathepsin B (R&D no. 965-CY-010, Minneapolis, MN) was activated in pH 5.5 buffer consisting of 20 mM Sodium Acetate (sodium acetate, Fisher Scientific #BP-333-500, Fair Lawn, NJ), 100 mM NaCl (Fisher Chemical no. S271-1, Pittsburgh, PA), 1 mM EDTA (Calbiochem #324503, Burlington, MA), 5 mM dithiothreitol (DTT, Promega, #V351, Madison, WI), incubated for 30 min at 37° C. Once activated, 0.04 ng/µL mouse cathepsin B was assayed in pH 4.6 and pH 7.2 buffer consisting of 40 mM Citrate Phosphate (citric acid monohydrate, Merck #1.00244.0500, Burlington, MA; sodium phosphate dibasic anhydrous, EMD no. SX-072305, Burlington, MA), 100 mM NaCl, 1 mM EDTA, 5 mM DTT, 0.01% Tween20, and 1.5% DMSO (Vehicle for substrate and inhibitor). Cathepsin B activity was measured using 40 µM Z-FR-AMC (Anaspec no. AS-24096, Fremont, CA) under the presence of inhibitor concentration ranging from 0 nM to 8,304 nM using 1.5-fold serial dilution for Z-R-K-AOMK in quadruplicates.

Substrate and inhibitor solutions were prepped in the 384-well plate first, then enzyme was added last, and then activity was immediately recorded using plate reader to ensure activity was detected from non-preincubation conditions of inhibitor and enzyme. Activity was measured in RFU/s as the highest slope value detected in 10 consecutive fluorescent readings (46 sec apart) observed in the 30 min assay using the microplate reader (Biotek Synergy HTX) with the following settings: Excitation=360 nm, emission=460 nm, gain=50, top optics with read height at 1 mm from 384-well plate. Relative activity % was obtained from the ratio of observed activity in presence of inhibitor over the activity observed for 0 nM DMSO control and then multiplying by 100. Cathepsin B relative activity % detected from its corresponding inhibitor concentration were plotted with SEM error bars using GraphPad Prism (Version 9) to determine the IC50.

5.4.2 Mouse Microglia BV2 Cell Culture

Embryonic mouse microglia BV2 cells, provided by Dr. Christopher Glass from UC San Diego, were cultured in a 5% CO_2 environment under humidified conditions at 37°C under sterile conditions. The growth media comprised varying concentrations of heat-inactivated fetal bovine serum, (FBS, Gibco, Grand Island, NY) and 90% RPMI (Gibco) specifically for BV2 cells. Cells were passaged every 3 to 4 days at an amount of approximately 4000 cells per ml of growth media. Experimental conditions included RPMI 1640 with no FBS (0% FBS) and the conventional growth media of RPMI 1640 containing 10% FBS.

5.4.3 Mouse Microglia BV2 Cells Treated with Inhibitors

Embryonic mouse microglia BV2 cells were cultured in media as described in previous sections. The cells underwent incubation with Z-Arg-Lys-AOMK (made by the Gerwick Lab (doi/10.1021/acsomega.3c08629) for 24 hours at 37°C. Z-Arg-Lys-AOMK was applied at a concentration of 2 µM, in media with varying proportions of 90% RPMI and either 10% or 0%

FBS. Following the treatment incubation periods with inhibitors, the cells were harvested for homogenization.

5.4.4 Cathepsin B Activity in Mouse Microglia BV2 Cells

Cathepsin B activity in homogenates was assessed using the fluorogenic peptide substrate Z-Nle-Lys-Arg-AMC. Proteolytic assays were conducted on embryonic mouse microglia BV2 homogenates and fractions, employing a substrate concentration of 60 µM in a buffer containing 40 mM citrate phosphate at pH 5.5, 1 mM EDTA, 100 mM NaCl, 5 mM DTT, and 1.2% DMSO. Incubation was carried out for 60 minutes with readings at 15, 30, and 60-minute intervals. The assays were performed in 96-well round bottom black plates at 37°C in a total volume of 100 µl. Fluorescence was measured using a Biotek Synergy HTX microplate reader (excitation 360 nm, emission 460 nm, gain 50, top optics, and read height of 1 mm). Cathepsin B proteolytic activity was quantified as nmol AMC per µg protein in the sample per 30 minutes and presented as the mean ± SEM. Statistical significance ($p < 0.05$) was determined by Student's t-test. Relative fluorescence units (RFU) readings were converted to nmol AMC using AMC standard curves for each plate. Protein content in homogenates was assessed using the DC protein assay kit, as described later.

5.4.5 Protein Measurement of Cells

Protein measurements of cell homogenates and fractions were carried out following the instructions provided in the Bio-Rad DC Protein Assay Kit (Bio-Rad, #500-0113, 500-0114). Protein standards, ranging from 0.125 to 1.5 µg/µl bovine serum albumin (BSA), were prepared. The assays were conducted in a 96-well clear flat-bottom plate. In each sample well, 25 µl of Reagent A was added, followed by 5 µl of standards and ½ to ¼ diluted samples. Subsequently, 200 µl of Reagent B was added to each well, and the contents were thoroughly mixed. The plate was incubated at room temperature (24°C) for 15 minutes, and absorbance was read at 750 nm

after 15 minutes, remaining stable for up to an hour. The undiluted sample protein concentration (µg/µl) was calculated by converting sample absorbance readings to protein concentration (µg/µl) using the standard protein curve for each plate and adjusted with the relevant dilution factor.

5.4.6 LDH assay of culture media as indicator of cell death

The cell culture media were collected according to the procedures outlined in previous sections. The LDH assay was conducted following the instructions provided in the CyQUANT LDH Cytotoxicity Assay kit (Invitrogen, #C20300 and C20301). NADH standards ranging from 2.0 to 50.0 nmol/50 µl per well were prepared. The assays were performed in 96-well clear flat-bottom plate, where 50 µl of standard or sample was added, followed by the addition of 50 µl of the reaction mixture and thorough mixing. The plate was then covered with aluminum foil and incubated at room temperature in a water bath (24°C). Absorbance readings were taken at 490 nm after 15, 30, and 60 minutes of incubation. At the 60-minute mark, 50 µl of stop solution was added, and a final absorbance was read at 680 nm. The amount of nmol NADH in a 50 µl sample was determined using the NADH standard. NADH in 1.5 ml media was calculated and divided by the amount of protein in the sample to ascertain the total nmol NADH in media per total µg protein.

5.5 References

1. De Duve C, Wattiaux R. Functions of lysosomes. Annu Rev Physiol. 1966;28:435-92. doi: 10.1146/annurev.ph.28.030166.002251. PMID: 5322983.

2. Lawrence RE, Zoncu R. The lysosome as a cellular centre for signalling, metabolism and quality control. Nat Cell Biol. 2019 Feb;21(2):133-142. doi: 10.1038/s41556-018-0244-7. Epub 2019 Jan 2. PMID: 30602725.

3. Turk V, Stoka V, Vasiljeva O, Renko M, Sun T, Turk B, Turk D. Cysteine cathepsins: from structure, function and regulation to new frontiers. Biochim Biophys Acta. 2012 Jan;1824(1):68-88. doi: 10.1016/j.bbapap.2011.10.002. Epub 2011 Oct 12. PMID: 22024571; PMCID: PMC7105208.

4. Mindell JA. Lysosomal acidification mechanisms. Annu Rev Physiol. 2012;74:69-86. doi: 10.1146/annurev-physiol-012110-142317. PMID: 22335796.

5. Ishida Y, Nayak S, Mindell JA, Grabe M. A model of lysosomal pH regulation. J Gen Physiol. 2013 Jun;141(6):705-20. doi: 10.1085/jgp.201210930. PMID: 23712550; PMCID: PMC3664703.

6. Wang F, Gómez-Sintes R, Boya P. Lysosomal membrane permeabilization and cell death. Traffic. 2018 Dec;19(12):918-931. doi: 10.1111/tra.12613. Epub 2018 Sep 12. PMID: 30125440.

7. Bright GR, Fisher GW, Rogowska J, Taylor DL. Fluorescence ratio imaging microscopy: temporal and spatial measurements of cytoplasmic pH. J Cell Biol. 1987 Apr;104(4):1019-33. doi: 10.1083/jcb.104.4.1019. PMID: 3558476; PMCID: PMC2114443.

8. Yoon MC, Phan V, Podvin S, Mosier C, O'Donoghue AJ, Hook V. Distinct Cleavage Properties of Cathepsin B Compared to Cysteine Cathepsins Enable the Design and Validation of a Specific Substrate for Cathepsin B over a Broad pH Range. Biochemistry. 2023 Aug 1;62(15):2289-2300. doi: 10.1021/acs.biochem.3c00139. Epub 2023 Jul 17. PMID: 37459182; PMCID: PMC10399199.

9. Phan VV, Mosier C, Yoon MC, Glukhov E, Caffrey CR, O'Donoghue AJ, Gerwick WH, Hook V. Discovery of pH-Selective Marine and Plant Natural Product Inhibitors of Cathepsin B Revealed by Screening at Acidic and Neutral pH Conditions. ACS Omega. 2022 Jul 12;7(29):25346-25352. doi: 10.1021/acsomega.2c02287. PMID: 35910167; PMCID: PMC9330179.

10. de Castro MA, Bunt G, Wouters FS. Cathepsin B launches an apoptotic exit effort upon cell death-associated disruption of lysosomes. Cell Death Discov. 2016 Feb 29;2:16012. doi: 10.1038/cddiscovery.2016.12. PMID: 27551506; PMCID: PMC4979493.

11. Xie Z, Zhao M, Yan C, Kong W, Lan F, Narengaowa, Zhao S, Yang Q, Bai Z, Qing H, Ni J. Cathepsin B in programmed cell death machinery: mechanisms of execution and regulatory pathways. Cell Death Dis. 2023 Apr 8;14(4):255. doi: 10.1038/s41419-023-05786-0. PMID: 37031185; PMCID: PMC10082344.

12. Droga-Mazovec G, Bojic L, Petelin A, Ivanova S, Romih R, Repnik U, Salvesen GS, Stoka V, Turk V, Turk B. Cysteine cathepsins trigger caspase-dependent cell death through cleavage of bid and antiapoptotic Bcl-2 homologues. J Biol Chem. 2008 Jul 4;283(27):19140-50. doi: 10.1074/jbc.M802513200. Epub 2008 May 9. PMID: 18469004.

13. Bai H, Yang B, Yu W, Xiao Y, Yu D, Zhang Q. Cathepsin B links oxidative stress to the activation of NLRP3 inflammasome. Exp Cell Res. 2018 Jan 1;362(1):180-187. doi: 10.1016/j.yexcr.2017.11.015. Epub 2017 Nov 28. PMID: 29196167.

14. Campden RI, Zhang Y. The role of lysosomal cysteine cathepsins in NLRP3 inflammasome activation. Arch Biochem Biophys. 2019 Jul 30;670:32-42. doi: 10.1016/j.abb.2019.02.015. Epub 2019 Feb 23. PMID: 30807742.

15. Hook V, Yoon M, Mosier C, Ito G, Podvin S, Head BP, Rissman R, O'Donoghue AJ, Hook G. Cathepsin B in neurodegeneration of Alzheimer's disease, traumatic brain injury, and related brain disorders. Biochim Biophys Acta Proteins Proteom. 2020 Aug;1868(8):140428. doi: 10.1016/j.bbapap.2020.140428. Epub 2020 Apr 17. PMID: 32305689; PMCID: PMC7261628.

16. G. R. Hook, J. Yu, N. Sipes, M. D. Pierschbacher, V. Hook, and M. S. Kindy, "The cysteine protease cathepsin B is a key drug target and cysteine protease inhibitors are potential therapeutics for traumatic brain injury," *J. Neurotrauma*, vol. 31, no. 5, pp. 515–529, Mar. 2014, doi: 10.1089/neu.2013.2944.

17. M. S. Kindy, J. Yu, H. Zhu, S. S. El-Amouri, V. Hook, and G. R. Hook, "Deletion of the cathepsin B gene improves memory deficits in a transgenic alzheimer's disease mouse model expressing AβPP containing the wild-type β-secretase site sequence," *J. Alzheimer's Dis.*, vol. 29, no. 4, pp. 827–840, 2012, doi: 10.3233/JAD-2012-111604.

18. G. Hook, J. S. Jacobsen, K. Grabstein, M. Kindy, and V. Hook, "Cathepsin B is a new drug target for traumatic brain injury therapeutics: Evidence for E64d as a promising lead drug candidate," *Frontiers in Neurology*, vol. 6, no. SEP. Frontiers Media S.A., 2015, doi: 10.3389/fneur.2015.00178.

19. G. Hook, V. Hook, and M. Kindy, "The cysteine protease inhibitor, E64d, reduces brain amyloid-β and improves memory deficits in Alzheimer's disease animal models by inhibiting cathepsin B, but not BACE1, β-secretase activity," *J. Alzheimers. Dis.*, vol. 26, no. 2, p. 387, 2011, doi: 10.3233/JAD-2011-110101.

20. Yoon MC, Solania A, Jiang Z, Christy MP, Podvin S, Mosier C, Lietz CB, Ito G, Gerwick WH, Wolan DW, Hook G, O'Donoghue AJ, Hook V. Selective Neutral pH Inhibitor of Cathepsin B Designed Based on Cleavage Preferences at Cytosolic and Lysosomal pH Conditions. ACS Chem Biol. 2021 Sep 17;16(9):1628-1643. doi: 10.1021/acschembio.1c00138. Epub 2021 Aug 20. PMID: 34416110; PMCID: PMC9104225.

21. Yoon MC, Christy MP, Phan VV, Gerwick WH, Hook G, O'Donoghue AJ, Hook V. Molecular Features of CA-074 pH-Dependent Inhibition of Cathepsin B. Biochemistry. 2022 Feb 15;61(4):228-238. doi: 10.1021/acs.biochem.1c00684. Epub 2022 Feb 4. PMID: 35119840; PMCID: PMC9096814.

22. Lai JQ, Shi YC, Lin S, Chen XR. Metabolic disorders on cognitive dysfunction after traumatic brain injury. Trends Endocrinol Metab. 2022 Jul;33(7):451-462. doi: 10.1016/j.tem.2022.04.003. Epub 2022 May 7. PMID: 35534336

23. Komura A, Kawasaki T, Yamada Y, Uzuyama S, Asano Y, Shinoda J. Cerebral Glucose Metabolism in Patients with Chronic Mental and Cognitive Sequelae after a Single Blunt Mild Traumatic Brain Injury without Visible Brain Lesions. J Neurotrauma. 2019 Mar 1;36(5):641-649. doi: 10.1089/neu.2018.5641. Epub 2018 Sep 14. PMID: 29921156.

24. Huynh LM, Burns MP, Taub DD, Blackman MR, Zhou J. Chronic Neurobehavioral Impairments and Decreased Hippocampal Expression of Genes Important for Brain Glucose Utilization in a Mouse Model of Mild TBI. Front Endocrinol (Lausanne). 2020 Sep 18;11:556380. doi: 10.3389/fendo.2020.556380. PMID: 33071972; PMCID: PMC7531511.

25. Bowman CE, Scafidi J, Scafidi S. Metabolic perturbations after pediatric TBI: It's not just about glucose. Exp Neurol. 2019 Jun;316:74-84. doi: 10.1016/j.expneurol.2019.03.018. Epub 2019 Apr 3. PMID: 30951705; PMCID: PMC6739863.

26. Blonz ER. Alzheimer's Disease as the Product of a Progressive Energy Deficiency Syndrome in the Central Nervous System: The Neuroenergetic Hypothesis. J Alzheimers Dis. 2017;60(4):1223-1229. doi: 10.3233/JAD-170549. PMID: 28946565; PMCID: PMC5676979.

27. Daulatzai MA. Cerebral hypoperfusion and glucose hypometabolism: Key pathophysiological modulators promote neurodegeneration, cognitive impairment, and Alzheimer's disease. J Neurosci Res. 2017 Apr;95(4):943-972. doi: 10.1002/jnr.23777. Epub 2016 Jun 27. PMID: 27350397.

28. Settembre C, Perera RM. Lysosomes as coordinators of cellular catabolism, metabolic signalling and organ physiology. Nat Rev Mol Cell Biol. 2023 Nov 24. doi: 10.1038/s41580-023-00676-x. Epub ahead of print. PMID: 38001393.

29. Gerónimo-Olvera C, Montiel T, Rincon-Heredia R, Castro-Obregón S, Massieu L. Autophagy fails to prevent glucose deprivation/glucose reintroduction-induced neuronal death due to calpain-mediated lysosomal dysfunction in cortical neurons. Cell Death Dis. 2017 Jun 29;8(6):e2911. doi: 10.1038/cddis.2017.299. PMID: 28661473; PMCID: PMC5520945.

30. Schechter I, Berger A. On the size of the active site in proteases. I. Papain. Biochem Biophys Res Commun. 1967 Apr 20;27(2):157-62. doi: 10.1016/s0006-291x(67)80055-x. PMID: 6035483.

31. Caglic D, Kosec G, Bojic L, Reinheckel T, Turk V, Turk B. Murine and human cathepsin B exhibit similar properties: possible implications for drug discovery. Biol Chem. 2009 Feb;390(2):175-9. doi: 10.1515/BC.2009.021. Erratum in: Biol Chem. 2009 May-Jun;390(5-6):517. PMID: 19040356.

32. de Araujo MEG, Liebscher G, Hess MW, Huber LA. Lysosomal size matters. Traffic. 2020 Jan;21(1):60-75. doi: 10.1111/tra.12714. Epub 2019 Dec 6. PMID: 31808235; PMCID: PMC6972631.

Acknowledgements

Chapter 5, in part, is material in preparation for submission. Von V. Phan, Sonia Podvin, Charles Mosier, Michael C Yoon, Dennis Wolan, Anthony J O'Donoghue, and Vivian Hook. The dissertation author was the primary researcher and author of this material.

Chapter 6 Traumatic Brain Injury Induces Translocation of Cathepsin B to the Cytosol of Brain Cortex during Motor Deficits

Chapter 6 Abstract. Traumatic Brain Injury (TBI) remains a pressing public health concern, with significant mortality and morbidity rates globally. This study investigates the role of cytosolic cathepsin B in TBI pathogenesis and evaluates the therapeutic potential of the novel inhibitor Z-R-K-AOMK. Using a controlled cortical impact (CCI) TBI model in mice, CCI-TBI-induced motor deficits and lysosomal leakage of cathepsin B into the cytosol were observed. Treatment with Z-R-K-AOMK mitigated motor deficits and inhibited cytosolic cathepsin B activity, suggesting its efficacy in ameliorating TBI-induced neuropathology. These findings underscore the importance of targeting cytosolic cathepsin B as a potential therapeutic strategy for TBI and pave the way for further research in developing innovative pharmacological interventions to improve patient outcomes.

6.1 Introduction

Traumatic Brain Injury (TBI) stands as a significant public health concern, often arising from external forces or trauma directed at the brain. (1) In the United States alone, TBI represents a major cause of both mortality and morbidity, with over 69,000 TBI-related deaths reported in 2021. (2) It encompasses both primary injury, which occurs immediately upon impact, and secondary injury, involving subsequent biochemical and cellular changes that exacerbate tissue damage. (3, 4) Secondary injury mechanisms include inflammation, cell death pathways, and oxidative stress, contributing to further neurological dysfunction. Despite advancements in understanding these processes, effective drug treatments for TBI remain elusive. However, research suggests that targeting cathepsin B may hold promise for improving TBI outcomes, as evidenced by positive results in animal models. (5)

Cathepsin B, an essential protease crucial for cellular homeostasis, primarily resides within lysosomes. (6-8) However, under neuropathological conditions like TBI, lysosomal membrane permeabilization occurs, leading to the translocation of lysosomal contents, including cathepsin B, into the cytosol. (9, 10) In the cytosol, cathepsin B retains its proteolytic activity, functioning at a neutral pH of 7.2. (9, 11, 13-15) Here, it continues to generate bioactive peptides that activate cell death (16-18) and inflammation pathways (19-20), precipitating neurodegeneration and neuroinflammation. Notably, elevated expression and activity of cathepsin B have been observed following TBI, where it significantly contributes to TBI-induced cell death. (21)

Moreover, TBI is recognized as a significant risk factor for Alzheimer's Disease (AD). TBI-induced disruptions in cellular and molecular pathways can accelerate the onset and

progression of AD pathology. (22-24) Therefore, mitigating TBI-induced neuropathology becomes crucial not only for TBI management but also for reducing AD risk.

Cathepsin B has emerged as a promising therapeutic target for mitigating secondary injury in TBI. (25, 26) Studies employing controlled cortical impact (CCI) TBI models have revealed increased expression and activity of cathepsin B post-injury. (21) Notably, genetic knockout of cathepsin B or chemical inhibition using E64d has shown improvements in behavioral dysfunctions and neuropathology in TBI animal models. (25, 26) However, E64d's lack of selectivity necessitated the development of a more specific inhibitor to target pathogenic cytosolic cathepsin B.

In this context, the novel inhibitor Z-Arg-Lys-AOMK, designed as a neutral pH-selective and cathepsin B-specific inhibitor, presents a significant advancement. (27) Leveraging cathepsin B's cleavage preferences in different pH environments, this inhibitor was engineered to selectively target pathogenic cytosolic cathepsin B. (27, 28) Herein lies the focus of the present study, which investigates the effects of Z-R-K-AOMK administration in a CCI-TBI animal model to elucidate the impacts of inhibiting cytosolic cathepsin B in TBI.

Through this study, we aim to demonstrate the efficacy of Z-Arg-Lys-AOMK treatment in CCI-TBI mouse models, offering insights into its potential for improving motor dysfunction and TBI outcomes, while also addressing its relevance in mitigating AD risk associated with TBI.

6.2 Results

6.2.1 *In vivo* CCI-TBI Elicits Motor Deficits and Triggers Lysosomal Leakage of Cathepsin B into the Cytosol

In mouse studies of controlled cortical impact traumatic brain injury (CCI-TBI), TBI induces both motor deficits and the leakage of lysosomal cathepsin B into the cytosol. Mice

subjected to CCI-TBI exhibited pronounced motor impairment at 1 and 3 days post-injury, as evidenced by rotarod assays (Figure 6.1a). This injury model also induced cortical lesions, quantified by measuring cortical tissue loss (Figure 6.1b, c). Western blot analysis revealed a notable translocation of cathepsin B to the cytosolic fraction within the brain cortex of the ipsilateral hemisphere, which received the CCI (Figure 6.1d). In contrast, sham controls displayed no detectable cytosolic cathepsin B (Figure 6.1d). The migration of cathepsin B into the cytosol following CCI-TBI was further confirmed through immunofluorescence, illustrating a shift from its typical lysosomal localization to a more diffuse distribution within cells (Figure 6.1e). Quantitative immunofluorescence analysis also demonstrated a decrease in lysosomal cathepsin B localization near nuclei post-CCI-TBI (Figure 6.1f). Collectively, these findings underscore the multifaceted impact of CCI-TBI, linking it to behavioral deficits, the relocation of cathepsin B to the cytosol, and cortical tissue loss.

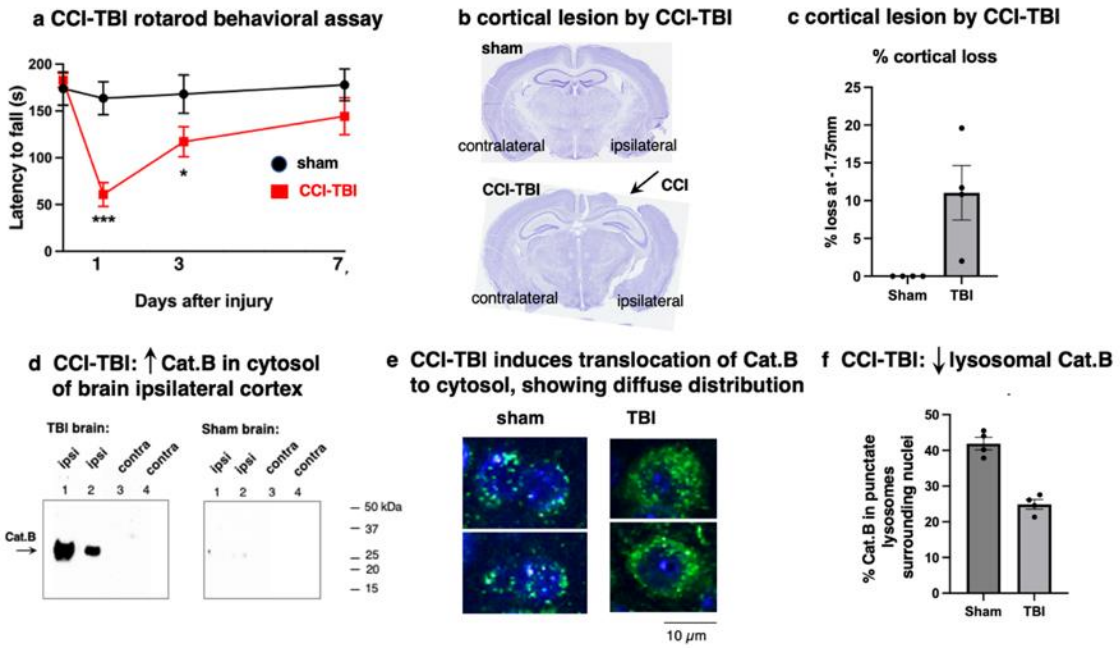

Figure 6.1 Effects of CCI-TBI on Behavioral Deficits, Cortical Tissue Integrity, and Cathepsin B Distribution in the Brain. (a) Motor function deficits observed via rotarod assay following CCI-TBI (*p<0.05; ***p<0.001, student's t-test). (b) Nissl staining of sham and TBI brains. (c) Increased cortical brain lesion following CCI-TBI. (d) Elevated cytosolic cathepsin B levels detected by western blot in brain cortex fractions post-CCI-TBI compared to sham controls. (e) Immunofluorescence reveals diffuse distribution of cathepsin B in cortical cells (ipsilateral) post-CCI-TBI, indicative of cytosolic localization. (f) Reduced lysosomal cathepsin B post-CCI-TBI evidenced by quantitative immuno-fluorescence (*p<0.01).

6.2.2 Z-Arg-Lys-AOMK Mitigates Behavioral Motor Deficits and Inhibits Brain Cytosolic Cathepsin B in CCI-TBI Mice.

Significant results indicate that administration of Z-Arg-Lys-AOMK leads to a marked improvement in CCI-TBI induced behavioral deficits (Figure 6.2). The inhibitor was administered daily via intraperitoneal injection at a dose of 20 mg/kg, beginning one day prior to CCI-TBI and continued with daily dosing thereafter. Importantly, the Z-Arg-Lys-AOMK inhibitor significantly mitigated motor deficits induced by CCI-TBI, as evidenced by rotarod assays conducted one day post-injury (Figure 6.2a).

Additionally, Z-Arg-Lys-AOMK treatment resulted in a reduction in cathepsin B activity within the brain cortex homogenate of CCI-TBI mice (Figure 6.2b). Notably, the inhibitor also

decreased cathepsin B activity specifically within the cytosolic fraction isolated from the brain cortex of CCI-TBI mice (Figure 6.2c). It is noteworthy that cathepsin B activity was elevated in the ipsilateral brain cortex, which received the CCI-TBI insult, as compared to the contralateral cortex, which remained uninjured.

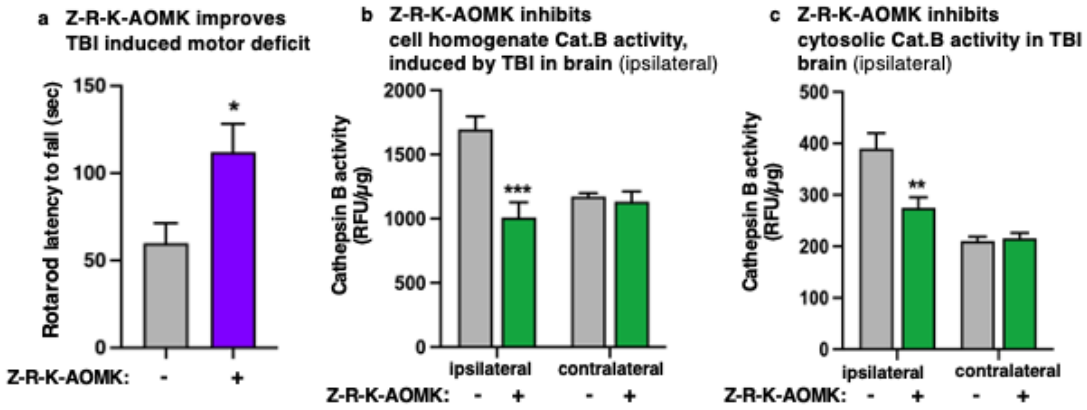

Figure 6.2 Efficacy of Z-Arg-Lys-AOMK in Alleviating Motor Deficits and Inhibiting Cytosolic Cathepsin B in CCI-TBI Mice. (a) Administration of Z-Arg-Lys-AOMK (20 mg/kg, intraperitoneal injection daily) improves motor dysfunction in CCI-TBI mice, as evidenced by a significant increase in latency to ~110 secs compared to 60 secs without the inhibitor in the rotarod assay conducted one day post-CCI-TBI (*$p<0.05$). (b) Z-Arg-Lys-AOMK treatment results in inhibition of cathepsin B activity in the brain cortex homogenate of CCI-TBI mice ($p<0.001$). (c) The inhibitor demonstrates significant inhibition of cytosolic cathepsin B activity within the brain cortex of CCI-TBI mice (**$p<0.001$).

6.3 Discussion

This investigation unveiled a cascade of events implicating lysosomal leakage and the involvement of cytosolic cathepsin B in the TBI injury process. Notably, CCI-TBI induced significant motor deficits in mice, provoking cortical lesions. Of particular interest was the observation of lysosomal cathepsin B translocating to the cytosolic fraction within the brain cortex of the ipsilateral hemisphere that sustained the CCI insult, as revealed by Western blot analysis (Figure 6.1d). In contrast, sham controls exhibited no discernible cytosolic cathepsin B. Immunofluorescence studies further corroborated this phenomenon, depicting a shift in cathepsin B's localization from the lysosomes to a diffuse distribution within cells following CCI-TBI

(Figure 6.1e). These findings collectively underscore the intricate interplay between CCI-TBI, motor deficits, lysosomal leakage, and the translocation of cathepsin B to the cytosol. The observed alterations in cathepsin B localization suggest its potential involvement in the neuropathological mechanisms underlying CCI-TBI-induced cortical tissue loss and associated motor impairments. Further elucidation of these pathways holds promise for the development of targeted therapeutic strategies aimed at mitigating the deleterious consequences of traumatic brain injury.

Additionally, the efficacy of Z-Arg-Lys-AOMK in ameliorating both motor deficits and brain cytosolic cathepsin B activity emerged as a significant breakthrough. The novel inhibitor was administered daily via intraperitoneal injection, with treatment beginning one day prior to CCI-TBI and continued daily thereafter. The results yielded improvements in CCI-TBI-induced motor deficits observed at one day post-injury, as demonstrated by rotarod assays. The rapid amelioration underscores the therapeutic potential of Z-Arg-Lys-AOMK in addressing the acute consequences of TBI.

Furthermore, the capability of Z-Arg-Lys-AOMK to penetrate the blood-brain barrier (BBB) and effectively inhibit cathepsin B activity within the brain cortex homogenate of CCI-TBI mice underscores its therapeutic potential. This feature highlights the compound's capacity to access the central nervous system and regulate key biological pathways involved in the pathology of TBI. It is worth noting that this ability to traverse the BBB may be facilitated by the compromise of its integrity, a common occurrence in the context of TBI. However, additionally understanding of the pharmacokinetics of Z-Arg-Lys-AOMK is necessary to fully elucidate its mechanisms of action and therapeutic efficacy in the context of TBI. Further research in this area will contribute to a more thorough comprehension of the inhibitor's potential.

Intriguingly, analysis revealed a marked reduction in cathepsin B activity within the cytosolic fraction isolated from the brain cortex of CCI-TBI mice following Z-Arg-Lys-AOMK treatment. This finding not only corroborates the inhibitor's ability to access intracellular compartments but also underscores its specificity in targeting cytosolic cathepsin B, an important enzyme in TBI-induced neuropathological processes.

Taken together, these findings underscore the therapeutic potential of Z-Arg-Lys-AOMK as a neutral pH-selective inhibitor of cathepsin B in ameliorating CCI-TBI-induced motor deficits by specifically targeting and inhibiting cytosolic cathepsin B activity. As research in this field continues to evolve, the insights from this study hold promise for the development of innovative pharmacological strategies aimed at addressing the complex pathophysiology of TBI and improving patient outcomes.

6.4 Methods

6.4.1 Animals

Female C57BL/6 mice obtained from Taconic Biosciences (#B6-F, La Jolla, CA) were individually housed and allowed to acclimate for a minimum of 7 days prior to experimentation, with 3-5 mice per cage for social enrichment. The mice, aged between 3 to 4 months, were provided free access to food and water throughout the duration of the study. All animal procedures were conducted according to the regulations by the National Institutes of Health and as approved by the institutional animal care and use committee at the Medical University of South Carolina (Charleston, SC) and Ralph H. Johnson CA Medical Center (Charleston, SC). Mice were euthanized either on day 8 for comparison between TBI and sham groups or on day 6 for comparison between TBI groups treated with vehicle and those treated with Z-Arg-Lys-AOMK. For the sacrifice procedure, mice were anesthetized with Ketaset ketamine solution (200mg/kg)

for a duration of 10 minutes (Zoetis #KET-00002R2, San Diego, CA) and perfused with 14 ml of sterile saline over a 2-minute period until the liver was clear of blood. For subsequent biochemical analysis, the brains were carefully extracted and dissected into ipsilateral (to TBI) and contralateral hippocampus, as well as ipsilateral and contralateral cortex regions. For histological analysis, a similar anesthesia procedure was performed, followed by a perfusion of 14 ml of sterile saline over 2 minutes, followed by 21 ml of 4% paraformaldehyde over 3 minutes. Whole brains were then extracted and submerged in 4% paraformaldehyde solution for further processing.

6.4.2 Controlled Cortical Impact Traumatic Brain Injury

The controlled cortical impact traumatic brain injury (CCI-TBI) mouse model was utilized to induce consistent brain injuries across all subjects. The procedure involved anesthetizing adult female mice with 3% isoflurane (VetOne #50217, Boise, ID) and 1.0 liter of oxygen flowrate, placing them in a stereotaxic frame (Kopf Instruments, #963, Tujunga, CA) atop a 37°C warming pad (RWD Life Science, #69027, San Diego, CA). The site was shaved and sterilized with betadine, followed by 70% ethanol. A midline incision was made anterior just above the orbital region, with retractors (Kent Scientific, #SURGI5001, Torrington, CT) used to secure the skin and expose the skull. A 5 mm diameter burr hole was created, using a 5 mm Trephine burr drill bit (DDS Gadget, #MCT-TPB03, Aventura, FL), in the skull with a stereotaxic microdrill (RWD Life Science, #78001, San Diego, CA) on the right side over the motor cortex positioned 0.5 mm to 5.5 mm posterior to bregma, 1 mm to 6 mm right of the sagittal suture, with the skull segment removed without disrupting the underlying dura. Using an impactor (Leica Biosystems, #39463920, Deer Park, IL) equipped with a 3 mm tip, set at an impact speed of 3 m/s, depth of 1 mm, and 100 ms dwell time, the exposed cortex was injured. Subsequently, a sterile circular glass cover slip (Electron Microscopy Sciences, #72295-03, Hatfield, PA) was placed over the craniotomy, and the scalp incision was closed with GLUture (Abbot Labs, #100-8170, Chicago, IL). Mice received

5 mg/kg buprenorphine into the scruff immediately after injury, and were allowed to recover in a cage placed over a 37°C warming pad until mobile, with continuous observation for signs of distress for at least 2 hours. If distress was noted, a second dose of 5 mg/kg buprenorphine (Par Pharmaceuticals, #42023-179-05, Irvine, CA) was administered before returning to the vivarium, and additional daily doses were given if necessary. Sham controls underwent anesthesia, scalp incision, GLUture, and analgesia.

6.4.3 Rotarod Assay for Assessment of Mouse Motor Function

The area injured by CCI-TBI was to the motor cortex. Accordingly, motor function was evaluated using an automated RotaRod (Ugo Basile, #47650, Gemonio, VA, Italy) to assess the efficacy of both CCI-TBI and 20 mg/kg Z-Arg-Lys-AOMK (made by the Gerwick Lab (doi/10.1021/acsomega.3c08629) therapeutic intervention to test the hypothesis of improved motor function by cathepsin B inhibition. Z-R-K-AOMK was administered one day prior to trauma and continued daily thereafter. Prior to injury, mice underwent a training regimen consisting of three trials, conducted two days before the TBI or sham procedure, at linear rotational accelerations of 5-10 rpm, 5-20 rpm, and 5-40 rpm for durations of 120 s, 240 s, and 240 s, respectively. The baseline latency was established by averaging the time to fall from the rotating cylinder during these pre-injury trials. Mice underwent trials one day before and one, three, and five days after surgery, consisting of three trials each at a linear rotational acceleration of 5-40 rpm for 240 s. The average latency to fall from the rod was recorded, with mice unable to maintain grip on the rotating rod assigned a latency of 0 seconds. If the mouse remained on the rotating rod for the entire trial, a time of 240 seconds was recorded. Throughout the experiment, the experimenter remained blinded to the animal groups to ensure unbiased evaluation.

6.4.4 Brain Tissue Homogenization and Synaptosome Enrichment

6.4.4.1 Hippocampus Homogenate Preparation

Hippocampi was flash-frozen at the time of sac. Later, each hemisphere of the hippocampus, ipsilateral or contralateral to TBI/sham, was homogenized in 0.4 ml of 0.32 M sucrose using a glass-teflon homogenizer (Grainger, #358010, Lake Forest, IL), at 900 rpm for 12 strokes, with each stroke lasting 5 s each.

6.4.4.2 Cortex Homogenization and Synaptosome Enriched Fraction P2

Each hemisphere of the cortex ipsilateral or contralateral to the TBI/sham was processed fresh and on ice the day of sac, and were homogenized in 5 ml of 0.32 M sucrose on ice with a Wheaton glass-teflon homogenizer at 900 rpm for 12 strokes, 5 s each. Following homogenization, 0.5 ml of the homogenate was reserved for further analysis. The remaining homogenate (4.5 ml) underwent low speed centrifugation at 1000 g for 5 minutes to pellet the nuclei and cell debris, resulting in the S1 supernatant. Subsequently, the S1 supernatant underwent high-speed centrifugation at 12,000 g for 20 minutes to pellet synaptosomes, mitochondria, and myelin fragments, resulting in the P2 pellet, while the S2 supernatant contained the cytosol.

6.4.5 Western Blot Analysis of Cathepsin B Protein Levels

Western blot analysis was employed to quantify cytosolic cathepsin B protein levels in the ipsilateral and contralateral cortex of both TBI and sham-operated mice. Each sample, containing 7 µg of protein, was subjected to electrophoresis, and cathepsin B protein levels were assessed in the S2 supernatant, representing the cytosolic compartments of brain homogenates. The primary antibody used for detection was anti-mouse cathepsin B (R&D Systems, #AF965) at a dilution of 1:500, incubated overnight at 4°C. Subsequently, membranes were probed with Rabbit Anti-goat IgG HRP (Biorad, #5160-2504, Hercules, CA) at a dilution of 1:5000 in 4% milk PBST at room temperature for 2 hours.

6.4.6 Cathepsin B Activity Assay on Brain Homogenate

Cathepsin B activity in homogenates was assessed utilizing the fluorogenic peptide substrate Z-Nle-Lys-Arg-AMC. The assays were conducted on mouse cortex homogenates and fractions. The assay utilized a substrate concentration of 60 µM, in a buffer solution containing 40 mM citrate phosphate at pH 5.5 (citric acid monohydrate, Merck #1.00244.0500, Burlington, MA; sodium phosphate dibasic anhydrous, EMD no. SX-072305, Burlington, MA), 1 mM EDTA (Calbiochem #324503, Burlington, MA), 100 mM NaCl (Fisher Chemical no. S271-1, Pittsburgh, PA), 5 mM dithiothreitol (DTT, Promega, #V351, Madison, WI), and 1.2% DMSO (Vehicle for substrate and inhibitor). Incubation proceeded for 60 minutes with fluorescence readings at 15, 30, and 60-minute intervals. The assays were performed in 96-well round bottom black plates, maintained at 37°C, in a total volume of 100 µl. Fluorescence was measured using a Biotek Synergy HTX microplate reader (excitation 360 nm, emission 460 nm, gain 50, top optics, and read height of 1 mm). Cathepsin B proteolytic activity was quantified as pmol AMC per µg protein in the sample per 30 minutes and presented as the mean ± SEM. Statistical significance ($p < 0.05$) was determined by Student's t-test. Relative fluorescence units (RFU) readings were converted to pmol AMC using AMC standard curves specific to each plate. Protein content in homogenates was determined using the DC protein assay kit, as elaborated later.

6.4.7 Protein Measurement of Homogenate Samples

Protein measurements of homogenates and fractions adhered to the instructions provided in the Bio-Rad DC Protein Assay Kit (Bio-Rad, #500-0113, 500-0114, Hercules, CA). Protein standards, ranging from 0.125 to 1.5 µg/µl bovine serum albumin (BSA) in concentrations were prepared. The assays were conducted within a 96-well clear flat-bottom plate. Each sample well received 25 µl of Reagent A, followed by 5 µl of standards and appropriately diluted samples (ranging from ½ to ¼ dilution). Subsequently, 200 µl of Reagent B was introduced to each well,

ensuring thorough mixing of the contents. The plate underwent a 15-minute incubation period at room temperature (24°C), with absorbance readings recorded at 750 nm after the incubation period, remaining stable for up to an hour. Calculation of undiluted sample protein concentration (µg/µl) was achieved by converting absorbance readings of samples to protein concentration (µg/µl) using the standard protein curve unique to each plate, and adjustments were made based on the relevant dilution factor.

6.4.8 Histological analysis of hippocampal disorganization and cathepsin B immunofluorescence

Analyses of CCI-TBI lesion volume, hippocampal disorganization, and cathepsin B subcellular distribution by immunofluorescence were conducted on coronal brain tissue sections of CCI-TBI and sham mice.

6.4.8.1 NISSL Staining for lesion volume and hippocampal disorganization

Tissues were rinsed twice for 5 minutes each with 1X PBS before mounting on positively charged slides (Fisher CAT#12-550-15). Slides were air-dried for 60 minutes at room temperature (RT) followed by overnight drying at 37°C. Subsequently, slides were brought to RT and fixed for 30 minutes in 10% formalin at RT. After fixation, tissues were rinsed thrice for 5 minutes each with 1X PBS, followed by a 1-minute rinse in deionized water (DH2O). NISSL staining was performed using 0.25% cresyl violet (Sigma CAT# C5042-10G) for 5 minutes, followed by a 1-minute rinse in DH2O. Sequential dehydration was carried out in 100%, 95%, 70%, and 50% ethanol for 1 minute each, followed by a 1-minute immersion in Citrisolv to clear tissue of the any remaining ethanol dehydrating reagent (Decon Labs, Inc. CAT# 1601) and two 5-minute washes in Citrisolv. Finally, coverslips were applied using Entellan (Sigma CAT# 1.07960.05000).

6.4.8.2 Immunolabeling with Cathepsin B Antibody for subcellular distribution of cathepsin B

Immunolabeling with cathepsin B antibody was conducted over two days following a standard protocol. On the first day, brain tissue sections were rinsed twice with 1X PBS for 5 minutes each, followed by incubation in a blocking solution consisting of 10% normal donkey serum (NDS) with 1X PBS and 0.3% Triton X-100 for 60 minutes. After a final rinse with 1X PBS for 5 minutes, the sections were stored overnight at 4°C. On the second day, the primary antibody, goat anti-cathepsin B, 8.3 µg/mL in 1X PBS, (R&D Systems, #AF965, Minneapolis, MN) was applied to the sections for 60 minutes at room temperature. Following two washes with 1X PBS for 5 minutes each, the sections were incubated with the secondary antibody, donkey anti-goat A-488, 1:400 in 1X PBS, (Invitrogen, #A11055, Waltham, MA) for 60 minutes. After two additional washes with 1X PBS, the sections were air-dried at room temperature in the dark and coverslipped with Prolong Gold with DAPI (Invitrogen, CAT# P36931).

6.4.8.3 Histology Analysis

NISSL stained sections were digitized using a NanoZoomer S60 Digital Slide Scanner (Hammamatsu, #C13210-01, Shizuoka, Japan) at 20X magnification. Regions of interest, specifically those at -1.75 bregma, were isolated using NDP.View2 and analyzed with Image J. The area of cortical loss was delineated and compared to the contralateral whole hemisphere to calculate the percentage of cortical loss in each mouse. Cathepsin B staining was visualized using a Leica DMI8000 confocal microscope with a 63X objective, focusing on two locations in the cortex near the site of TBI damage, one at CA1 of the hippocampus and one at the dentate gyrus. Similar areas were imaged on the contralateral side for comparison. Image analysis using ImageJ with the Coloc2 plugin determined the fluorescence intensity and distribution of cathepsin B immunoreactive puncta features in the nuclear and paranuclear region, reporting the percent co-localization with the DAPI-stained nucleus. Additionally, qualitative analysis of hippocampal

structure post-TBI was performed on NISSL-stained sections at -1.75 bregma, utilizing a scale rating from 0 to 4 to compare the hemisphere containing TBI with the contralateral hemisphere, with scores ranging from normal structure to complete loss of hippocampus. Briefly; (0) – normal hippocampus structure; (1) – minor architectural alterations; (2) – major architectural alterations; (3) major architectural alterations accompanied by loss of cells; (4) – complete loss of hippocampus. Funding support from the UCSD Light Microscopy Core with NIND NS047101 was acknowledged.

6.5 References

1. Menon DK, Schwab K, Wright DW, Maas AI; Demographics and Clinical Assessment Working Group of the International and Interagency Initiative toward Common Data Elements for Research on Traumatic Brain Injury and Psychological Health. Position statement: definition of traumatic brain injury. Arch Phys Med Rehabil. 2010 Nov;91(11):1637-40. doi: 10.1016/j.apmr.2010.05.017. PMID: 21044706.

2. Centers for Disease Control and Prevention. (2015). Report to Congress on Traumatic Brain Injury in the
3. United States: Epidemiology and Rehabilitation. National Center for Injury Prevention and Control; Division of Unintentional Injury Prevention. Atlanta, GA.

4. Werner C, Engelhard K. Pathophysiology of traumatic brain injury. Br J Anaesth. 2007 Jul;99(1):4-9. doi: 10.1093/bja/aem131. PMID: 17573392.

5. Veenith T, Goon SSh, Burnstein RM. Molecular mechanisms of traumatic brain injury: the missing link in management. World J Emerg Surg. 2009 Feb 2;4:7. doi: 10.1186/1749-7922-4-7. PMID: 19187555; PMCID: PMC2646711.

6. Hook V, Yoon M, Mosier C, Ito G, Podvin S, Head BP, Rissman R, O'Donoghue AJ, Hook G. Cathepsin B in neurodegeneration of Alzheimer's disease, traumatic brain injury, and related brain disorders. Biochim Biophys Acta Proteins Proteom. 2020 Aug;1868(8):140428. doi: 10.1016/j.bbapap.2020.140428. Epub 2020 Apr 17. PMID: 32305689; PMCID: PMC7261628.

7. De Duve C, Wattiaux R. Functions of lysosomes. Annu Rev Physiol. 1966;28:435-92. doi: 10.1146/annurev.ph.28.030166.002251. PMID: 5322983.

8. Lawrence RE, Zoncu R. The lysosome as a cellular centre for signalling, metabolism and quality control. Nat Cell Biol. 2019 Feb;21(2):133-142. doi: 10.1038/s41556-018-0244-7. Epub 2019 Jan 2. PMID: 30602725.

9. Turk V, Stoka V, Vasiljeva O, Renko M, Sun T, Turk B, Turk D. Cysteine cathepsins: from structure, function and regulation to new frontiers. Biochim Biophys Acta. 2012 Jan;1824(1):68-88. doi: 10.1016/j.bbapap.2011.10.002. Epub 2011 Oct 12. PMID: 22024571; PMCID: PMC7105208.

10. Wang F, Gómez-Sintes R, Boya P. Lysosomal membrane permeabilization and cell death. Traffic. 2018 Dec;19(12):918-931. doi: 10.1111/tra.12613. Epub 2018 Sep 12. PMID: 30125440.

11. Lin Y, Epstein DL, Liton PB. Intralysosomal iron induces lysosomal membrane permeabilization and cathepsin D-mediated cell death in trabecular meshwork cells exposed to oxidative stress. Invest Ophthalmol Vis Sci. 2010 Dec;51(12):6483-95. doi: 10.1167/iovs.10-5410. Epub 2010 Jun 23. PMID: 20574010; PMCID: PMC3055766.

12. Bright GR, Fisher GW, Rogowska J, Taylor DL. Fluorescence ratio imaging microscopy: temporal and spatial measurements of cytoplasmic pH. J Cell Biol. 1987 Apr;104(4):1019-33. doi: 10.1083/jcb.104.4.1019. PMID: 3558476; PMCID: PMC2114443.

13. Yoon MC, Phan V, Podvin S, Mosier C, O'Donoghue AJ, Hook V. Distinct Cleavage Properties of Cathepsin B Compared to Cysteine Cathepsins Enable the Design and Validation of a Specific Substrate for Cathepsin B over a Broad pH Range. Biochemistry. 2023 Aug 1;62(15):2289-2300. doi: 10.1021/acs.biochem.3c00139. Epub 2023 Jul 17. PMID: 37459182; PMCID: PMC10399199.

14. Phan VV, Mosier C, Yoon MC, Glukhov E, Caffrey CR, O'Donoghue AJ, Gerwick WH, Hook V. Discovery of pH-Selective Marine and Plant Natural Product Inhibitors of Cathepsin B Revealed by Screening at Acidic and Neutral pH Conditions. ACS Omega. 2022 Jul 12;7(29):25346-25352. doi: 10.1021/acsomega.2c02287. PMID: 35910167; PMCID: PMC9330179.

15. de Castro MA, Bunt G, Wouters FS. Cathepsin B launches an apoptotic exit effort upon cell death-associated disruption of lysosomes. Cell Death Discov. 2016 Feb 29;2:16012. doi: 10.1038/cddiscovery.2016.12. PMID: 27551506; PMCID: PMC4979493.

16. Xie Z, Zhao M, Yan C, Kong W, Lan F, Narengaowa, Zhao S, Yang Q, Bai Z, Qing H, Ni J. Cathepsin B in programmed cell death machinery: mechanisms of execution and regulatory pathways. Cell Death Dis. 2023 Apr 8;14(4):255. doi: 10.1038/s41419-023-05786-0. PMID: 37031185; PMCID: PMC10082344.

17. Droga-Mazovec G, Bojic L, Petelin A, Ivanova S, Romih R, Repnik U, Salvesen GS, Stoka V, Turk V, Turk B. Cysteine cathepsins trigger caspase-dependent cell death through cleavage of bid and antiapoptotic Bcl-2 homologues. J Biol Chem. 2008 Jul 4;283(27):19140-50. doi: 10.1074/jbc.M802513200. Epub 2008 May 9. PMID: 18469004.

18. Bai H, Yang B, Yu W, Xiao Y, Yu D, Zhang Q. Cathepsin B links oxidative stress to the activation of NLRP3 inflammasome. Exp Cell Res. 2018 Jan 1;362(1):180-187. doi: 10.1016/j.yexcr.2017.11.015. Epub 2017 Nov 28. PMID: 29196167.

19. Campden RI, Zhang Y. The role of lysosomal cysteine cathepsins in NLRP3 inflammasome activation. Arch Biochem Biophys. 2019 Jul 30;670:32-42. doi: 10.1016/j.abb.2019.02.015. Epub 2019 Feb 23. PMID: 30807742.

20. Luo CL, Chen XP, Yang R, Sun YX, Li QQ, Bao HJ, Cao QQ, Ni H, Qin ZH, Tao LY. Cathepsin B contributes to traumatic brain injury-induced cell death through a mitochondria-mediated apoptotic pathway. J Neurosci Res. 2010 Oct;88(13):2847-58. doi: 10.1002/jnr.22453. PMID: 20653046.

21. Armstrong RA. Risk factors for Alzheimer's disease. Folia Neuropathol. 2019;57(2):87-105. doi: 10.5114/fn.2019.85929. PMID: 31556570.

22. Li Y, Li Y, Li X, Zhang S, Zhao J, Zhu X, Tian G. Head Injury as a Risk Factor for Dementia and Alzheimer's Disease: A Systematic Review and Meta-Analysis of 32 Observational Studies. PLoS One. 2017 Jan 9;12(1):e0169650. doi: 10.1371/journal.pone.0169650. PMID: 28068405; PMCID: PMC5221805.

23. Schaffert J, LoBue C, White CL, Chiang HS, Didehbani N, Lacritz L, Rossetti H, Dieppa M, Hart J, Cullum CM. Traumatic brain injury history is associated with an earlier age of dementia onset in autopsy-confirmed Alzheimer's disease. Neuropsychology. 2018 May;32(4):410-416. doi: 10.1037/neu0000423. Epub 2018 Feb 1. PMID: 29389151; PMCID: PMC5975092.

24. G. R. Hook, J. Yu, N. Sipes, M. D. Pierschbacher, V. Hook, and M. S. Kindy, "The cysteine protease cathepsin B is a key drug target and cysteine protease inhibitors are potential therapeutics for traumatic brain injury," *J. Neurotrauma*, vol. 31, no. 5, pp. 515–529, Mar. 2014, doi: 10.1089/neu.2013.2944.

25. G. Hook, J. S. Jacobsen, K. Grabstein, M. Kindy, and V. Hook, "Cathepsin B is a new drug target for traumatic brain injury therapeutics: Evidence for E64d as a promising lead drug candidate," *Frontiers in Neurology*, vol. 6, no. SEP. Frontiers Media S.A., 2015, doi: 10.3389/fneur.2015.00178.

26. Yoon MC, Solania A, Jiang Z, Christy MP, Podvin S, Mosier C, Lietz CB, Ito G, Gerwick WH, Wolan DW, Hook G, O'Donoghue AJ, Hook V. Selective Neutral pH Inhibitor of Cathepsin B Designed Based on Cleavage Preferences at Cytosolic and Lysosomal pH Conditions. ACS Chem Biol. 2021 Sep 17;16(9):1628-1643. doi: 10.1021/acschembio.1c00138. Epub 2021 Aug 20. PMID: 34416110; PMCID: PMC9104225.

27. Yoon MC, Christy MP, Phan VV, Gerwick WH, Hook G, O'Donoghue AJ, Hook V. Molecular Features of CA-074 pH-Dependent Inhibition of Cathepsin B. Biochemistry.

2022 Feb 15;61(4):228-238. doi: 10.1021/acs.biochem.1c00684. Epub 2022 Feb 4. PMID: 35119840; PMCID: PMC9096814.

Acknowledgements

Chapter 6, in part, is material in preparation for submission. Sonia Podvin, Jzamin Florio, Charles Mosier, Brian Spencer, Michael Mante, Michael C Yoon, Von V Phan, Jehad Almaliti, William Gerwick, Anthony J O'Donoghue, Robert Rissman, and Vivian Hook. The dissertation author was a co-author of this material.

Chapter 7 Conclusions

7.1 Conclusion: Utilizing Neutral pH inhibitor to Assess the Role of Cytosolic Cathepsin B

Our research has shed light on the pH-dependent properties of cathepsin B and their significance for enzyme function, inhibitor design, substrate specificity, and disease mechanisms, and implications for understanding the role of cathepsin B in health and disease. Remarkably, our findings have highlighted the potential of targeting cathepsin B in neurological diseases, particularly AD and TBI. Our studies opens new avenues for the development of novel therapeutic strategies for neurodegenerative disorders.

Future studies should continue to investigate the role of cathepsin B in disease pathogenesis using advanced experimental approaches and disease models. These studies will provide further insights into the contribution of cathepsin B to disease progression and potential therapeutic interventions. Additionally, building upon the findings of this thesis, future efforts should focus on the development of novel cathepsin B inhibitors with improved potency, selectivity, and pharmacokinetic properties. These inhibitors could offer promising therapeutic interventions.

In summary, this thesis has advanced our understanding of the pH-dependent properties of cathepsin B and their implications for enzyme function, inhibitor design, substrate specificity, disease mechanism, and drug discovery efforts. Our findings highlighted the therapeutic potential of targeting cytosolic cathepsin B in neurological diseases, paving the way for the development of novel therapeutic strategies for these disorders.

7.2 pH-Dependent Inhibitory Properties of CA-074 on Cathepsin B

In chapter 2, we conducted a comprehensive investigation into the pH-dependent inhibitory properties of CA-074 on cathepsin B, shedding light on its potency, molecular features, and protease specificity. Our findings underscore the preferential inhibition of cathepsin B by CA-074 at acidic lysosomal pH 4.6 compared to neutral pH 7.2, highlighting the importance of considering

pH-dependent enzyme properties in drug design. The distinct cleavage preferences of cathepsin B at different pH environments have significant implications for understanding its role in disease mechanisms, particularly in the cytosol and extracellular locations where it may play a role in carious human diseases. Furthermore, our molecular docking studies have provided insights into the pH-dependent interactions between CA-074 and cathepsin B, further elucidating the structural basis of pH-dependent inhibition. These findings contribute to our understanding of the molecular mechanisms underlying cathepsin B inhibition and pave the way for the development of novel pH-selective inhibitors.

Building upon the insights gained from this study, future research should focus on the development of additional pH-selective inhibitors targeting cathepsin B. These inhibitors could offer valuable tools for probing the role of cathepsin B in different cellular compartments and disease states. Additionally, in vivo studies using animal disease models will be crucial for assessing the efficacy of pH-selective inhibitors. These studies will provide valuable insights on the therapeutic potential of pH-selective inhibitors for treating cathepsin B-associated pathologies.

7.3 pH-Dependent Modulation of Cathepsin B by Pure Natural Products

In chapter 3, we investigated the impact of pH environments on the screening of natural product modulators of cathepsin B, highlighting the importance of considering the distinct pH environment of biological locations and conditions in drug discovery efforts. Our findings underscore the pH-dependent properties of cathepsin B inhibitors and their potential applications in probing the role of cathepsin B in different cellular compartments. Furthermore, the identification of pH-selective modulators through chemical screening of natural product libraries offer new avenues for investigating the function of cathepsin B in physiological and pathological processes. By elucidating the pH-dependent modulation of cathepsin B activity, this study

contributes to our understanding of the complex interplay between enzymes and their environments.

Future studies should continue to explore chemical libraries under various pH conditions to identify pH-selective modulators of cathepsin B. These modulators could serve as valuable tools for dissecting the role of cathepsin B in different cellular compartments as well as disease contexts.

7.4 Design and Characterization of Z-Nle-Lys-Arg-AMC Substrate to Monitor Cathepsin B Activity

In chapter 4, we focused on the design and characterization of a novel substrate, Z-Nle-Lys-Arg-AMC, for specific monitoring of cathepsin B activity over a broad pH range. Our findings underscore the importance of considering pH-dependent substrate cleavage properties in the development of specific fluorogenic substrates for cathepsin B. The identification of Z-Nle-Lys-Arg-AMC as a specific substrate for cathepsin B offers new opportunities for studying the role of cathepsin B in different cellular compartments and disease states. By providing a substrate with enhanced specificity and broad pH activity, this study advances our ability to accurately measure cathepsin B activity under physiologic and pathologic conditions.

Future research should incorporate Z-Nle-Lys-Arg-AMC in experimental designs as it serves as a useful tool, capable in many different environmental conditions. Further validation studies should be done to confirm the specificity and sensitivity of Z-Nle-Lys-Arg-AMC in clinical samples from patients with neurologic diseases. These studies would provide important clinical insights into the diagnostic and prognostic utility of cathepsin B activity measurements.

7.5 The role of Cytosolic Cathepsin B in Stress-Induced Cell death

In chapter 5, we elucidated the role of cathepsin B in stress-induced cell death and its implications for neurologic disorders such as Alzheimer's disease and traumatic brain injury. Our findings highlight the pathogenic involvement of cytosolic cathepsin B in mediating cell death under conditions of nutrient deprivation, a common stressor in neurologic disorders. Moreover,

the efficacy of the pH-selective inhibitor Z-Arg-Lys-AOMK in mitigating cell death induced by nutrient deprivation underscores the therapeutic potential of targeting cathepsin B in neurological diseases. By validating the protective effects of cathepsin B inhibition in cell death, this study provides valuable insights into potential therapeutic strategies for neurodegenerative disorders.

Future research should further explore the role of cathepsin B in cellular compartments and what biological pathways cathepsin B is involved in. These studies will provide important insights into the role of cathepsin B in biological and pathogenic contexts. Additionally, further studies that explore the therapeutic inhibition of cytosolic cathepsin B in neurologic diseases will provide important preclinical data on the efficacy of targeting pathogenic cathepsin B.

7.6 The role of Cytosolic Cathepsin B in Traumatic Brain Injury

The focus of chapter 6 elucidated a cascade of events implicating lysosomal leakage and the involvement of cytosolic cathepsin B in the TBI process. The significant motor deficits induced by CCI-TBI in mice, coupled with cortical lesions, underscore the severity of the injury. In particularl, the translocation of lysosomal cathepsin B to the cytosolic fraction within the brain cortex of the ipsilateral hemisphere affected by CCI, as evidenced by Western blot and immunofluorescence analyses. These findings highlight the interplay between CCI-TBI, motor deficits, lysosomal leakage, and cytosolic cathepsin B translocation, suggesting its involvement in the neuropathological mechanisms underlying the pathology of TBI. Further exploration of these pathways is crucial for the development of targeted therapeutic strategies to mitigate the consequences of TBI.

In addition, the efficacy of Z-Arg-Lys-AOMK in ameliorating motor deficits and reducing brain cytosolic cathepsin B activity represents a significant advancement. When administered, Z-Arg-Lys-AOMK improved motor deficits following CCI-TBI. Evidently, Z-Arg-Lys-AOMK

treatment led to a marked reduction in cathepsin B activity within the cytosolic fraction of the brain cortex in CCI-TBI mice, demonstrating its specificity in targeting this enzyme. These findings collectively underscore the therapeutic potential of Z-Arg-Lys-AOMK as a neutral pH-selective inhibitor of cathepsin B in alleviating CCI-TBI-induced motor deficits. Future directions should focus on further elucidating the mechanisms underlying the therapeutic effects of Z-Arg-Lys-AOMK and optimizing its clinical application in the treatment of TBI.